Optical characterisation of non polar nanostructures quantum wells ZnO/(Zn,Mg) O

Mohammed Jassim Mohammed Ali

Mohammed Jassim Mohammed Ali. Optical characterisation of non polar nanostructures quantum wells ZnO/(Zn,Mg) O. Physics [physics]. Université Montpellier, 2018. English. NNT : 2018MONTS096 . tel-02155700

HAL Id: tel-02155700
https://theses.hal.science/tel-02155700
Submitted on 13 Jun 2019

THESE POUR OBTENIR LE GRADE DE DOCTEUR DE L'UNIVERSITE DE MONTPELLIER

En **Physique**

École doctorale **I2S**

Laboratoire Charles Coulomb L2C-UMR 5221

Caractérisation optique de nanostructures à base de puits quantiques non polaires ZnO/ (Zn, Mg) O

Présentée par Mohammed **Jassim MOHAMMED ALI**
Le 13 juillet 2018

Sous la direction de Thierry BRETAGNON

Devant le jury composé de

Brahim GUIZAL, Université de Montpellier	Président
Mathieu GALLART, Université de Strasbourg	Rapporteur
Joël LEYMARIE, Université Clermont Auvergne	Rapporteur
Jean-Michel CHAUVEAU, Université de Nice Sophia Antipolis	Examinateur
Pierre LEFEBVRE, CNRS-Université de Montpellier	Examinateur
Thierry BRETAGNON, Université de Montpellier	Directeur de thèse

UNIVERSITÉ
DE MONTPELLIER

UNIVERSITY OF MONTPELLIER

Optical characterisation of ZnO/(Zn, Mg)O nanostructures based on non polar quantum wells

Author:

MOHAMMED JASSIM MOHAMMED ALI

Supervisor:
Professor Thierry BRETAGNON

A thesis submitted in fulfillment of the requirements for the
degree of Doctor of Philosophy
in the
University of Montpellier
Laboratoire Charles Coulomb – UMR 5221 CNRS-UM
Information Structures Systems (I2S)

July, 2018

UNIVERSITÉ
DE MONTPELLIER

Acknowledgements

To my father and mother whose kindness knows no bounds. To all my family, my three wonderful sisters and my brothers Saif and Ali, to my wife and my beautiful daughters (Meyar, Zina) for all their constant support. To my good friends, there are too many to be cited, I here want to thank them for the help and support they have given since beginning my PhD.

My thanks go to my supervisor Professor Thierry Bretagnon, who always provided a critical ear for my ideas throughout this project and who supported me, in every endeavour with strong encouragement.
I thank Jean-Michel Chauveau obviously for the exceptional quality of his samples.
Special thanks also to Professor Brahim Guizal and Professor Bernard Gil whose doors was always open to me. Thanks also go to Professor Pierre Lefebvre, who always found time for me and who tirelessly facilitated our work over the years. My sincere thanks with a special mention to Pierre VALVIN of the laboratory Charles Columb for his technical support. Thanks also to Professor Lucyna Firlej for all the help she gave to me. I thank also Joël Leymarie and Mathieu Gallart for having accepted to judge my work.
To all my office colleagues (Phuong, Huong, Maha, Waseem, , ...) and to all the members of the team (Christelle Brimont, Thierry Guillet...) of the Charles Coulomb laboratory for making my time here so enjoyable.

My acknowledgements also to Physics Department - Faculty of Science - University of Al-Mustansiriyah, and for the funding of my PhD by the Ministry of Higher Education and Scientific Research of Iraq.

Mohammed 2018

TABLE OF CONTENTS

Chapter 1: Properties of zinc oxide (ZnO)

Chapter 2: Optical properties of ZnO/(Zn, Mg)O quantum wells

Chapter 3: Optical properties of the (Zn, Mg)O barriers

Chapter 4 : Exciton complexes in ZnO/(Zn, Mg)O quantum well

Chapter 5 : Time resolved study of a ZnO/(Zn, Mg)O quantum well

LIST OF FIGURE

LIST OF TABLE

Introduction

Zinc oxide material, II-VI semi-conductor, has an extensive research history dating back to the early beginning of the 20th century. This is due to its attractive features such as deposition as a crystalline material at room temperature, relatively low cost compared to most oxides. ZnO is a wide and direct bandgap II-VI semiconductor (Eg=3.37 eV at room temperature). The powder of zinc oxide is moreover used as additive in very numerous products, for example, plastic arts, ceramic, paints, pigments, cosmetics, etc. The growth of thin layers and low-dimensionality hetero-structures (quantum wells, nano-columns, etc.) with a good crystalline quality recently revived the effort of research on ZnO, in particular with the aim of obtaining effective devices for optoelectronics in the blue and the ultraviolet as a complement to the nitride of gallium. In this objective, the main advantage of the ZnO in front of GaN is a lower cost, allowed by the relative abundance of zinc compared with gallium.

In materials science, another major advantage of zinc oxide is its strong exciton binding energy, which allows preserving the excitonic properties up to ambient temperature. The cohesion energy of the exciton is indeed twice as great in ZnO (60 meV) than in GaN (25 meV) and more than ten times higher than in GaAs (4.8 meV). Excitonic transitions also have a large force of oscillator in ZnO, which enhances the light-matter interaction. These characteristics make of the zinc oxide an excellent material for the study of the effects resulting from the coupling between the photon and exciton, as the condensation of Bose-Einstein and polaritons laser and this until room temperature. In these perspectives, the crystalline good quality realization of nanostructures is essential. The first samples of quantum wells of ZnO/(Zn, Mg)O were developed by L-MBE (laser molecular beam epitaxy) in 2000. The epitaxy by molecular jet technique quickly turned out to be an excellent method of growth of the quantum wells of ZnO/(Zn, Mg)O. Our study takes place within the framework of the characterization of such structures by the optical ways.

One of the peculiarities of zinc oxide lies in its hexagonal crystalline structure, called wurtzite. This crystalline structure is at the origin of several original properties of hetero-structures based on this material, which will be listed in the first chapter of this manuscript. We will see in particular that arguments of symmetry predict the existence of an internal electric field in quantum wells of ZnO/(Zn, Mg)O elaborated along the principal axis of the ZnO, said axis c. The presence of this internal electric field has been observed experimentally in 2005. It has several detrimental effects on the optical properties. One of the main effects is the spatial separation of electrons and holes due to their opposite charge. We will see that the radiative lifetime of the electron-hole pairs is greatly increased in wide quantum wells. The effective lifetime resulting from the competition between radiative and non-radiative processes is quickly degraded in such samples. The binding energy of the exciton is also decreased under the effect of the electric field. They are actually less stable, which means is harmful for the achievement of the two objectives presented above.

There are two solutions to this problem. The first is the growth of quantum wells along non-polar axes. These axes, perpendicular to the c axis, allow to get rid of the internal electric field. The main axes used in growth are the a and m axes. The first quantum well samples of ZnO/(Zn, Mg)O non-polar plane A were grown in 2007 on sapphire substrates. Another way of improving the radiative efficiency of these hetero-structures is to decrease the density of the crystalline defects, responsible for non-radiative losses. Most of non-radiative centers are dislocations of the crystal, which arise from the lattice mismatch inherent in the heteroepitaxy method. Homoepitaxy, and therefore the use of bulk ZnO substrate, theoretically promises a clear improvement in the crystalline quality. A significant improvement was observed only recently.

The first chapter introduces some general information about the properties of zinc oxide and crystal structure and lattice parameters of wurtzite II-VI semiconductors.

The next one presents the most standard growth techniques used for elaborated ZnO hetero-structures. After, we review the experimental and theoretical work about the optical properties of excitons in ZnO/(Zn, Mg)O-based QWs published in the past twenty years.

The third, fourth and fifth chapters are dedicated to the study of the optical properties of homoepitaxial non-polar (A plane) ZnO/(Zn, Mg)O quantum wells growth by MBE. According to the studied physical information, we used three types of experiments: reflectivity, continuous wave photoluminescence (CW-PL) and time-resolved photoluminescence (TRPL).

We dedicate a chapter to the presentation of the optical properties of the ZnO substrate and the (Zn, Mg)O barriers. In this last case we present a detailed study of the lifetime of the exciton in this alloy. A model is proposed to report experimental results including the non-radiative recombination and the effects of localization.

The next one is devoted to the results obtained by continuous wave optical spectroscopy, including the effects at the same time of the polarization and the temperature, on a single

ZnO/(Zn, Mg)O quantum well growth by MBE on A-oriented ZnO substrate. The various lines of photoluminescence observed are attributed to the radiative recombination of excitonic complexes.

In the last chapter, we present the results of time-resolved investigation of the non-polar quantum well. This technique allows us to characterize the dynamic of the recombination of the exciton complexes. The analysis leads to the determination of the behavior of the optical properties according to the temperature among which the evolutions of the radiative and non-radiative contributions in the photoluminescence. We can also get information about the localization of the exciton complexes.

Chapter 1

Properties of zinc oxide (ZnO)

1.1 Introduction

Zinc oxide has an extensive research history dating back to the early beginning of the 20th century due to its attractive features such as its capability of growth as a crystalline material at room temperature, relatively low cost compared to most oxides. It is a wide and direct bandgap II-VI semiconductor (E_g =3.37 eV at room temperature). Moreover, it has a great interest in optoelectronic devices, such as light emitting diodes or laser diodes, due to a large exciton binding energy of 60 meV.[mor09] Another benefit of ZnO is that its components are earth abundant materials, as opposed to gallium or indium, moreover its cost is low compared to GaN.

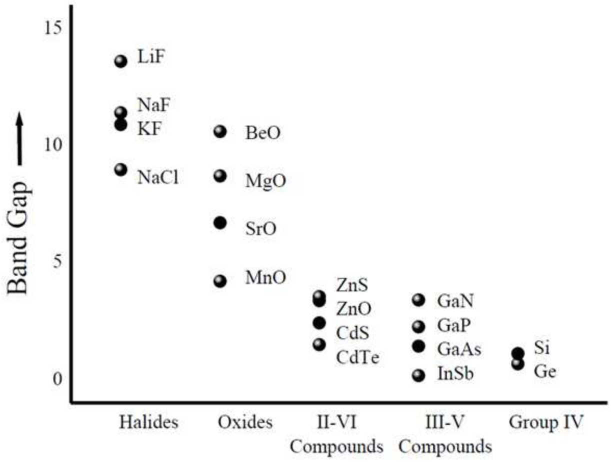

Figure 1.1: Bandgap variations of compounds taken from different columns of the periodic table. Values are presented for room temperature bandgap.[chi11]

ZnO is part of a broader family of semiconductor binary compounds including elements from group II and group VI of the periodic table. This group includes metals such as zinc (Zn), cadmium (Cd) and mercury (Hg) in binary compounds with elements of chalcogens (O, S, Se, Te). Overall, these compounds tend to have lower band gaps than metal-oxides and alkali-halides and larger band gaps of the elementary semiconductors, Si and Ge.[Yu2010] Figure 1.1 presents the band gap of some widespread semiconductors plotted as a function of their chemical composition going from elementary semiconductors to binary semiconductors. The band gap of ZnO is larger than the one of the semiconductors usual (Si, Ge, GaAs). Its value is comparable to that of the GaN.

1.2 Crystal Structure

The organization of a solid as well as the nature of the atoms forms the imprint of the material. It ensues from these elements all its properties; their knowledge thus takes on a major importance that we summarize here. In the natural state, the zinc oxide meets under the shape of an ore bearing the name of zincite the preferential morphologies of which are needles of hexagonal sections.[pal44] ZnO crystallizes (fig. 1.2) according to three different allotropic forms (cubic centered faces, cubic centered blende, and hexagonal of type Würtzite). The crystalline form depends upon the thermodynamic conditions of the environment.[des98], [ski92]

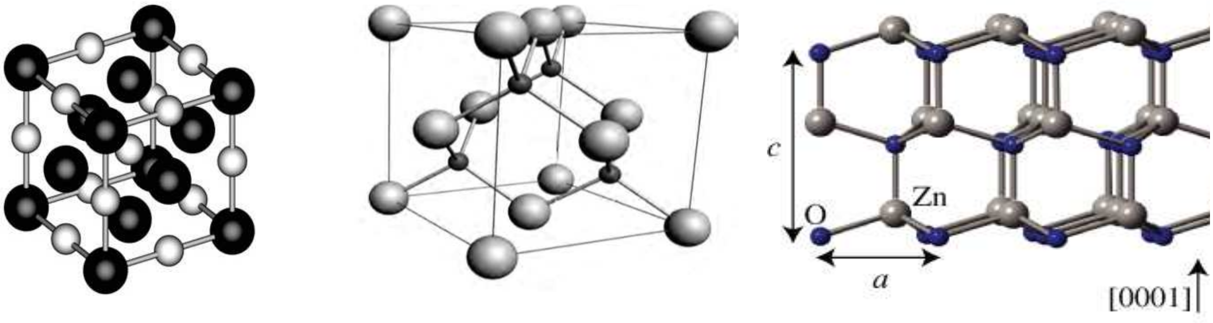

(a) (b) (c)

Figure 1.2: Schematic representation of the crystalline structures of ZnO (a) cubic centered faces, (b) zinc of blende, (c) hexagonal Würtzite. The large and small spheres represent respectively the atoms of zinc and oxygen.

ZnO with most of the group II–VI binary compound semiconductors crystallize in either cubic zinc blende or hexagonal Würtzite (Wz) structure where each anion is surrounded by four cations at the corners of a tetrahedron (fig. 1.3), therefore characterized by two interconnecting sublattices of Zn^{2+} and O^{2-}, such that each zinc ion is surrounded by a tetrahedral of oxygen ions, and vice versa.[mor09] Furthermore ZnO is a II–VI compound semiconductor whose ionicity resides at the borderline between the covalent and ionic semiconductors. In this structure, this tetrahedral coordination is typical of sp^3 covalent bonding nature, but these materials also have a substantial ionic character that tends to increase the bandgap beyond the one expected from the covalent bonding. The ionicity of ZnO is estimated at 51,4 %, which confirms the iono-covalent character of the connection Zn-O.

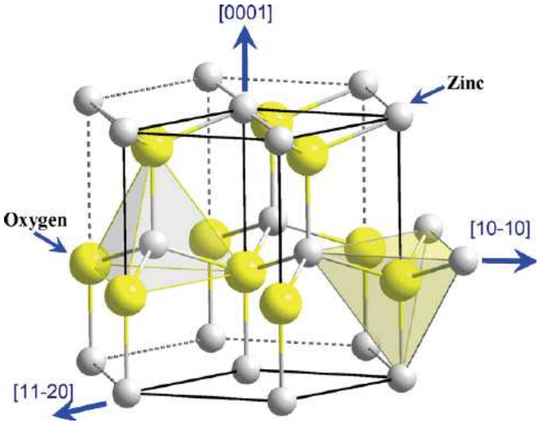

Figure 1.3: The hexagonal Würtzite crystal structure of ZnO.

During our study, we shall be interested exclusively in the hexagonal structure Würtzite of the zinc oxide because it is the structure that is the most thermodynamically stable under ambient conditions.[jaf93] Consequently, it is the commonly crystalline structure observed for zinc oxide samples fabricated using different growing techniques.

Würtzite structure. The Würtzite structure has been resolved in 1914 by W. L. Bragg through the analysis by X-Ray diffraction.[bra20] The Bravais lattice corresponding to this structure is an hexagonal lattice of space group C_{6v}^{4} in the Schoenflies notation and $P6_3mc$ in the Hermann–Mauguin notation. It defines itself by the hexagonal shape of its unit cell (a=b≠c and $\alpha = \beta = 90°, \delta = 120°$), and by the lattice constants (a and c). The values of these constants are closely linked to the chemical nature of the constituent atoms of the lattice. The distance d separating two reticular plans of index (h, k, l) deducts of the relation:

$$\frac{1}{d^2} = \frac{4\left(h^2 + hk + k^2\right)}{3\ a^2} + \frac{1}{c^2} \quad \text{......} \quad (1.1)$$

The following relation give the u parameter for a Würtzite crystal, which is a measure of the amount by which each atom is displaced with respect to the next along the c-axis:

$$u = \frac{1}{3}\,\frac{a^2}{c^2} + \frac{1}{4} \quad \text{......} \quad (1.2)$$

Moreover, in an ideal Würtzite crystal, the axial ratio c/a and the u parameter are correlated by the relationship $uc/a=(3/8)^{1/2}$, where $c/a=(8/3)^{1/2}$ and u= 3/8 for an ideal crystal.

In the ZnO the values of lattice constants are: a=0.32495 nm and c=0.52069 nm. The value of the ratio of $c/a = 1.60$ is close to the one of an ideal Würtzite structure. A schematic representation of the wurtzitic ZnO structure is shown in figure 1.3. The structure can be thus described (fig. 1.4) as a succession of perpendicular plans from the [0001] direction of quotation z equal in 0, 1/8, 4/8, 5/8, ... alternately populated with ions Zn^{2+} and ions oxygen O^{2-} (type ABABAB's pile).

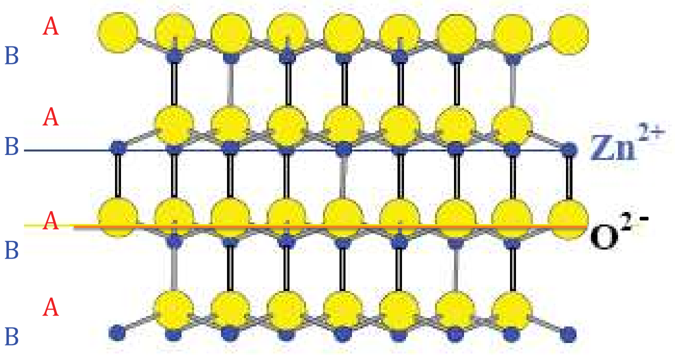

Figure 1.4: Representation of the hexagonal structure Würtzite, the highlighting of the pile of type ABABAB...

One of the fundamental points concerning the ZnO Würtzite is that it does not possess a plan of symmetry perpendicular to the axis c. Two arrangements are thus possible for the atoms of zinc and oxygen, defining the polarity of the structure. Surfaces are either of polarity Zn, if the connection Zn-O is directed to the surface, or of polarity O should the opposite occur.

The tetrahedral coordination gives rise to polar symmetry along the hexagonal axis. This polarity is responsible for a number of the properties of ZnO, including its piezoelectricity and spontaneous polarization, and is also a key factor in crystal growth, etching and defect generation.[gru06]

Miller indices and planes in Würtzite symmetry. The different crystal orientations of the unit cell can therefore be indexed in the Würtzite structure (figure 1.5), with four Miller indices (hkil) for the four vectors (a_1, a_2, a_3) and c spanning the unit cell. The a_i vectors are not linearly independent thus the value of "i" is given by $\{i=-(h+k)\}$.

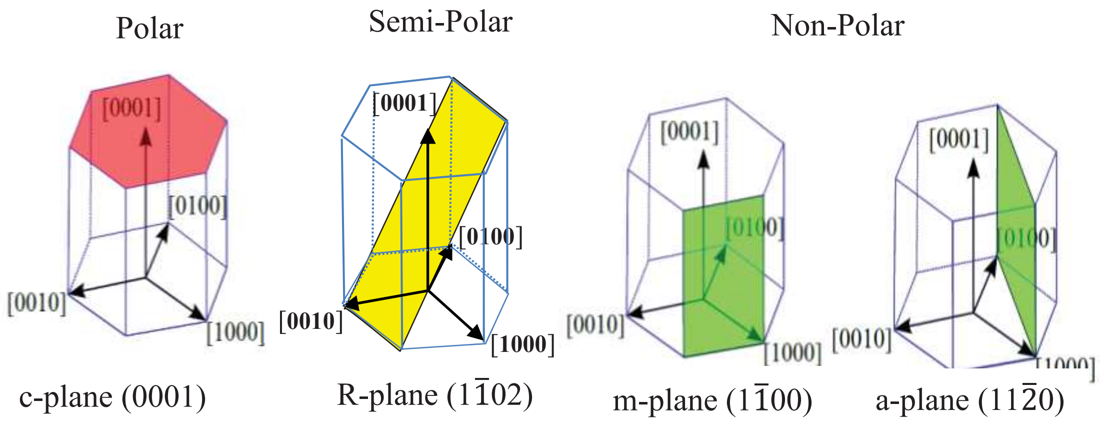

Figure 1.5: The most planes used in Würtzite symmetry. C plane (0001) is a polar plane, R plane $(1\bar{1}02)$ plane is a semi polar. The M plane $(1\bar{1}00)$ and A plane $(11\bar{2}0)$ orthogonal to the C plane are non-polar planes.

The four most common face terminations of Würtzite ZnO (figure 1-5) are: the polar Zn terminated (0001) and O terminated ($000\bar{1}$) faces (C-plane), and the non-polar faces ($11\bar{2}0$) (A-plane) and ($10\bar{1}0$) (M-plane) which both contain an equal number of zinc and oxygen atoms.[des98]

However, it is important to note, before finishing this paragraph, that several factors can affect the value of the lattice constants:

- The concentration in defects and impurities incorporated, because of the difference of length existing between their ionic beam and that of the constituent atoms of the ionic matrix of ZnO.
- The external constraints applied to the crystal.
- The temperature of the material.[ree70]

1.3 Band structure of ZnO

The optical properties of semi-conductors report their electronic structure which results itself from the crystalline structure of the material. Thus it seems essential to possess a good knowledge of the structure of band of ZnO to interpret the results of optical spectroscopy. ZnO is a direct band gap semiconductor, its highest valence band and lowest conduction band are located at the Γ-point of the Brillouin zone (fig. 1.6).[mor09]

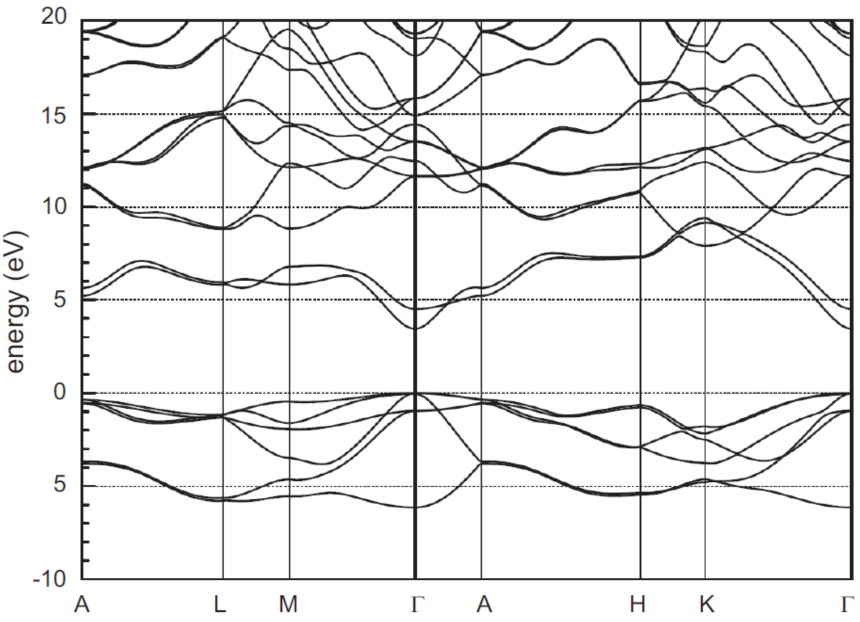

Figure 1.6: Band structure of ZnO.[mor09]

The conduction band is s-like and the valence band is p-like of ZnO. The valence band of ZnO is split by the combined action of the hexagonal crystal field and the spin-orbit interaction, resulting in a band structure as shown in the following diagram in (Fig. 1.7 and 1.8). More clearly, in bulk ZnO the valence band is split by the crystal field and spin-orbit interaction into three states, labeled A, B and C, as depicted in figure 1.8. The highest energy A band has Γ_9 symmetry whist the B and C bands, as well as the conduction band, have Γ_7 symmetry.[rey99] For electric fields polarized perpendicular to the c-axis only the three Γ_5 excitons (A, B and C) are optically active, whereas for electric fields polarized parallel to the c-axis only the two Γ_1 excitons (B and C) are optically active.[rey99]

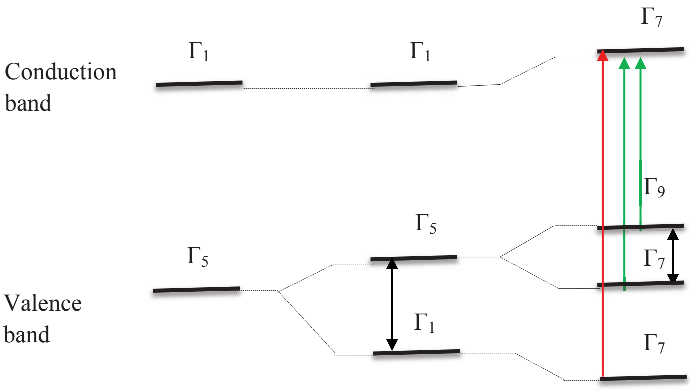

Figure 1.7: Band structure and selection rules Würtzite symmetry.

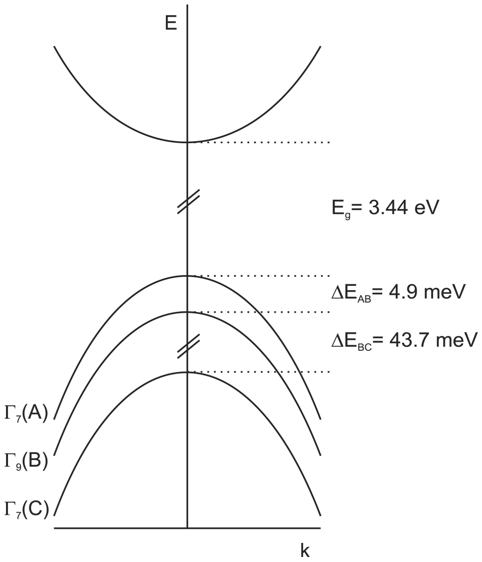

Figure 1.8: Schematic diagram representing the crystal-field and spin-orbit splitting of the valence band of ZnO into 3 subband states A, B and C at 4.2 K.[col06]

In ZnO quantum wells that are grown c-axis oriented, only the three Γ_5 excitons are observed for emission perpendicular to the plane of the well, with the A exciton typically dominating the optical spectrum. Excitons formed with holes in the A band can have Γ_5 or Γ_6 symmetry, which are optically allowed and forbidden, respectively. Excitons formed with holes in the B or C band can have Γ_5, Γ_1 or Γ_2 symmetry, the first two of which are optically allowed and the Γ_2 exciton is optically forbidden.[rey99]

Moreover, there has been a controversial discussion about the symmetry of the uppermost A subvalence band (Γ_7[tho60] or Γ_9[par66]) since the first studies on bulk ZnO. The symmetry of the uppermost A subvalence band, which appears to be currently determined in favor of the Γ7 symmetry, presented by Puls *et al.*[pul12]

Three upper bands occur at the valence top band, leading to three corresponding intrinsic exciton states denoted free exciton A, B and C. Exciton series exists for all three combinations of valence band (VB) and conduction band (CB). The binding energy of the electron with the hole is called excitonic binding energy. This energy varies slightly depending on whether the hole in the exciton is built from the valence band stats A, B or C. The exciton binding energies are taken to be equal to the same value for the three excitons $E_X = 60$ meV.

1.4 Properties of zinc oxide

1.4.1 Electrical properties

ZnO with a bandgap of 3.37 eV at room temperature acts as an insulator in absence of foreign atoms or electric active defects. However, ZnO is most of the time an n-type material. It is attributed to defects in the material such as interstitial zinc atoms or oxygen vacancies. The hydrogen that is present in the majority of the growing technics can be also at the origin of the n-type conductivity of nid ZnO material. The control of the conductivity has been subject to many investigations. For example, one of the stakes is the realization of transparent electrodes for the photovoltaic applications.[chu95]

The p-type doping is much more difficult to be obtained. Indeed, the elements of the columns IA and IB that by substitution in zinc atoms would play acceptors' role tend because of their low size to be located on the interstitial sites, so not playing acceptors' role anymore but that of the donors. The p-doping remain one of the most important issues for the development of electronic devices with ZnO related material

1.4.2 Dielectric function

The macroscopic optical properties of materials are described by the tensor of the dielectric function, linking the vector of the electric flux density to the electric field:

$$\vec{D} = \varepsilon_0 \vec{E} + \vec{P} = \varepsilon_0 \bar{\varepsilon}_r \vec{E} \qquad (1.3)$$

It is possible to demonstrate that the dielectric tensor $\bar{\varepsilon}_r$ of a transparent non-magnetic environment is symmetric real, and thus diagonalizable. By choosing an axis z parallel to the axis c, we obtain in the case of a Würtzite structure:

$$\bar{\varepsilon}_r = \begin{vmatrix} \varepsilon_r^{\perp} & 0 & 0 \\ 0 & \varepsilon_r^{\perp} & 0 \\ 0 & 0 & \varepsilon_r^{//} \end{vmatrix} \qquad (1.4)$$

Thus the optical properties of the ZnO Würtzite are in essence anisotropes uniaxial, of optical axis parallel to the c axis. According to this axis, a plane wave propagates with the same velocity whatever is the polarization. For waves propagating according to any other direction, the velocity is dependent on the polarization. By using the equations of Maxwell, it is possible to demonstrate that the vector refractive index is connected with the dielectric tensor via the equation of Fresnel:

$$\left(n^2-\varepsilon_r^{\perp}\right)\left(\varepsilon_r^{//}\ n_z^2+\varepsilon_r^{\perp}\left(n_x^2+n_y^2\right)-\varepsilon_r^{\perp}\ \varepsilon_r^{//}\right)=0 \quad (1.5)$$

Both solutions of this equation form two surfaces of ellipsoids:

$$n^2=\varepsilon_r^{\perp}$$
$$\frac{n_z^2}{\varepsilon_r^{\perp}}+\frac{n_x^2+n_y^2}{\varepsilon_r^{//}}=1 \quad (1.6)$$

The ZnO Würtzite is consequently birefringent: two types of plane waves can propagate. In the case of a propagation according to the optical axis, the crystal is considered isotropic with a refractive index $n_o=\sqrt{\varepsilon_r^{\perp}}$ (ordinary index). Otherwise, the refractive index depends on the angle between the direction of propagation and the optical axis. It is between n_o and $n_e=\sqrt{\varepsilon_r^{//}}$ (extraordinary index). We see that in the zone of transparency of the ZnO the optical properties present a light anisotropy.

1.4.3 Physical parameters of ZnO

The most important chemical and physical parameters of the ZnO are summarized in table 1.1.

Chemical and Physical parameters	*Values*
Crystal Structure	*Hexagonal & Cubic*
Color	*White*
Density	*5.6760 g/cm*^{3}
Stable phase at 300K	*Würtzite*
Melting point	*1975 °C*
Thermal conductivity	*100 mW/cm.K at 300K*
Molecular weight	*81,38 g.mol-1*
Hardness	*4-5 on the Moh scale*
Static dielectric constant	*8.656*
Refractive index	*2.008*
Energy gap	*3.37 eV, direct*
Exction binding energy	*60 meV*
Electron effective mass	*0.24m°*
Electron Hall mobility at 300K for low n-type conductivity	*200 cm2/Vs*
Hole effective mass	*0.59*
Hole Hall mobility at 300K for low p-type conductivity	*5-50 cm2/Vs*

Table 1.1: The most physical properties of the material ZnO.[pea05]

1.4.4 Optical properties and luminescence

The optical properties of a material are related to the interaction between the light (electromagnetic wave) with the material (electrons of the material). The photoluminescence (PL) is the optical radiation from a physical system, it is the re-emission of light after absorbing a photon of higher energy.[fox14] In a compound semiconductor system like ZnO, the thermal equilibrium is broken by the external optical excitation, from which the electrons are excited from the valence band to the conduction band. The system tends to return to its equilibrium state through the recombination of electron-hole pairs. This process is usually achieved by either band-to-band transitions, or transitions through discrete levels in the band gap related to dopants or defects. The spectrum is then recorded, and peaks with different energies are related to different recombination processes. The electronic band structure of the material can be investigated by analyzing its PL spectrum. Detects radiative transition from an excited electronic state to a lower electronic state. Also, it allows having information about the presence of certain impurities in the characterized material, but only impurities that produce radiative transitions can be detected.

The sample is excited with an optical source, typically a laser with hν > Eg, which is for an example, for example a HeCd laser emitting at a wavelength of 325 nm in the case of ZnO. A photon allows an electron promotion from a bound state in the valence band, to a free state in the conduction band, this phenomenon is named fundamental absorption, as shown in following figure 1.9.[mor09], [mak02b], [li03] This figure also illustrates the different recombination processes of the electron-hole pairs.

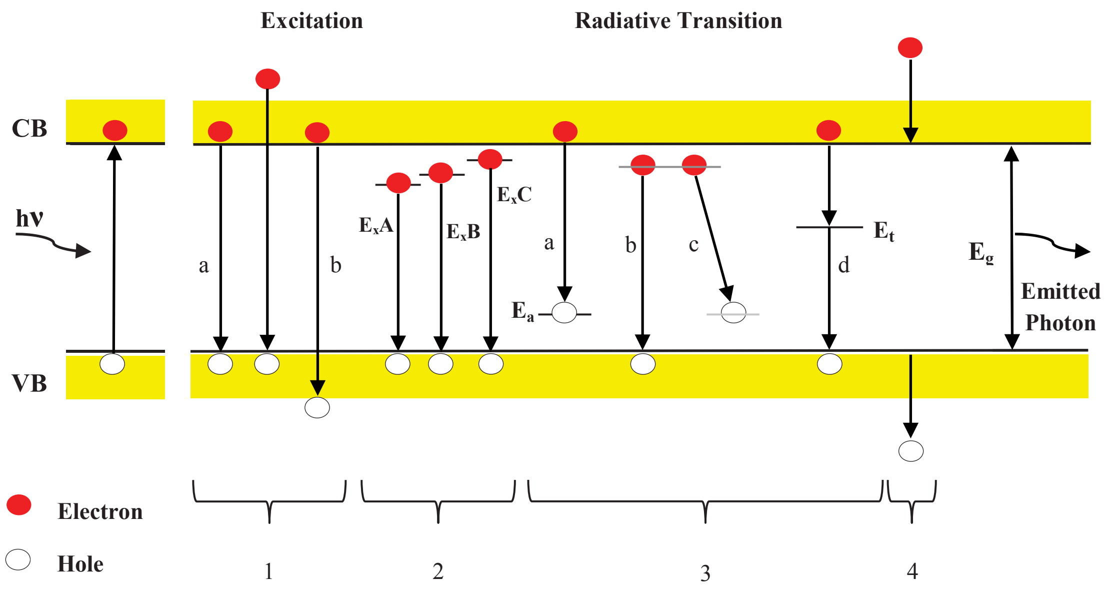

Figure 1.9: Schematic diagrams the band transition of the photoluminescence.

Inter-band transition: Intrinsic emission corresponding in energy to the band gap.

Higher energy emission involving energetic or hot carriers, sometimes related to avalanche emission.

Excitonic transitions due to the A, B or C exciton. These emission energies are corresponding very close in energy to the band gap.

Transitions involving chemical impurities or physical defect. Conduction band to acceptor, donor to valence band, donor to acceptor, and deep level.

Intra-band transitions involving hot carrier, sometimes called deceleration emissions.

In pure ZnO, the photoluminescence at low temperature is usually dominated by the excitonic transitions. When an electron-hole pair is created, coulomb attraction can lead to the formation of an excited state, in which an electron and hole remain bound to each other. This excited state is referred as a free exciton, with slightly less energy than the band-gap energy. The exciton can be bound to a donor or acceptor and recombine to yield neutral donor or acceptor exciton transitions.

1.4.4.1 Excitons (X)

Excitons are electron-hole pairs bound together in stable orbits by the mutual Coulomb attraction between them. Excitons are mainly important for the optical properties of a material. Usually optical recombination causing the emission of photons from a semiconductor occurs between free electrons and holes. For both there is a continuum of possible energies and therefore will also get a rather broad range of photon emission energies. In a semiconductor, the absorption of a photon creates an electron in the conduction band and a hole in the valence band. The oppositely charged particles are created at the same point in space and can attract each other through Coulomb interaction. This attractive interaction increases the probability of the formation of an electron-hole pair, and therefore increases the optical transition rate. Moreover, if the right conditions are satisfied, a bound electron-hole pair can be formed. This neutral bound pair is called an **exciton**. In the simplest picture, the exciton may be conceived as a small hydrogenic system similar to a positronium atom with the electron and hole in a stable orbit around each other.[fox14]

There are two common forms of excitons that are observed in many crystalline materials.

- Wannier-Mott excitons, often known as free excitons.
- Frenkel excitons, also known as tightly bound excitons.

If the electrons and holes are only weakly bound, these excitons are known as **Wannier–Mott excitons.** While, as in ionic crystals, the electron and the hole are tightly bound to each other by strong attraction, such excitons are known as **Frenkel excitons.** In this case the two carriers are localized within the same or nearest-neighbor unit cells. **Frenkel excitons,** occurs in large band gap materials with small dielectric constants and large effective masses. The Wannier-Mott excitons are often observed in semiconductors, whereas the Frenkel excitons are observed in insulator crystals and molecular crystals.

In the case of Wannier-Mott excitons or weakly related excitons, the problem is reduced to that of an hydrogenoic system in which the effective mass μ and total mass M are written as a function of the effective masses of the electron and of the hole (equations 1.7).

$$\frac{1}{\mu} = \frac{1}{m_e^*} + \frac{1}{m_h^*}; \qquad M = m_e^* + m_h^* \quad \text{......} (1.7)$$

The solutions of such a system are well known and the relation of dispersion of Exciton it is written by equation (1.8).

$$E_X\left(\vec{k}\right) = E_g + E_n + \frac{\hbar^2\ k^2}{2\ M} \quad \text{with} \quad E_n = \frac{E_{Ry}}{n}\ \frac{\mu}{m_0\ \varepsilon^2} \quad \text{......} (1.8)$$

Where E_n is the exciton binding energy for the (n^{th}) excited state and $\frac{\hbar^2 k^2}{2M}$ the kinetic energy of the center of mass, m_0 is the rest mass of the electron, ε the background dielectric constant and E_{Ry} =13.6 eV is the Rydberg energy of the hydrogen model.[tho60], [lia67] Like any hydrogenic system the exciton is characterized by two primitives parameters the binding energy of the exciton state 1s (n=1), otherwise noted E_B^X = 60 meV and a_B^* denotes the Bohr radius including in the formula (1.9).

$$a_B^* = \frac{\hbar^2\ \varepsilon}{\mu\ e^2} \quad \text{......} (1.9)$$

which amounts for ZnO with ε ≈ 6.5 to a value of $a_B^* = 1.8\ nm$. Consequently, the excitons in ZnO are therefore Wannier excitons, because their radius is considerably larger than the lattice constant.[tek04] Table 1.2 summarize the parameters of excitons in different semiconductors.

	GaAs	*CdTe*	*GaN*	*ZnO*
a_B^* (nm)	*13.6*	*7*	*2.8*	*1.8*
E_B^X (meV)	*4.8*	*10.8*	*25*	*60*

Table 1.2:Parameters of excitons in different semiconductors.

We indicated in this section the definition of the **free exciton** (X). But if a further charge binds to such an exciton, it forms a charged exciton, which is likewise referred to as a **Trion**. They are classified into two types, negative (**X^-**, with two electrons and one hole) and positive (**X^+**, with two holes and one electron) trions depending on whether an electron or a hole is added to the exciton. It should be noted that more complex exciton states can also exist like, **Biexciton (XX)**.[pee02]

1.4.4.2 Trion (X^-)

During the past few years, the three-particle bound state, as proposed by Lambert,[lam58] of an exciton with an additional carrier (X^-, electron trion or hole X^+, hole trion) has been subject of numerous works. The experimental signatures of trions are more clearly in semiconductor quantum wells because of an enhanced binding energy due to the confinement effect.[ess00a] Since the pioneering work by Kheng *et al.*[khe93] both types of trions (X^- and X^+) have been found in PL and absorption experiments on quantum wells in III–V compounds as well as in II–VI materials. [fin95], [man96], [pag98], [Ciu00], [pee02],

The formation of (X^-) by a neutral exciton (X) and a free electron (e^-) can be described by an atomic or chemical equation:

$$X + e^- \leftrightarrow X^- \quad \text{.......} \quad (1.10)$$

The concentration of free excitons in the quantum well depends on the excitation energy. J. Siviniant *et al*[siv99] explain the dependence of the ratio of X to X^- densities on the excitation power with a chemical law of action of masses (equation 1.11). He connects the densities of neutral exciton (n_X), charged excitons (n_{X-}), and free electrons (n_e), by the relation:

$$\frac{n_X \ n_{e^-}}{n_{X^-}} = K(T) = \frac{4 \ m_e \ k_B \ T}{\pi \ \hbar^2} \exp\left(- \frac{E_B^{X^-}}{k_B \ T} \right) \quad \text{.......} \quad (1.11)$$

Here, m_e is the electron effective mass in the QW, T is the temperature, and E_B^{X-} is the binding energy of the negatively charged exciton.

By comparing experimental data for different semiconductor QW and for the wide range of Lz R.A. Sergeev *et al*[ser05] propose a universal formula (equation 1.12) to calculate the trion binding energy in quantum wells.

$$\frac{E_B^{X^-}}{R_y} \approx \frac{1}{\sqrt[3]{\frac{L_Z}{a_B}}} \quad \text{.......} \quad (1.12)$$

Where E_B^{X-} is the trion binding energies, R_y is exciton Rydberg, L_z is the width of QW and a_B is the exciton Bohr radius.

1.4.4.3 Biexciton (XX)

Excitons are mainly important for the optical properties of a material. It is well established that, at high density of excitation, two excitons with opposition spins may interact and form a bound state known as biexciton. Moreover, the biexcitons can play an important role in optical properties such as threshold density for stimulated emission of laser action and gain coefficient. The relation between (I_X) intensity of exciton and (I_{XX}) intensity of biexciton can be described by the simplest relation:[sun00]

$$n_X \propto \left[\left(1+\frac{G}{G_0}\right)^{1/2} - 1\right] \qquad n_{XX} \propto \left[\left(1+\frac{G}{G_0}\right)^{1/2} - 1\right]^2 \qquad (1.13)$$

Where $G_0 = (n^{*}\tau_{XX}/4\tau_X^2)(1 + \tau_c\ /\ \tau_X\ )$ is the characteristic generation rate that separates the exciton-dominant from the biexciton-dominant region. G is the generation rate, τ_X *and* τ_{XX} are the exciton and biexciton lifetimes, and τ_C is the characteristic interconversion time when $n_X = n_{XX} = n^{*}$.

1.5 ZnO alloys

In the framework of development of electronic devices, band gap engineering is a crucial issue especially in reference to optoelectronic devices. By alloying the starting semiconductor with other material of different band gap, the band gap of the resultant alloy material can be fine tuned, thus affecting the wavelength of exciton emissions. Alloying with MgO and/or CdO, in the same way that the GaN that may be alloyed with AlN and/or InN in order to respectively increase or decrease the bandgap, may carry out bandgap engineering in ZnO. One of the differences between the nitride and the oxide families is that AlN and InN have the same Würtzite crystal structure as the GaN, whereas MgO and CdO have a rock-salt structure. This crystal structure is not the same that the one of ZnO, which is Würtzite structure. As a consequence, phase separation is expected to occur for ZnO based alloys with high content of MgO or CdO.[oht98], [oht00], [mak04a], [gru04] In summary, the bandgap of ZnO can be increased by alloying with MgO and can be reduced as well by alloying with CdO.[gru03] Some of the main properties of ZnO, MgO and CdO are shown in table 1.3.

	ZnO	*MgO*	*CdO*
Eg (eV)	*3.37*	*7.8*	*2.2*
*m*e (m0)*	*0.28*	*0.35*	-
*m*hh (m0)*	*0.78*	*1.60 [001], 2.77 [111]*	-
*m*lh (m0)*	-	*0.35 [001], 0.31 [111]*	-
a (Å)	*3.2*	*4.2*	*4.7*
c (Å)	*5.2*	-	
Stable crystal structure	*Würtzite*	*Rocksalt*	*Rocksalt*

Table1.3: Some properties of the binary II-VI oxides compounds.[pea12]

These ZnO, MgO, and CdO isoelectronic materials span the entire blue ultraviolet spectral range (fig. 1.10).[mak04a] These alloys are potentially good candidates for the realization of quantum wells. However, the change of crystalline structure limits the possibilities of incorporation of the magnesium (colbat) in the alloy. The main idea behind the invention of heterostructures was to create artificial potential wells and barriers for electrons and holes combining different semi-conductor materials. The crystalline quality and the separation of the phases are consequently the main problems that must be overcome for making a device. Moreover, the complication of the lattice mismatch, which strongly affects the electronic states and the valence band offset, must be taken into consideration.

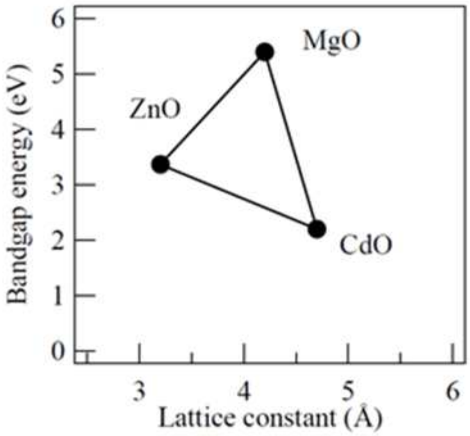

Figure 1.10: Energy gap at 300 K versus lattice constant for a few relevant II-VI-oxide semiconductors. [mak04]

Experimental and theoretical[hu2015] researches on Mg incorporation into ZnO have achieved an affordable understanding of the action of incorporating on both the crystalline structures and the electronic properties.[oht98], [mak01] The first results on the synthesis of $Mg_xZn_{1-x}O$ material on $ScAlMgO_4$ substrates using pulsed-laser deposition has been reported by Ohtomo *et al.*[oht98b] The band-gap increases up to 3.99 eV for 33% of Mg. Accordingly, the lattice parameter *a* increases and *c* decreases with increasing Mg concentration.[oht99] Since this pioneering work, several teams have reported on the grown of (Zn, Mg)O alloy.[mak01], [gru04], [hei07] An increase of the band gap of 20 meV by percent of Mg in the alloy has been reported.[mak01], [gru04] The Mg incorporation into ZnO can increase the width of band gap from 3.37 eV to 4.1 eV, so (Zn, Mg)O is a promising candidate for the optoelectronic devices.[ozg05] For the growth of ZnO quantum well (QW) structures, (Zn, Mg)O was used as a barrier material, due to its larger bandgap compared to ZnO. Usually, the ZnMgO are grown at relatively higher temperatures in order to achieve epitaxial layers with good crystal quality. Accordingly, the increase in the exciton binding energy in (Zn,Mg)O/ZnO quantum well leads to an even higher stability of the excitons well above room temperature, and will improve the performance of ZnO based excitonic devices.[gru04], [sha99] In heterostructures the optical properties of (Zn, Mg)O are usually not investigated directly, but it is evident that the optical characteristics of the barriers influence the optical performance of ZnO quantum wells, so there is a need to explore (Zn, Mg)O features separately as an alloy system.[sha99], [mak04], [pie99], [des98]

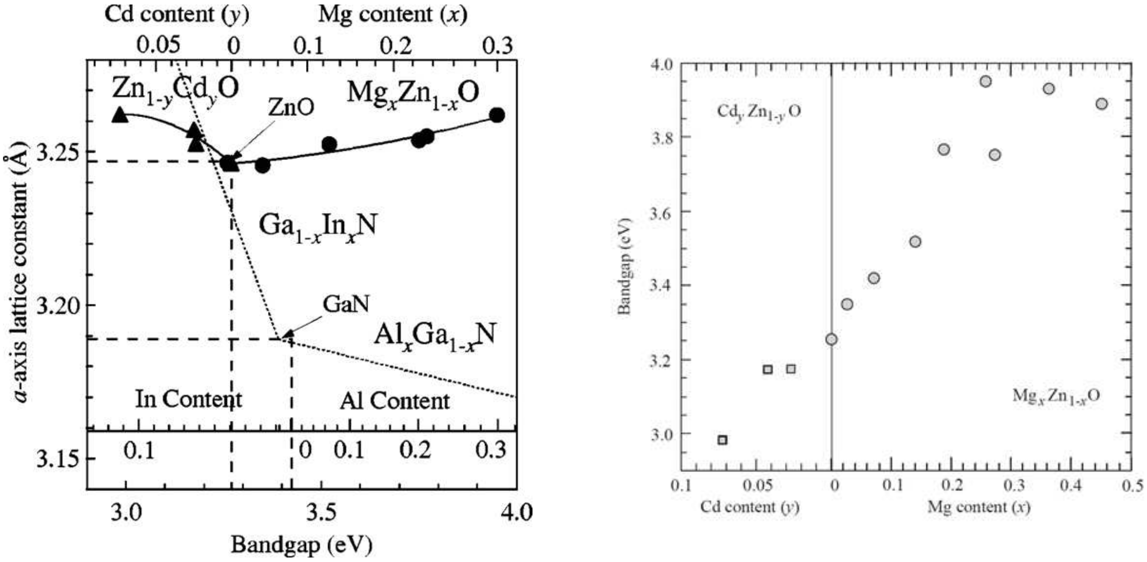

Figure 1.11: Optical bandgaps of $Cd_yZn_{1-y}O$ and $Mg_xZn_{1-x}O$ alloys as a function of Cd and Mg composition in the ZnO lattice on to different representation left panel[mak01] right panel.[mor09], [oht98]

In the case of CdZnO, both lattice parameters *a* and *c* increase with the Cd content, consistent with the larger atomic size of Cd compared with Zn. For example Makino *et al*[mak01] reported on the grown of the CdZnO alloys with Cd concentrations of 7% and band gap of 3.0 eV were grown on sapphire (0001) and $ScAlMgO_4$ substrates using pulsed-laser deposition.

1.6 Conclusion

We have presented the main properties of ZnO and its related alloys. In the next chapter, we review the main results reported in literature on optical characterization of ZnO/(Zn, Mg)O quantum wells.

Chapter 2

Optical properties of ZnO/(Zn, Mg)O quantum wells

2.1 Introduction

Since the paper of Ohtomo *et al*[oht98a] in 1998, ZnO/(Zn, Mg)O QWs have ben successfully grown by different techniques such as laser pulsed deposition (LPD), metal–organic chemical vapor deposition (MOCVD), and Molecular Beam Epitaxy (MBE). Sapphire (0001) oriented substrates were originally used.[oht99a] The resulting structures are oriented according to the c-axis. To grow ZnO and its related alloys, other substrates such as SCAM, Si(111), GaN and bulk ZnO have been successfully used since then.

ZnO has been research attention for a long time because of its applications in many scientific and industrials areas. All these applications have boosted research related to the growth of high quality ZnO thin films by a lot of different techniques that need high quality substrates[tri14] . The main technique for the growth of ZnO bulk crystals is the hydrothermal method (growth from aqueous alkaline solutions). Optical and structural properties have been improved when the ZnO/(Zn, Mg)O heterostructures were grown using ZnO substrates.[cha10]

As for nitride, the more stable structure for the Zinc Oxide is the wurtzite. In strained group III-nitride based quantum structures grown along the c direction internal electric fields were found to appear naturally. In spite of the fact that theoretical calculations[gop06], [mal07] predict value of spontaneous and piezoelectric constants for the ZnO comparable to those of the GaN, the first experimental results reported on ZnO/(Zn, Mg)O QWs, do not mention the presence of such a field.

In order to prevent the detrimental effects of the internal electric field, it is possible to grow the quantum heterostructures along the non-polar directions, i.e., with the polar c-direction of ZnO lying in the growth plane. ZnO/(Zn, Mg)O based QWs have been successfully grown on the A-plane $(11\bar{2}0)$ or the M-plane $(10\bar{1}0)$.

In this chapter, we present the most standard growth techniques used for elaborated ZnO heterostructures. After, we summarize the experimental and theoretical work about the optical properties of excitons in ZnO/(Zn, Mg)O-based QWs published in the past twenty years.

2.2 Excitons in quantum wells

2.2.1 Quantum wells

The techniques of growth allow building heterostructures mono-layer by mono-layer. It is thus possible to achieve artificial materials where the carriers will be confined according to one or several directions. Here we have studied 2D systems, where the carriers are free in two directions of space. In the third directions the barriers confine the carriers. The quantum wells are the simplest 2D system; they can be obtained by superimposing the layers of semiconductors with different bandgap. However, in order to get a good crystalline structure the lattices parameters of the semiconductors must be close. If the thickness of the layer of the semiconductor with smaller bandgap is thin enough (i.e. weak in front of the de Broglie wavelength of the carrier) a quantification of the energy is observed. It results in an increase of the effective bandgap when the width of the quantum wells decreases. In 1974 Dingle *et al* [din74] report the first observation of the quantification in 2D-system in GaAs/(Ga, Al)As heterostructures.

By adding magnesium in the zinc oxide the bandgap of the alloy increases. A linear increase of the bandgap has been reported with a slope of around 25 meV by percent of magnesium in the alloy until a composition of about 40 %.[oht99b], [koi05] Furthermore, the lattice parameters remain close enough for avoiding interface constraints. Thus the ZnO/(Zn, Mg)O is a good candidate for the realization of UV devices.

2.2.2 Excitons

In a quantum well the coulombic interaction between the hole and the electron gives birth to excitons as in the case of the 3D materials. As a consequence of the two-dimensional character of the quasi particle the bounding energy of the exciton is more important in quantum well than in the bulk material. In pure 2D material, the exciton bounding energy is four times the one in 3D material. In practice, quantum wells are not pure 2D systems, however the exciton bounding energy is higher than in the bulk material.[din74] The excitons are consequently more stable in quantum wells than in bulk material, which is an advantage for optoelectronic devices operating at room temperature. This is not always true, in particular in quantum wells when an internal electric field is present.

2.2.3 Excitons in quantum wells with internal electric field

In polar material such as GaN or ZnO the polarization is neutralized by the free carriers and the surface charges, this is not the case in the heterostructures. Thus the polarization field created gives birth to an internal electric field, which is profoundly going to modify the optical properties. We are going to illustrate these effects by considering a layer of thickness L_W (well) of polarization P_W sandwiched between two layers of thickness L_B (barriers) and polarization P_B grown according to the [1000] direction. Assuming the same value for the dielectric constant for the wells and the barriers, it can be easily demonstrated[ler99a] that the electric field resulting from the polarization shift (in the wells and in the barriers) is given by:

$$\vec{E}_w = \frac{L_B}{L_B + L_W}\frac{\left(\vec{P}_B - \vec{P}_w\right)}{\varepsilon} = \frac{L_B}{L_B + L_W}\vec{E}_{max} \qquad (2.1)$$

$$\vec{E}_B = \frac{-L_W}{L_B}\vec{E}_w$$

The first obvious remark is that the electric field in the well will be of opposite sign to that of the barrier. Furthermore, we see that the electric field inside the quantum well depends on the geometry of the sample. The maximum of the electric field in the quantum well is obtained when the width of the barriers are large enough ($L_B >> L_W$).

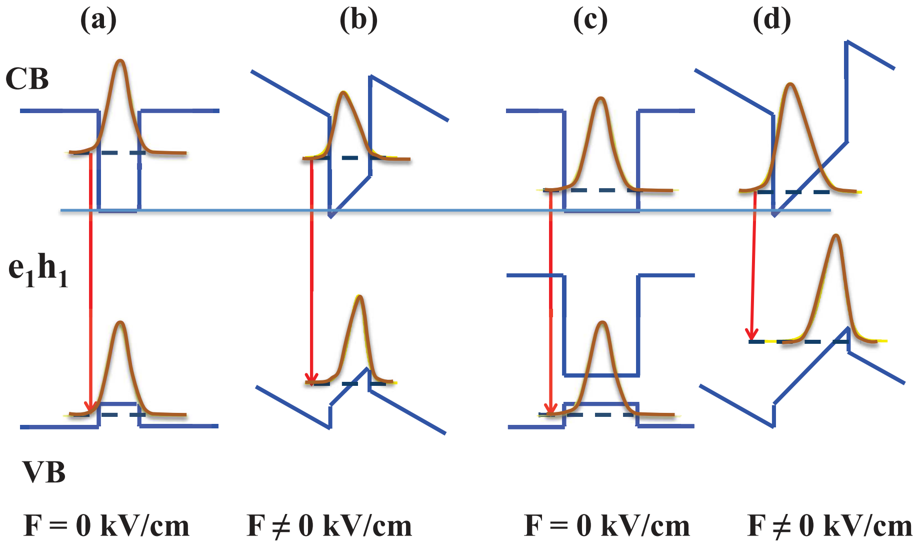

Figure 2.1: Schematic representation of band structure for narrow (a) and (b) and wide (c) and (d) QW without (a) and (c) and with (b) and (d) internal electric field.

The effect of such an internal electrical field is known as the quantum-confined Stark effect (QCSE). It has been investigated in detail in heterostructures based on wurtzite group-III nitrides[lef01] GaN/(Ga,Al)N. They are type I quantum well, where both electron and hole are confined in the same layer. This is illustrated in figure 2.1, which shows the calculated transition energies and electron and hole wave functions without (a and c) and with (b and d) electric field for narrow (a and b) and wide (c and d) quantum wells. The quantum-confined Stark effect (QCSE) red shifts the fundamental optical transition. In addition, it induces spatial separation of electron and hole. As a consequence, there is a decrease of the overlap between the electron and hole ground state wave functions. Thus the oscillator strength of the fundamental transition reduces. From the experimental results on group-III nitrides QW two regimes can be defined: (a) for narrow QWs the emission energy is above the material bandgap and the excitonic lifetimes are in the range of nanoseconds, the quantum confinement dominates; (b) for wide QWs the emission energy is below bandgap and decreases almost linearly with increasing QW width (Lw), whereas the exciton lifetime increases exponentially, the QCSE dominates.

2.3 Growth techniques

Different type of growth techniques have been used to growth ZnO/(Zn, Mg)O quantum wells. The technique the most used so far is the Pulse Laser Deposition.

The Pulsed Laser Deposition (PLD)[vis99] or Laser Molecular-Beam Epitaxy (LMBE) gave the first multi-quantum wells.[oht98a] In this method, a polycrystalline target is ablated by a pulse laser in an ultrahigh vacuum chamber. When the laser is absorbed by the target surface a strong plasma plume is generated which then condenses onto the substrate surface. The growth process is monitored in situ by reflection high-energy electron diffraction (RHEED). In order to form the targets high purity ZnO and MgO powders are mixed, calcined, and sintered in a predetermined amount. The important parameters in the PLD technique are the deposition temperature, background gas pressure, target to substrate distance, laser fluence, and pulse repetition rate. Single-phase thin film of $Zn_{1-x}Mg_xO$ c-oriented has been successively growth with a magnesium concentration up to $x=0.33$.[oht98b] ZnO/(Zn, Mg)O heterostructures such as superlattices,[oht99a] MQW[mak00] or single QW[mak08] have been also successfully elaborated.

Metalorganic vapour-phase epitaxy (MOVPE) is a very important industrial epitaxy standard and offers the advantages of controlled growth and large-scale production.[gru04], [zha05] Different combinations of precursors were chosen to fabricate this structures. For example Gruber *et al*[gru04] used diethylzinc (DEZn), bis(methylcyclopentadienyl)magnesium ($MeCp_2Mg$), and nitrous oxide are used as the zinc, magnesium and oxygen precursors, respectively. N_2O, DMZn:TEN and $(MCP)_2Mg$ have been used as oxygen, zinc and magnesium precursor, respectively by Thiandoume *et al.*[thi10]

In 1996, a team of the North Carolina State University have investigated the growth of ZnO using molecular beam epitaxy (MBE).[joh96] The modified set-up called plasma-assisted MBE[mor05a], [lu05] or radical-source MBE[sad05] has been successfully used to growth high quality quantum wells. Here the metals (Zn and Mg) being evaporated using Knudsen cells and atomic O being activated in a radio-frequency plasma cell. The oxygen gas flow rate is controlled by a leak valve. As in PLD the growth process is monitored in situ by reflection high-energy electron diffraction (RHEED).

For the heteroepitaxy of ZnO and related alloys the choice of the substrate is crucial, he must be chosen so as to minimize the lattice-matched. Table 2.1 summarises the lattice properties and lattice mismatch of several materials used as substrate for the growth of ZnO heterostructures. Sapphire substrate (0001) are regularly used for the growth of ZnO according (0001)[oht98a], [mor05a] or $(11\bar{2}0)$. Non polar structure (A-plane $(11\bar{2}0)$ and M-plane $(10\bar{1}0)$ ZnO) can be grow using r-oriented[cha07] and m-oriented[cha08] sapphire substrates respectively. In addition, ZnO polar heterostructure have been grown on SCAM ($ScAlMgO_4$),[mak00] Si (1111),[gu07] GaN and SiC.

Material	*Crystal structure*	*Lattice parameters* *a (Å)* *c (Å)*	*Lattice mismatch (%)*	*Orientation*
ZnO	*Hexagonal*	*3.252* *5.213*	*0*	*c, m, a*
GaN	*Hexagonal*	*3.189* *5.185*	*1.8*	*c*
a-Al2O3	*Hexagonal*	*4.757* *12.983*	*(18.4 after 30° in plane rotation)*	*(0001) c* *(10-12) a*
ScAlMgO4	*Hexagonal*	*3.246* *25.195*	*0.09*	*c*
6H-SiC	*Hexagonal*	*3.080* *15.117*	*3.5*	*c*
Si	*Cubic*	*5.430*	*40.1*	*c*

Table 2.1: Lattices parameters of different substrate material for ZnO.

2.4 Polar ZnO/(Zn, Mg)O based quantum wells

In strained hetero-layers in wurtzite structure grown along the c-axis both piezoelectric and spontaneous polarization effects are expected. But even though the ZnO presents coefficients of spontaneous and piezoelectric polarizations comparable to those of wurtzite III–V nitrides only few experimental papers[mak02], [gru04] suggest the presence of internal electric fields between 1998 and 2005. The magnitude of the electric field has been a subject of controversy. For example, we can read in a paper published in 2005: "*ZnO/MgZnO QW structures with relatively low Mg composition (x≤0.2) and thin well width (Lw<46 Å) have the negligible internal field effect due to the cancellation of the sum of piezoelectric and spontaneous polarizations between the well and the barrier.*"[par05] In the same time, the calculations of excitonic transition in quantum wells (QWs)[col01], [sen03] have neglected the presence of such internal field.

For quantum well large enough, the presence of built-in electric fields in the QWs can be evident in the pump-power dependence of the emission energy[mor05b] as illustrated in Figure 2.2(left). In this figure a shift of the PL peak to higher energy of ~80 meV is observed by increasing the pump power density over six orders of magnitude. To demonstrate the effect of the carriers density on both transition energy and overlap of the electron and hole wave function we performed calculation for a 7.1 nm wide QW, solving the Schrodinger and Poisson equation. Figure 2.2(right) show the change in potential profile of the QW and wave function. The corresponding transition energy and electron-hole overlap integral are indicated on the figure. The shift of the photoluminescence line results from the screening of the internal electric field by densities of electron-hole dipoles. Such effects can also be produced for the wider QWs at moderate excitation densities because of the large recombination time as discussed below.

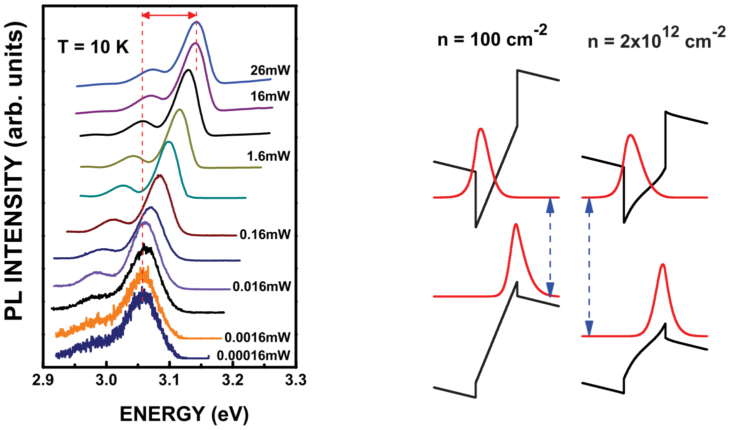

Figure 2.2: Continuous-wave PL spectra of the 7.1 nm QW recorded at low temperature, for various pump-power densities.

To determine the magnitude of the internal electric field it is necessary to measure unambiguously both transition energy and lifetime of the system in its lowest excitation state whatever the wide of the QWs. That is to say, it is necessary to quantify as precisely as possible the minimum PL energy that the system can reach. To that end time-resolved photoluminescence (TRPL) measurements are very helpful.[bre06b] Figure 2.3 gives an illustration of the evolution of the PL spectrum over time. The most noticeable feature is the energy move of the peak with time after the pulsed laser excitation. Firstly, the spectrum peaks around 3.08 eV and, with time, and a shift to lower energy is observed down to a value of 3.02 eV. This comportment is attributed to the screening and de-screening of the internal electric field due to the electron-hole pairs concentration change along time. Immediately after the pulse laser excitation, the density of electron-hole dipoles induces an effective electric field that opposes the internal one. The latter is thus partially screened and the PL line is shifted to higher energy in comparison to the very low excitation regime. The progressive loss of carriers after the pulse due to recombination processes induces a de-screening of the electric field and, hence, a shift to lower energy of the transition energies by restoration of the QCSE.

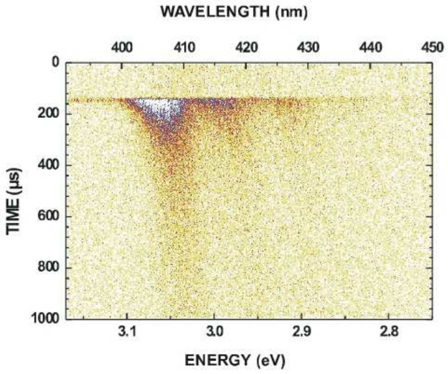

Figure 2.3: Image of the TR-PL of the 7.1 nm thick ZnO/(Zn, Mg)O QW measured at low temperature (T=10 K).[bre14]

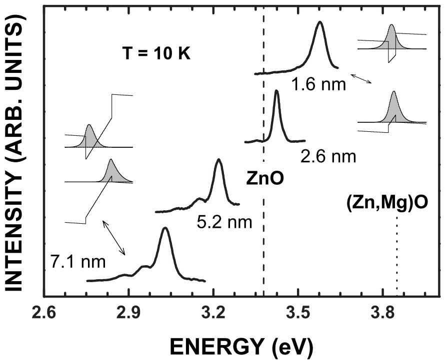

Figure 2.4: Time-integrated PL spectra of single ZnO/Zn_{078} $Mg_{0.22}$ O QWs. The inserts illustrate the effect of internal electric field on electron and hole wave function.[bre06a]

The real value of the transition energy is obtained more accurately from time-integrated PL (TIPL) instead of CW-PL. The time-integration window is restricted to delays large enough to ensure the constancy of the PL line energy. Moreover, the repetition rate is adapted to the slowness of the observed decay, in order to get a full de-excitation between two consecutive pulses. Using this careful procedure, the excitonic transition energy and exciton lifetime are measured. Figure 2.4 shows the TIPL spectra, recorded at 10K, of a serie of ZnO/ $Zn_{0.75}Mg_{0.25}O$ single quantum wells with different width (Lw). The PL lines of the two wider QWs lie below the ZnO excitonic gap. Furthermore, it can be noted that the QW PL lines are accompanied by a series of longitudinal-optical phonon replicas separated by 72 meV. The ratio of the intensities of the first phonon replica line and the zero-phonon line increases when the width of the QW increases. The internal electric field separates the electron and hole wave functions toward either side of the QW. Consequently, for wide QW a strong dipole is formed, which enhances the coupling with polar phonons.[mak02], [sun02], [mak05], [lan12], [bea13]

The results of such measurements are presented in figure 2.5. For wells with width smaller than 3 nm, the exciton transition energies are higher than of the ZnO bulk, and the exciton lifetimes are in the range of nanosecond. For these narrow QWs, the quantum confinement effects dominates the exciton properties. For wide QWs, with widths larger than 3 nm, the exciton transition energies are lower than those of the ZnO bulk. The transition energy decreases linearly with the well width while the lifetime increases exponentially. The exciton properties are governed by the QCSE. The energy of the fundamental transition, the binding energy, and the oscillator strength of the ground-state exciton can be calculated by a variational method[mor05b] that includes the electric field. The calculation taking into account an electric field of 0.9 MV/cm is in a very good agreement with the experimental energies and lifetimes (Fig. 2.5).

Before going further, let us now comment the influence of the built-in electric field on the exciton binding energy. The exciton binding energy is higher than the bulk value in a QW without internal electric field. This is the normal effect of quantum confinement. The interaction between the two particles increases, consequence of the reduction of the distance between the electron and the hole. In polar QW, for wider one the electric field pushes the electron and the hole towards either side of the QW, thus weakening their Coulombic interaction. Consequently, the exciton binding energy decreases when the width increases (Fig. 2.6).

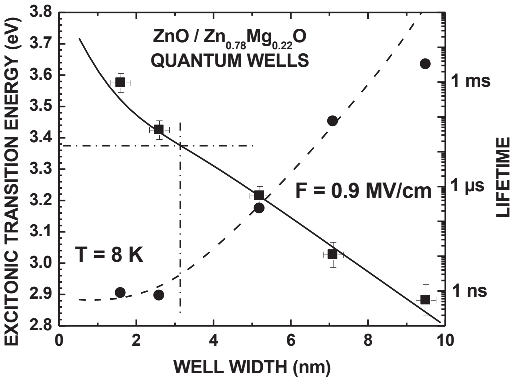

Figure 2.5: Comparison of experimental PL peak energies and PL decay times to the result of variational calculation.[mor05b]

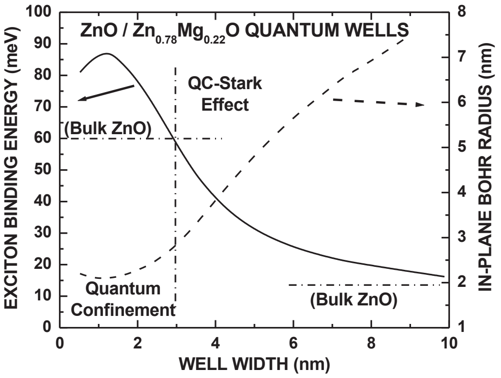

Figure 2.6: Calculated binding energy and pseudo-Bohr radius versus well width, obtained by assuming an electric field of 0.9 MV/cm.[mor05b]

In a first approximation, the built in electric field in ZnO/(Zn, Mg)O single QW varies linearly with the magnesium concentration in the barrier, x (fig. 2.7), with a coefficient of A = 3.95 (MV/cm).[bre07] In MQW, the distribution of electric field among the well and barrier layers[ler99a] should be taken into consideration. Then the resulting electric field in the QW is given by:

FW = Fmax LB / (LB + LW), ... *(2.1)*

where Fmax is the maximum electric field. It is obvious from this formula that the electric field in the well layer is close to Fmax for samples having very thick barriers (LB >> LW). In contrast, relatively narrow barrier layers will significantly reduce the effective field in the QW. The modelling illustrated the effect of the barrier width on the transition energy in MQW having a constant barrier width (Fig. 2.8). The energies shift are calculated in three different situations: no electric field (as a reference), taking in consideration the distribution of the field in well and barrier layers and maximal electric field (thick barriers). In the last situation, for QW width wider than 3 nm the energy falls below the ZnO excitonic gap, whereas the same crossing it obtains only for QW wider than 4 nm in the second situation. Indeed, the effective field in the QWs decreases steadily with LW (see insert in Fig. 2.8). In the such MQWs the electric field declines in the layers with increasing QW width and therefore the QCSE is reduced if compared to SQW designs. It could be an explanation why the magnitude of piezoelectric and spontaneous polarization in ZnO/(Zn, Mg)O hetrostructures has been underestimated in MQWs.[mak04], [koi06] Generally, in MQWs, the electric field in the well layers decreases with increasing LW and therefore the

QCSE is reduced if compared to SQW designs. In summary, the polarization effects are underestimated in analysing the experimental results, if the barrier width dependence of FW is not taken into account.

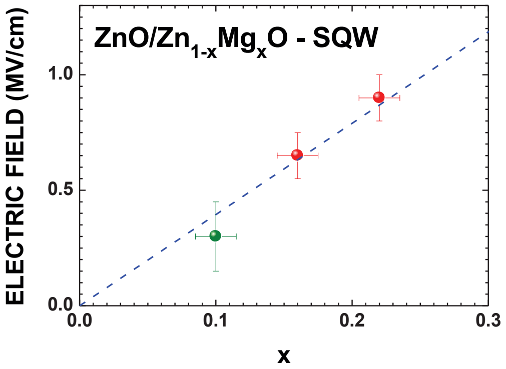

Figure 2.7: Dependance of the internal electric field in ZnO/(Zn, Mg)O with contration of Mg in the barriers.[bre07]

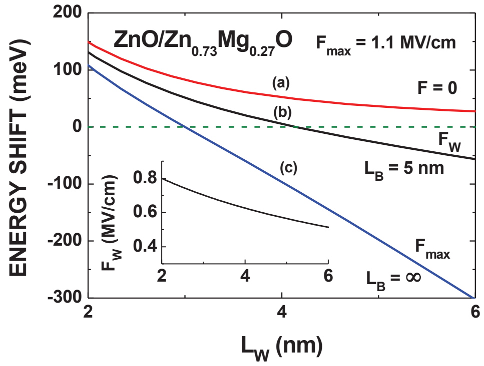

Figure 2.8: Calculated energy shift of the excitonic transition for (a) no electric field, (b) a width-dependent electric field (shown in insert for constant barrier width) (c) the maximum value of built in electric field.[bre07]

The Quantum Confined Stark Effect is damaging for the performance of optoelectronic devices based on these structures. From the study of the variation of the PL integrated intensity as a function of temperature a comparison between the radiative efficiency of two QW separated by a barrier of 200 nm width has been achieved.[bre14] In a simple model the radiative efficiency (η), which is proportional to PL intensity (I_{PL}), is given by:

$$I_{PL} \approx \eta = \tau_{rad} \big/ \left(\tau_{rad} + \tau_{nonrad} \right) \quad \text{.......} \quad (2.2)$$

where τ_{nonrad} and τ_{rad} are, respectively, the non-radiative and radiative decay times. In a 7.1 nm width QW, the intensity of photoluminescence decreases by two orders of magnitude between 8 K and 50 K. In a 1.6 nm width QW it is necessary to increase the temperature to 300 K to reach the same variation in intensity (Fig. 2.9). Both quantum wells are in the same sample thus the non-radiative phenomena are even in both wells. This observation is simply understandable if we take into account the fact that in the wide well the radiative lifetime is very long in comparison with that of the narrow well.

The profits of the homoepitaxie on the optical properties of these wells have been also demonstrated.[lau11] The intensity is almost constant for a homo-epitaxial sample while it divided by a factor ten (fig. 2.10) for a hetero-epitaxial sample.

Despite the high value of the polarization induced electric field exciton complexes have been observed in multi-quantum wells growth along the c-axis. Biexciton formed by two excitons in interaction or charged exciton (negatively charged trions) have been detected in these systems.

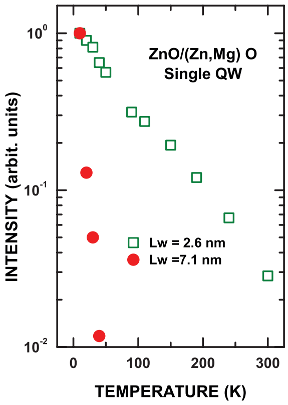

Figure 2.9: Photoluminescence intensity normalysed as function of temperature for two QWs.[bre14]

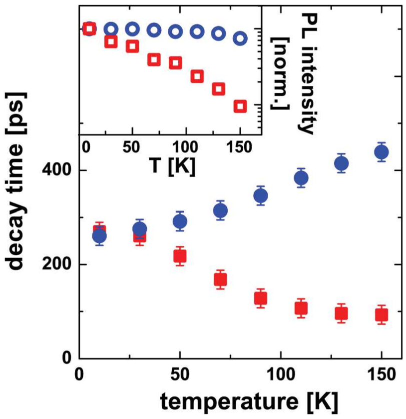

Figure 2.10: Temperature-dependent PL decay times for the homo- (full circles) and heteroepitaxial SQW (full squares) with a well width of 2.0 nm. The corresponding normalized PL intensities are shown in the inset by the open symbols.[lau11]

In ZnO/$Zn_{0.74}Mg_{0.26}O$ multi-quantum wells, grown by PLD on SCAM substrate, luminescence due to the radiative recombination of biexcitons has been observed at low temperature.[sun01] The identification of the biexciton PL line is supported by their relative energy positions and intensity dependence as a function of the excitation power density (Fig 2.11). The binding energy of biexcitons in multi-quantum wells is enhanced by quantum confinement effect and it is a monotonically decreasing function of well width (Fig. 2.12).[chi03] Its value is comparable to the thermal energy of room temperature for the MQWs with Lw smaller than 2.5 nm. The high value of the binding energy is confirmed by the observation of the emission associated to biexciton at the room temperature reported by Davis *et al*[dav06] in narrow MQWs.

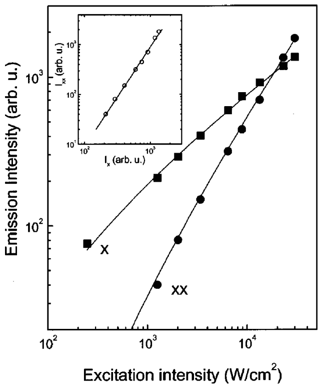

Figure 2.11: Exciton and biexciton spectral weights at a temperature of 5 K asfunctions of excitation power densities for a ZnO/$Zn_{0.74}Mg_{0.26}O$ MQWs sample with well width of 1.75 nm. The inset plots the spectrally integrated intensity I_{XX} as a function of I_X. The solid line denotes the square-power law relation.[sun01]

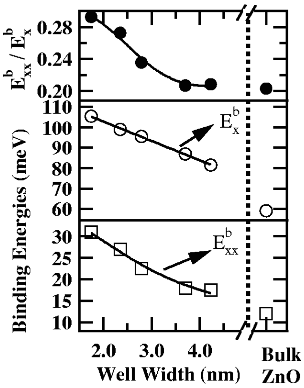

Figure 2.12: Well-width dependence of biexciton binding energy (open squares). Binding energies of free excitons (open circles), and the Exx/Ex ratios (filled circles) as a function of the Lw, are also shown. We plotted the corresponding values of bulk ZnO for comparison at the right part of graph.[chi03]

Magneto-optical studies of ZnO/(Zn, Mg)O multi-quantum wells provide clear evidence of negatively charged excitons (trions, X^-).[pul12] The sample here is grown on c-plane sapphire substrates by radical-source molecular-beam epitaxy. The width of QW is 3.5 nm. However, the distribution of the field in well and barrier layer and the low concentration of magnesium in the barriers (x ≈ 0.09) leads to a very low value of the effective electric field. Biexcitons are also evidenced in these quantum wells (Fig 2.13) by increasing the excitation power density. The PL polarization reflects the occupation of the split-off angular momentum state of the Γ_7 hole (Fig 2.13). Trion transition scheme in magnetic field with optical selection rules is also presented in figure 2.14. In agreement with the widely accepted situation for bulk ZnO a Γ_7 symmetry is founded for the uppermost band in the quantum well.

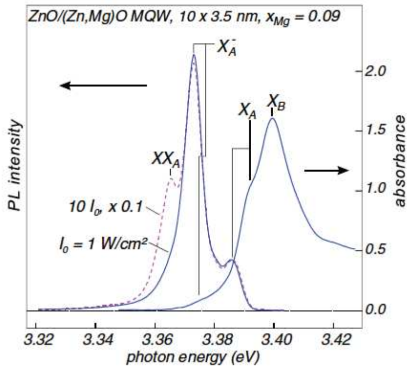

Figure 2.13: Solid blue lines: PL and absorbance derived from the measured transmission T and reflectivity R, where d is the total thickness of all QWs. The indices A and B refer to the incorporated hole(s) from the A and B subvalence band, respectively, in the exciton (X), charged exciton (X-), and biexciton (XX). Dashed (magenta) line: PL spectrum at excitation intensity $10xI_0$.[pul12]

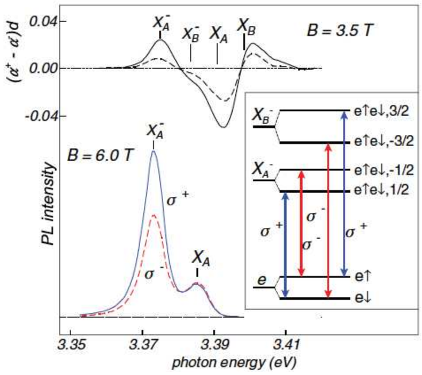

Figure 2.14: Upper black solid and dashed curve: circular absorption difference spectrum at B = 3.5 T and T = 1.5 and 9 K, respectively. Lower solid blue and dashed red curve: circularly polarized PL spectra for σ_+ and σ_-polarization taken at B = 6 T. Inset: Derived trion transition scheme in magnetic field with optical selection rules.[pul12]

2.5 Non polar ZnO/(Zn,Mg)O based quantum wells

In order to prevent the detrimental effect of QCSE, it has been proposed the growth the quantum heterostructures along so-called nonpolar directions. Here, there is no component for spontaneous fields of polarization in growth direction as the polar c-axis is contained in the growth plane. Sapphire substrates were first used in to grow nonpolar ZnO and its related alloys. Indeed it is possible to make grow $a-\left(11\bar{2}0\right)$ ZnO and $m-\left(10\bar{1}0\right)$ ZnO using r-oriented[cha07], [li10], [ko10], [lau10], [chen2015] and m-oriented[cha08], [kim09], [bea11a] sapphire substrates respectively. However, nonpolar growths on sapphire substrates give rise to a large density of defects.[ven08] A drastic improvement of the optical and structural properties has been obtained when using bulk ZnO substrates.[zip10], [cha10] In this paragraph, we focus only on the optical properties of homoepitaxial ZnO/(Zn, Mg)O single quantum wells (QW) grown on A-plane and M-plane ZnO substrate.

The transition energies are plotted in figure 2.14 as a function of the thickness of the QW grown on A-plane[cha10] and M-plane oriented ZnO.[bea11a] Here, the most important feature is that the exciton transition energy is above the value of that of the bulk material, independent of the well width. This results indicate that there is no QCSE in these structures.

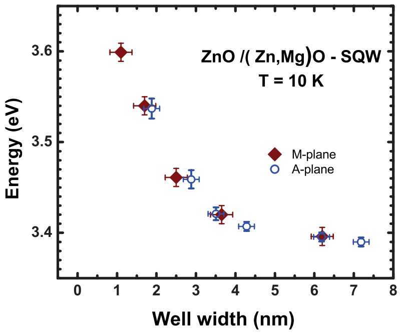

Figure 2.15: Exciton energy in a serie of QW growth on A plane[cha10] (open symbols) and M plane[bea11a] (closed symbols).

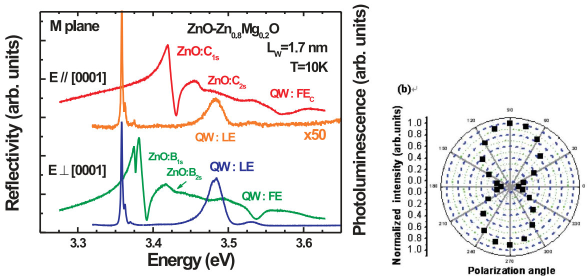

Figure 2.16: (a) Low temperature polarized (red and green plots) reflectance spectra of single quantum well grown on an M-plane oriented ZnO substrate showing the excitonic selection rules.[bea11a] (b) Normalized PL intensities for a-plane ZnO/ZnMgO MQWs as a function of the polarizer angles at low temperature.[ko10]

As predicted by group theory, the CW-PL and reflectance spectra[ko10], [bea11a] of non-polar QW reveal strong in-plane optical anisotropies. In reflectance, confined states analogous to A and B bulk excitons are detected in experiments performed using light polarized perperdicular to the c-axis. The spectral signature of confined excitons built from spin-orbit split-off band in the valence band, analogous to C-exciton in bulk ZnO, is detected in orthogonal polarization is detected.

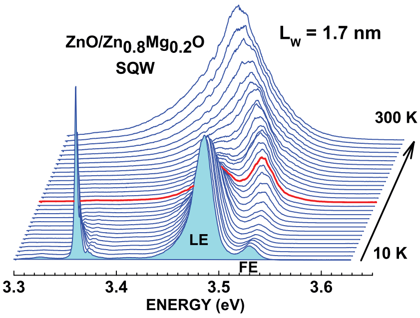

Figure 2.17: Evolution of the PL lines corresponding to confined free and localized excitons in case of a single quantum well grown on an M plane oriented ZnO substrate.[bea11a]

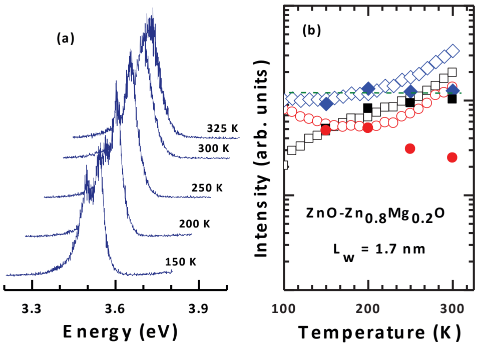

Figure 2.18: (a) Evolution of the ITRPL. (b) Evolution of the intensities in CW-PL (ITRPL) measurement of free, open (full) square and localized open (full) circle exciton bands together with the total photoluminescence intensity open (full) diamond with temperature.[bea11a]

As it has pointed out before, the optical properties of the QW are improved by the used of ZnO substrate. An illustration in given in figure 2.17 that shows a series of CW-PL spectra of non polar ZnO QW measured at different temperatures.[bea11a] It is interesting to note the intensities reversal between the two peaks associated with free and localized excitons, which indicates an efficient de-trapping of the bound exciton. The intensity of the two peaks is extracted from a deconvolution procedure of the photoluminescence band. It is remarkable that the total intensity (Fig. 2.18) does not collapse with increasing temperature. This result is a clear indication that non-radiative processes in this sample are not efficient even beyond room temperature, which is extremely promising for optoelectronic devices.

This property is confirmed by measurement by time resolved photoluminescence (TRPL) of the lifetime of free and localized excitons. Both decay times show identical behavior with temperature (Fig. 2.19). They increase linearly from ~750 ps to ~2.4 ns when the temperature increases from 100 K to room temperature. This linear increase, with a slope of about 7 ± 1 ps/K,[bea11a] of the decay time is typical of free excitons in 2D-system.

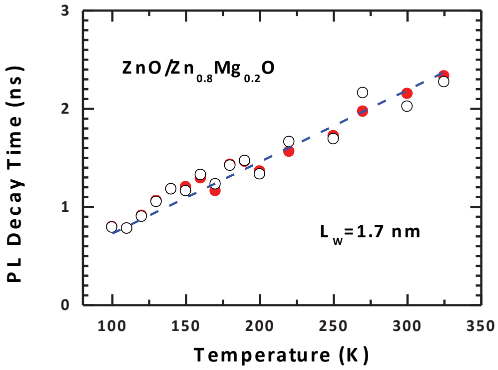

Figure 2.19: Evolution of the PL decay times of the localized (full symbol) and free excitons (open symbol) versus temperature.[bea11a]

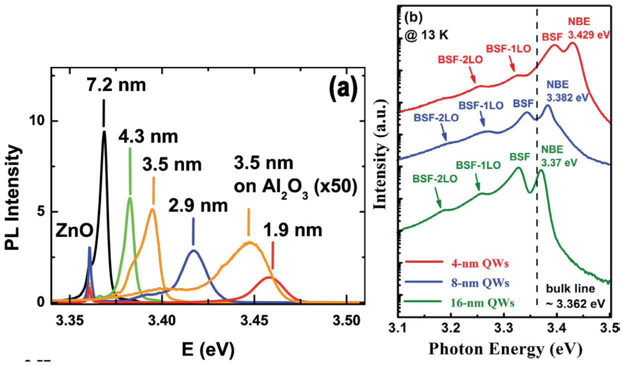

Figure 2.20: Photoluminescence spectra of (a) homoepitaxial A-plane QW[cha10] (b) heteroepitaxial M-plane QW.[che16]

The most remarkable feature in the published results of non-polar QW is the presence of two peaks in the optical response of the quantum well (Fig. 2.17, Fig. 2.20). Different interpretations of the two lines are given. In M-plane the low energy line is attributed to exciton recombination in localized states[bea11a] or excitons bound to plane stacking faults (BSFs).[che16] In A-plane QW, the dominant PL peak is attributed to exciton localization due to the interface fluctuations such as well-width variations, local strain modulations or Mg inhomogeneities.[cha10] On the basis of our results on non-polar quantum wells we shall discuss again these interpretations in the chapter three.

2.6 Conclusions

In this chapter, the optical properties of ZnO based QWs were presented. For single quantum wells grown along the (0001) axis, the drastic effect of QCSE on recombination energy the exciton and oscillator strength as well as radiative efficiency has been illustrated through the discussion of CW-PL and TRPL experimental results published by several authors. The detrimental effect of QCSE could be avoided by using QWs grown on non-polar planes (A-plane or M-plane). Here, reflectance, CW-PL and TRPL properties of single quantum wells grown on non-polar substrates reveal strong in-plane optical anisotropies. In non-polar M-plane QW, the temperature dependence of the intensity of the photoluminescence indicates a very moderate contribution from non-radiative recombination channels in. Above 100 K, the radiative decay times of the excitons show linear increase as a function of temperature characteristic of 2D-system. Such high-quality QWs open up possibilities for UV optoelectronic devices. However, an important obstacle still remains: the attainment of p-type conductivity in ZnO.

Other directions[gru16] more exotic are possible for the growth of the wells of ZnO; they are semi-polar plane as the plane R.[cha13] However very few results were published on semipolar QW.

Chapter 3

Optical properties of the (Zn, Mg)O barriers

3.1 Introduction

In order to avoid the disastrous effects of the internal electric field in the ZnO/(Zn, Mg)O heterostructure it is possible to grow them along the non-polar directions, *i.e.*, with the polar c-direction of ZnO lying in the growth plane. ZnO/(Zn, Mg)O based QWs without QCSE have been successfully grown on the A-plane (11-20) or the M-plane (10-10). Before exposing the results of our investigation of the optical properties of the quantum well on an A-plane, we dedicate this chapter to the presentation of the optical properties of the ZnO substrate and the (Zn, Mg)O barriers.

Figure 3.1 presents two spectra of the sample taken at low density of excitation in two different conditions for the energy of the excitation photon. With high-energy photons (4.3 eV) the barriers and the quantum well are excited. Whereas with low energy photons (3.8 eV) the quantum well and the substrate are excited. The energy range presented on the figure can be divided in three zones. The low energy part (3.34-3.37 eV) corresponds to the substrate response. The high-energy part (3.65-3.9 eV) corresponds to the signal arising from the barriers. Between these two signal we find the response of the quantum well.

In the second paragraph we gathered the results obtained on the luminescence of the substrate in the various experiences made to characterize the quantum well. In the third part, we examine the optical properties of (Zn, Mg)O barriers by using CW and time resolved photoluminescence spectroscopies.

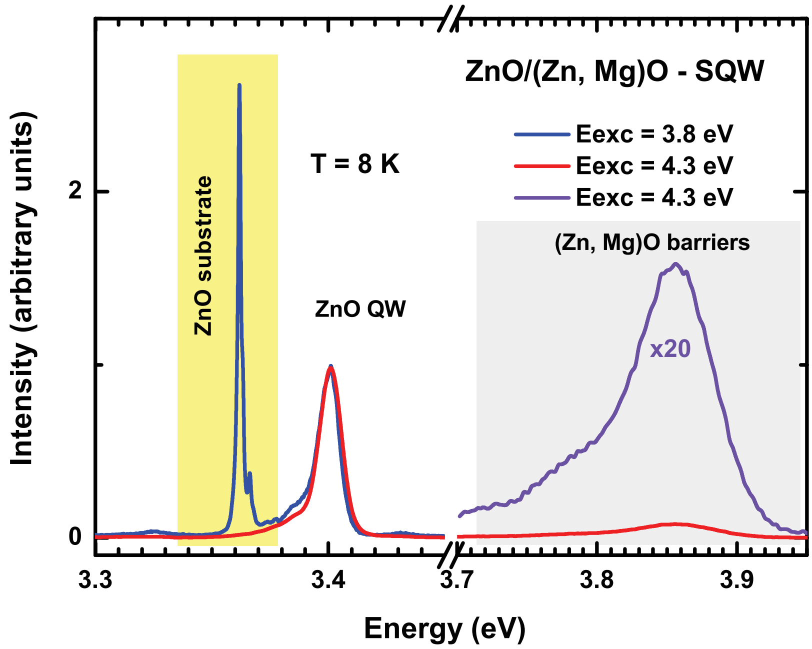

Figure 3.1: PL spectra measured at low temperature in two excitation conditions, with 4.3 eV photons (red and purple) and 3.8 eV photons (blue). The spectra are normalized to the QW PL line.

3.2 Optical properties of the ZnO substrate

In the case of excitation with photons at energy below the bandgap of the barriers (Figure 3.2) the PL spectra present three lines at 3.360, 3.362, and 3.365 eV below. These lines of photoluminescence present a maximum to energies lower than those attributed to the recombination of the free exciton in ZnO (3.376 eV). In agreement with Meyer *et al*[mey04] we attribute these peaks of photoluminescence to the recombination of excitons bound to the donors in the substrate, which is n-type material.

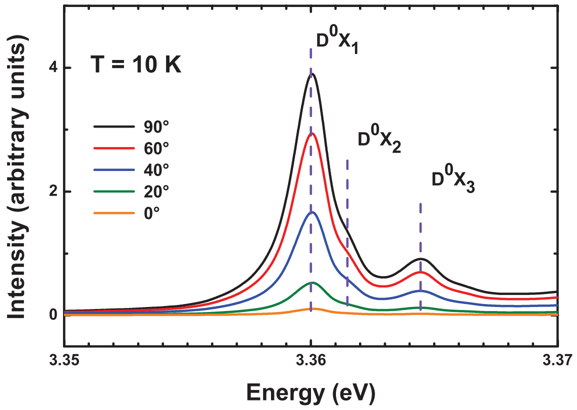

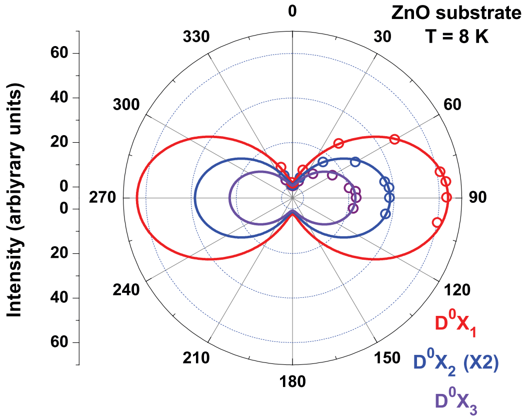

Figure 3.2: PL spectrum measured at 10 K as a function of the angle between the c-axis of the structure, chosen as zero, and the electric field of the outgoing light.

Figure 3.3: Representation in polar coordinates of the intensity of photoluminescence measured at 10 K according to the angle of polarization of the electric field of the emitted light. The c-axis of the structure is chosen as zero.

We present (Fig. 3.2 and Fig. 3.3) the experimental measures of the anisotropy of the optical response of the substrate. To determine the rate of anisotropy, we analyze the photoluminescence spectra collected in the perpendicular direction to the growth plane. We polarize linearly and in a selective way the electric field of the emission of photoluminescence by means of a polarizer consisted by two birefringent crystals. The regulation of crystals is made according to an angle associated with the orientation of the electric field of the light (perpendicular to the axis of propagation). This orientation is called direction of linear polarization. A first conclusion is that the whole spectrum associated to the substrate presents the same anisotropy. The degree of polarization (DOP) of the signal is calculated from the data using the following formula:

$$\mathrm{DOP} = \frac{I_{90} - I_0}{I_{90} + I_0} \quad \text{.......... (3.1)}$$

The degree of polarization for three peaks is of the order of 95 %. These results correspond to the value waited for a non-polar material for which the c axis of the structure wurtzite is contained in the plan of growth.

Intensity of the photoluminescence. The emission of photons is due to the radiative recombination of carriers, its rate is inversely proportional to τ_R, the radiative lifetime. Besides the radiative processes, non-radiative processes can involve the carriers such as phonons emission or Auger process. These processes affect the carrier lifetime by a contribution, which is inversely proportional to τ_{NR}, the non-radiative lifetime. Then, under optical injection condition the evolution of the exciton population is given by:

$$\frac{dn}{dt} = G - \frac{n}{\tau_R} - \frac{n}{\tau_{NR}} \quad \text{.......... (3.2)}$$

Where n is the density of exciton concerned, G is the generation rate. The non-radiative recombination rates are mostly thermally activated whether they correspond to the activation of a non-radiative recombination center or to level depopulation. It may be written in the following form:

$$\tau_{NR}(T) = \tau_{NR0}\ \exp\left(E_A/kT\right). \quad \text{.......... (3.3)}$$

Where τ_{NR0} is a constant and E_A the activation energy of the non-radiative process. Under steady state condition, such as in CW-PL measurement, we get:

$$\frac{dn}{dt} = 0 = G - n\left(\frac{1}{\tau_R} + \frac{1}{\tau_{NR}}\right) = G - n\ \left(\Gamma_R + \Gamma_{NR}\right) \Rightarrow n = \frac{G}{\Gamma_R + \Gamma_{NR}} \quad \text{.......... (3.4)}$$

where Γ_R and Γ_{NR} are respectively the radiative and non-radiative rate. Moreover the PL intensities are proportional to $n/\tau_R = n\ \Gamma_R$, one obtains the following expression for PL intensity:[ler99a]

$$I(T) = \frac{G\,\Gamma_R}{\Gamma_R + \Gamma_{NR}} = \frac{G}{1 + \Gamma_{NR}/\Gamma_R} = \frac{I_0}{1 + A\,\exp\left(-\frac{E_A}{kT}\right)} \quad (3.5)$$

where $A = \tau_R/\tau_{NR0}$. The temperature dependence of exciton radiative lifetime is determined by thermally induced exciton redistribution in momentum space and depends on dimensionality of the investigated structure,[fel87], [and91], [cit92a], [cit92b] it can be written:

$$\tau_R = \tau_{R0}\,T^{n/2} \quad (3.6)$$

where n is an integer between 0 and 3, corresponding to the degree of freedom of the excitons. The constant τ_{R0} is depending of the studied material.

Let us consider now the decrease in intensity of the D^0X_1 and D^0X_2 lines (Fig. 3.4-a), it is due non-radiative process. The dashed lines are least-square fits to their variations using expression 3.5. Here, A is independent of T because we deal with localized excitons on the donors (n=0). Activation energy of 9.5 meV and 8.5 meV are found for respectively D^0X_1 and D^0X_2. This low activation energy quenching is due to the thermal detrapping of the bound excitons towards the free A exciton band in ZnO substrate.

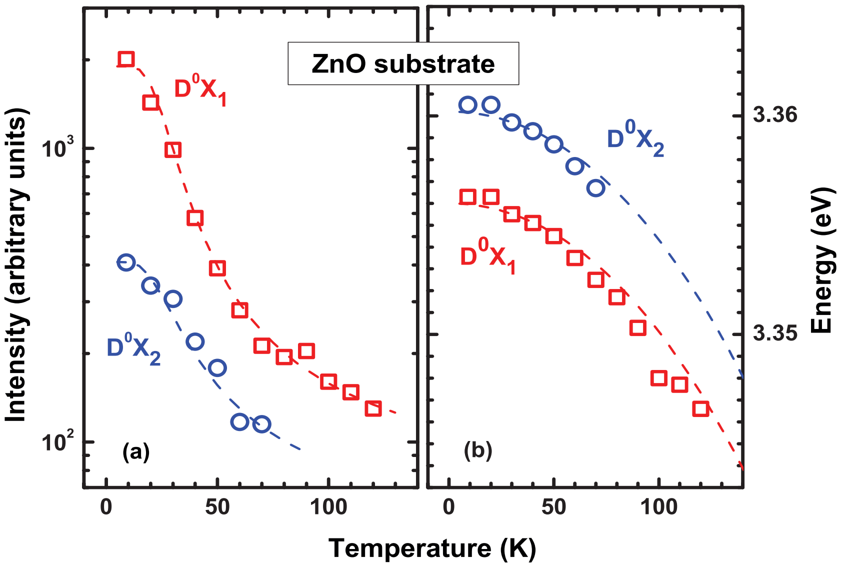

Figure 3.4: (a) Intensity of the PL lines D^0X_1 and D^0X_2 according to temperature the dashed lines correspond to formula 3.3. (b) Energies of the D^0X_1 and D^0X_2 PL lines. The dashed lines correspond to the model of Varshni (3.4).

Energy of emission of the photoluminescence. The model of Varshni[var67] is a good approximation to model the low-temperature dependence (T <300 K) of the energy of an electronic band-to-band transition. The expression is the following:

$$E_g = E_0 - \alpha\,T^2/(T+\beta) \quad (3.7)$$

where E_0 is the energy of the bandgap at 0 K. This phenomenological formula takes into account two main physical effects responsible for the variation of the gap of a semiconductor with the temperature, i.e. the temperature dependence of both the dilation of the lattice and the electron lattice interactions.

To reproduce the variation of the transitions energy with the temperature we use the low-temperature value as parameter E_0 in the formula of Varshni. A good agreement with the experimental values is obtained (Fig. 3.4-b) using the parameters $\alpha = 4.7\ 10^{-4}\ (\mathrm{eV/K})$ and $\beta = 900\ (\mathrm{K})$ these values are close to the ones proposed by Meyer *et al.* [mey04]

3.3 Optical properties of the (Zn, Mg)O barriers

3.3.1 Introduction

Several studies have been done on the incorporation of magnesium in ZnO.[oht98b], [mak01], [oga03], [sch03], [hei07], [was09], [neu11], [lau13], [kam16] The main result is an increase of the bandgap of the alloy with the magnesium incorporation. However, the growth of this alloy with an important concentration of magnesium is difficult because the stable structure of the binary MgO is the cubic structure.[oht98b], [mak01] It has been reported on the growth of films with a good crystalline quality with magnesium concentration up to 36 %.[oht98b], [kam16] Moreover, due to the difference in the lattice parameters the layers are strained when their thickness is less than 600 nm.[kam16] The observed dependencies of the photoluminescence energies, measured at low temperature, with magnesium content follow a linear behavior. The slope of the line is 18 meV by percent of magnesium.[hei07]

Localization of excitons in the alloys. Studies on the solid solutions of semiconductors evidenced the phenomenon of localization of the excitons at low-temperature.[kim00], [che10] In the case of an alloy the exciton is sensitive to local variation of potential resulting on the local concentration and/or arrangement of the substituting elements. This effect is larger in ZnO alloys than in III-V semiconductors due to the small radius of the exciton (1.8 nm in ZnO), they are therefore more sensitive to local inhomogeneity. As a consequence, the Stockes shift between luminescence and absorption edge increases with x in $Zn_{1-x}Mg_xO$ alloys.[oht98b], [was09] This is translated by a behavior in S shape of the position of the maximum of the peak of photoluminescence when the temperature increases.[was09] This behavior is simply understandable in term of localization of excitons on the fluctuations in potential as illustrated in Fig. 3.5.

At very low temperature ($kT \ll \Delta E$), the excitons are trapped by potential fluctuations (Fig. 3.5-a). These localized excitons do not have enough thermal energy to be mobile. They recombine in the minima of potential occupied. A small increase in the temperature ($kT \approx \Delta E$) drive a migration of the excitons toward the minima of potential (Fig. 3.5-b), which leads to a decrease in the emission energy. A further increase in the temperature (kT>ΔE) allows the excitons to migrate toward others potential minima in the crystal (Fig. 3.5-c). Therefore an increase of the emission energy is observed. Above a certain temperature (kT>>ΔE), the excitons are no longer localized (Fig. 3.5-d). Then the emission energy follows the temperature dependence of the bandgap.

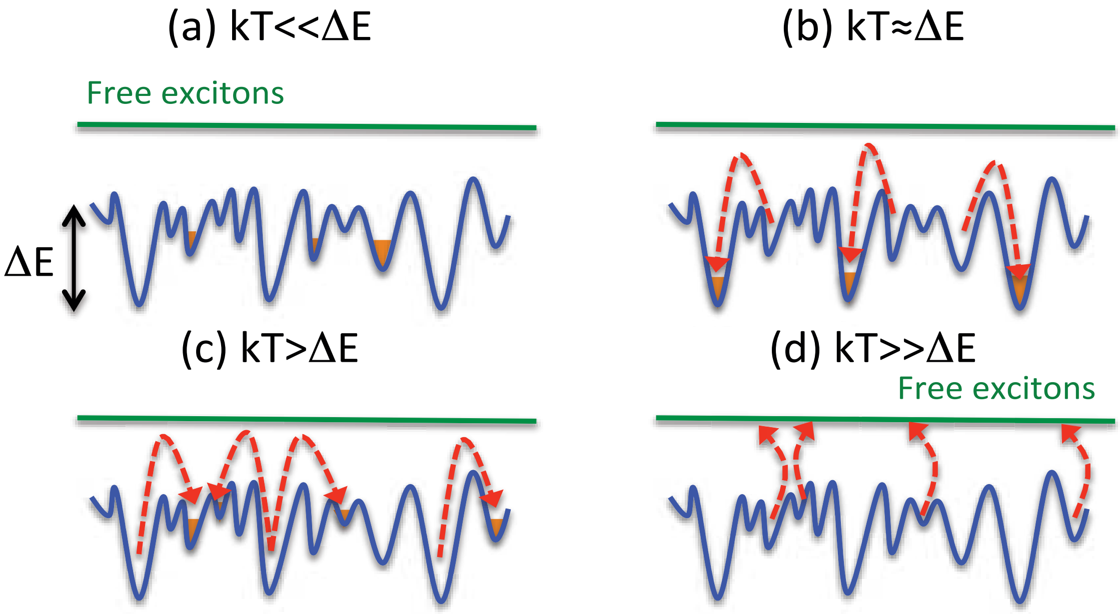

Figure 3.5: Schematic representation of the behavior of the excitons in the fluctuation of the potential resulting from the disorder of the alloy (for the details see text below).

3.3.2 CW photoluminescence investigation

Figure 3.6 presents a photoluminescence spectrum of the barriers measured at low temperature. The luminescence was excited at 4.3 eV using a monochromator. Three Gaussians of the same full width at half maximum (FWHM) are used to fit the signal. The energy of the maximum of the main line give an estimation of the magnesium content, which is about 25 %.[hei07] The two companions lines, separated by 71 meV, are identified as the phonons replicas of the main line. The strength of the phonon replicas confirm that we are dealing with localized excitons.[kon08] The large value of the FWHM (65 meV) compared to the one of the PL line in ZnO (3-4 meV) is attributed to the alloy disorder.[sch03]

Polarization of the signal. The variation of the intensity of the PL line as a function of the outgoing light electric field orientation is summarized in figure 3.7. The zero of the polar graph corresponds to light electric field oriented parallel to the [0001] axis. The maximum intensity is obtained when the light electric field is perpendicular to the c-axis. The DOP is 88 %, this value is much smaller than the one determined from the luminescence of the substrate. The difference could be explained taking in consideration the strain[kam16] in the barrier, which mixes the different states of the valence band.[gil00]

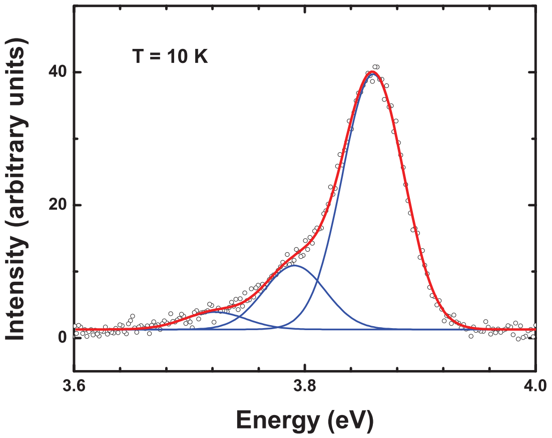

Figure 3.6: PL spectrum of the (Zn, Mg)O barriers measured at 10 K. Lines blue correspond to the deconvolution of the signal in Gaussian, the red one is the sum of three contributions.

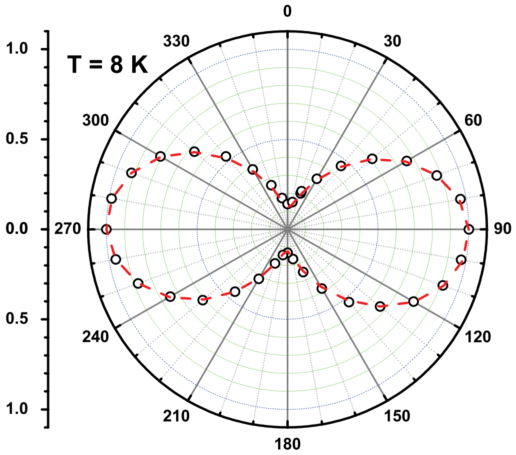

Figure 3.7: Representation in polar coordinates of the intensity of photoluminescence measured at 10 K according to the angle of polarization of the electric field of the emitted light. The c-axis of the structure is chosen as zero.

Temperature investigation. The figure 3.8 gathers the normalized spectra measured in various temperatures. The position of the maximum of luminescence begins by moving towards the high energies when the temperature increases. Beyond 70 K its energy decreases with the temperature. This behavior is waited for the localized excitons as it has been discussed before. The figure 3.9 groups the variations of the parameters used in order to replicate the behavior with temperature of main line of photoluminescence of the barrier.

When the temperature increases the energy of the transition (Fig. 3.9-a) first increases before decreasing for temperatures superior to 70 K. The dotted line corresponds to the formula of Varshni. This expression reproduces correctly the high-temperature behavior. The values of the parameters are: $E_0 = 3.871\ \text{eV}$, $\alpha = 9.14\ 10^{-4}\ (\text{eV}/\text{K})$ and $\beta = 560\ (\text{K})$. A difference of 11 meV is obtained in 10 K between the measure and the curve of Varshni. In a first explanation this difference can be interpreted as an effect of localization of the excitons

Thermal broadening of the photoluminescence line is generally interpreted as a consequence of the exciton–phonon interaction. The temperature dependence of the full width at half maximum (FWHM) presented in figure 3.8-b can be approximately described by the following equation:[hel93], [one93], [gru09]

$$\text{FWHM}(\text{T}) = \Gamma_{\text{inh}} + \gamma_{\text{ph}}\ \text{T} + \frac{\Gamma_{\text{LO}}}{\exp\left(\hbar\ \omega_{\text{LO}}/k_{\text{B}}\ \text{T}\right) - 1} \quad \text{..} \ (3.8)$$

where Γ_{inh} and Γ_{LO} are the inhomogeneous line-width at zero temperature and the strength of the exciton-LO-phonon coupling, respectively. $\hbar\ \omega_{\text{LO}}$ is the LO-phonon energy we take its value to be 71 meV. γ_{ph} is the coupling strength of the exciton-acoustic phonon. The dashed line represents the fitted result based on equation 3.8. The best fit is obtained for the parameter values: $\Gamma_{inh} = 64.7$ meV, $\Gamma_{LO} = 7.16$ eV and $\gamma_{ph} = 27.5\ \mu eV$.

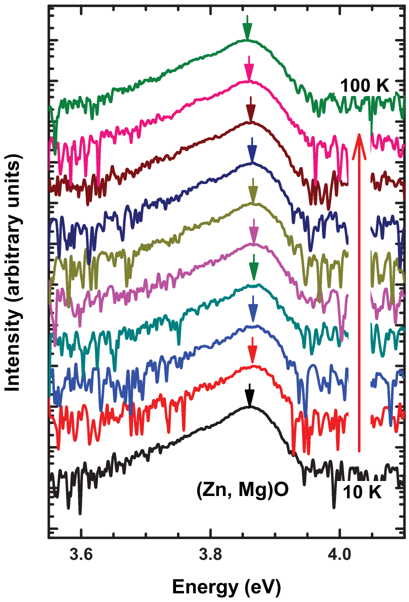

Figure 3.8: Normalized photoluminescence spectra of the (Zn, Mg)O barrier recorded at temperatures range from 10 to 100 K.

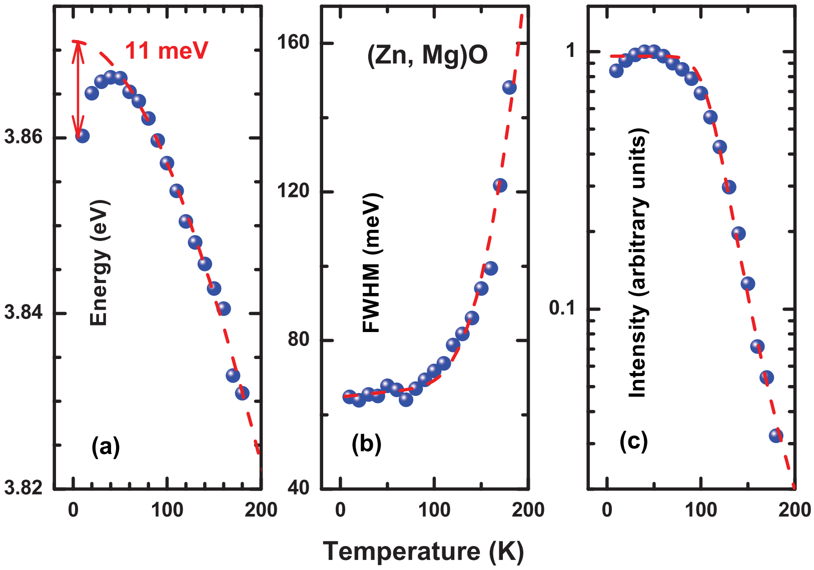

Figure 3.9: Energy of the transition, full width at half maximum (FWHM) and intensity of the line according to temperature.

The intensity of the photoluminescence stays nearly constant until 70 K (Fig. 3.8-c). For temperatures above this value it decreases rapidly. The decrease of the intensity is associated to the disappearance of the excitons, which can be due to its dissociation or its diffusion toward non-radiative centers. The parameters of the equation 3.3 are deducted from the variation of the intensity with the temperature. Here, A is dependent of the temperature because we deal with free excitons in bulk material ($A = A_0\ T^{3/2}$). The dashed lines is calculated for A_0=1.136 and an activation energy E_A of 72 meV.

3.3.3 Time-resolved photoluminescence

The time-resolved photoluminescence spectroscopy is also help to understand better the behavior of the excitons in material. In this paragraph, we present the results of this study and propose a model to account the observed properties. For it, we shall keep in mind on the results obtained by photoluminescence in continuous wave excitation. In particular on the fact that those results demonstrate that at low temperature regime we have to deal with localized excitons. At the contrary at high temperature regime we deal with free excitons in 3D system.

For the time-resolved photoluminescence experiment, the excitation was provided by a mode-locked frequency tripled titanium-sapphire laser, with a 2 ps pulse width and a wavelength of 266 nm. Due to the slow photoluminescence decays, we have adapted a laser repetition rate of 800 kHz by using an acousto-optic modulator. The photoluminescence signal was dispersed by an imaging spectrometer and then temporally resolved by a streak camera.

3.3.3.1 Experimental results

The TRPL experiments can give different information. If we integrate temporarily the signal on all the time-window (ITRPL) one can get similar information as CW photoluminescence experiment. The spectral integration of the signal on the window (TRPL) gives information about the time-dependence of the decline of the intensity. From the spectra one get the PL time decay, which give information about the different process involved in the recombination of the excitons.

Integrated time-resolved photoluminescence (ITRPL). ITRPL spectra are presented in Fig. 3.10-a. These spectra and the CW-PL spectra present a similar dependence on temperature. The energy of the line moves toward higher energy when the temperature increases. The intensity stays nearly constant until 90 K, then decreases monotonously with temperature (Fig. 3.10-b). The independence of the intensity with temperature at low temperature regime (T<90K) is a clear indication that the excitons recombinations are dominated by radiative process. On the other hand, at high temperature regime (T>150K) most of the carriers recombine through non-radiative channels. In the following, we will consider these two temperature domains, then we will merge them in a model.

The energy of the transition shows the same behavior at low temperature as the one we have discussed in the previous paragraph. However for the temperatures in the range 200-300 K a new S-shape appears. This behavior is attributed to the delocalization of the excitons with temperature.

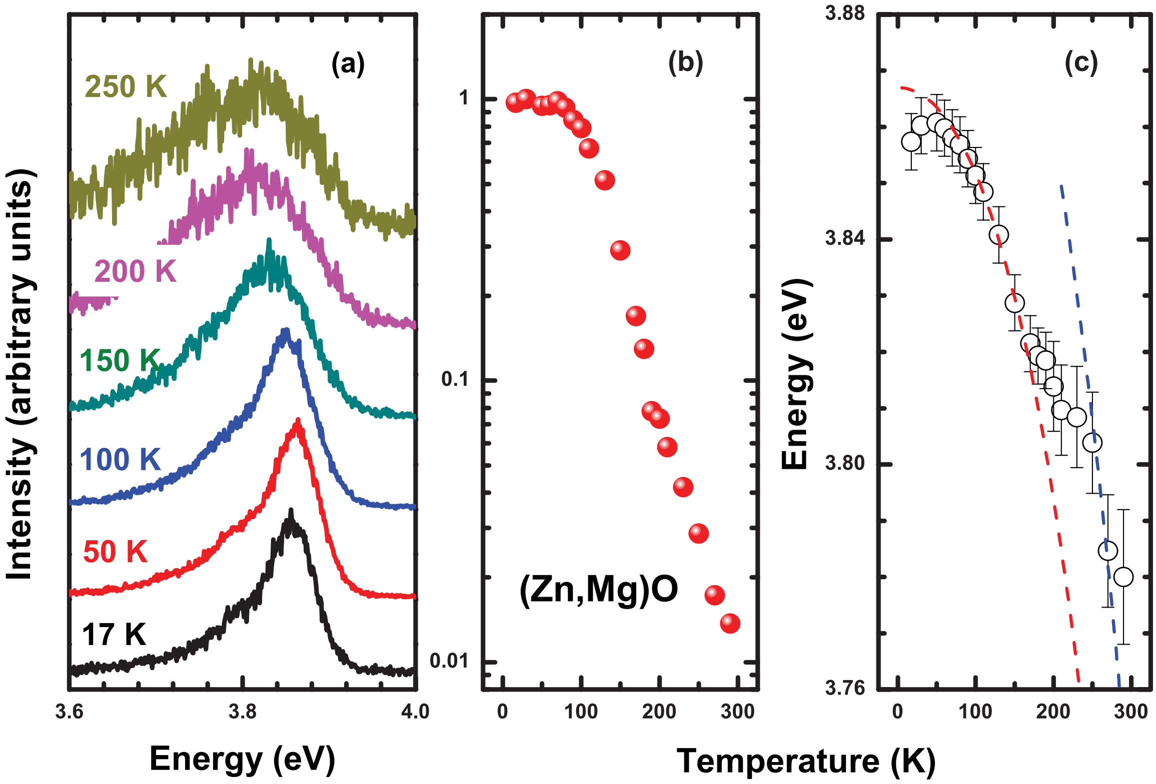

Figure 3.10: (a) Normalized integrated time-resolved photoluminescence spectra of the (Zn, Mg)O barrier recorded at different temperatures. **(b)** Dependence of the intensity of the integrated time-resolved photoluminescence spectra of the (Zn, Mg)O barrier with the temperature. (c) Energy of the transition according to temperature.

From these results we can propose the following scenario. At very low temperature the excitons are localized. When the temperature increases, they can occupy a second localized state separated by 11 meV from the fundamental state. The energy of the transition increases, after which the energy decreases and follow the classical behavior of the bandgap until 200 K. For higher temperature the excitons start to delocalize. At room temperature the majority of the excitons are free excitons. The energy of localization can be estimated from these data to be 60 meV.

PL decays. The photoluminescence decays are non-exponential until 90 K (Fig. 3.11). They become mono exponential at higher temperatures. The low-temperature decays shows two regimes: at the short time the decline is fast; on the other hand it is much slower at the long time. The slow regime accelerates when the temperature increases. For temperature above 90 K both decays seem to decrease with the same time constant. Non-exponential photoluminescence decays at low temperature have been previously reported in alloys such as (Al, Ga)N[kim00], [onu04] or (Zn, Mg)O.[che10] The non-exponential behavior is attributed to the fact that in this case we are in the presence of a mixed population of localized and free excitons.

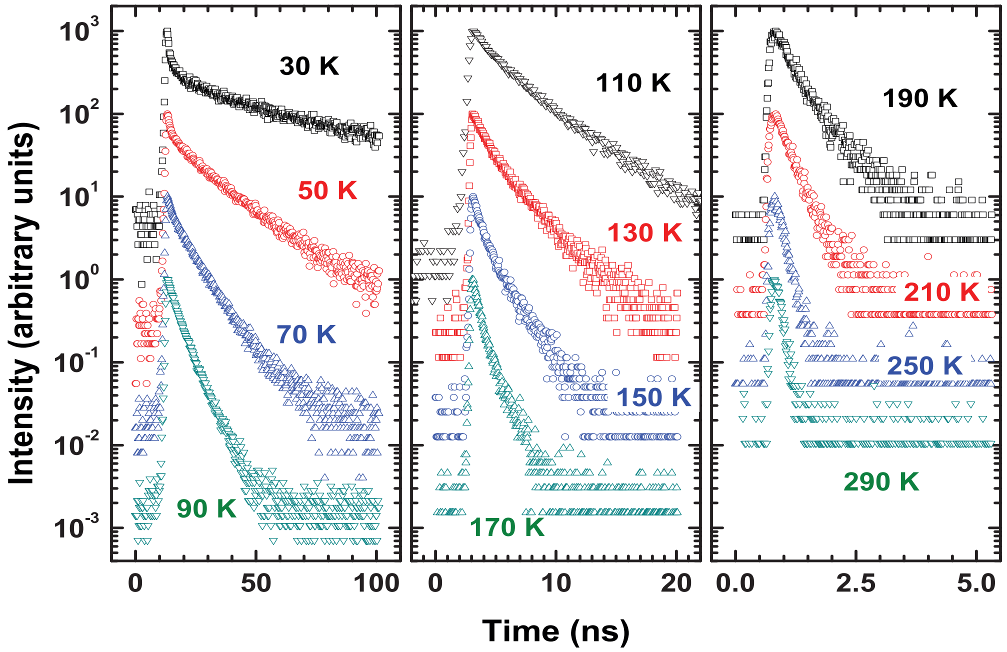

Figure 3.11: Normalized photoluminescence decays measured at different temperatures. Note that, the time scale goes from 100 ns to 5 ns from left to right.

The PL decay curve, for temperature below 90 K, can be well fitted using a biexponential line shape:

$$I(t) = y_0 + I_a \exp(-t/\tau_a) + I_b \exp(-t/\tau_b) \qquad (3.9)$$

where I(t) is the PL intensity at time t, y_0 the background, I_i and τ_i represent the initial intensity and the decay constant of the ith component. An example of the decomposition of the decay of photoluminescence in two components is presented on the Fig 3.12. Monoexponential line shape is used for the others. The results are shown in Fig. 3.13. The shorter decay time constant (τ_a) is nearly constant in a range of temperature from 18-90 K. The second decay time constant (τ_b) is substantially longer than the first decay time constant in the same range of temperature. After 90 K, only one decay time constant is required to fit the PL decay. Subsequently the time constants decline with the temperature.

The localized excitons are known to present a long lifetime independent of the temperature in the range of 0.5 to 5 nanoseconds.[cor11], [ros14] This correspond to the dependency according to the temperature and value of the τ_a lifetime, so it is attributed to recombination of localized exciton. The τ_b lifetime shows a decrease in temperature. Moreover, the value at low temperature is large as compared to the value reported in the literature. At 17 K, its value is about 130 ns. Of such important values are observed very often in a system with an internal electric field, which separate the electron and hole wave-function.[mor05b] Similar observations are reported for the indirect excitons[zhu17] or dark excitons.[smo15] In the first case, the carriers have different space localization. The long lifetime of dark exciton are related to "forbidden" transitions. This second lifetime is also attributed to the recombination of localized excitons.

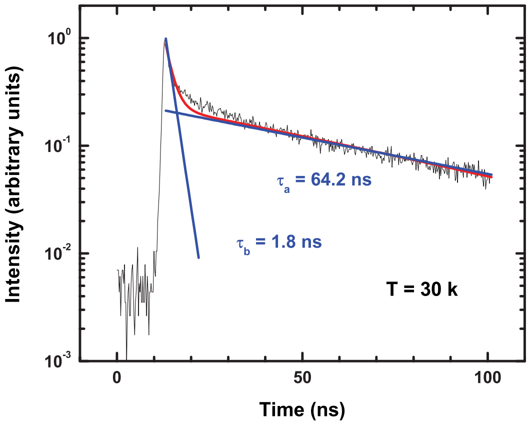

Figure 3.12: Example of the decomposition of the decay of photoluminescence in two exponential decays.

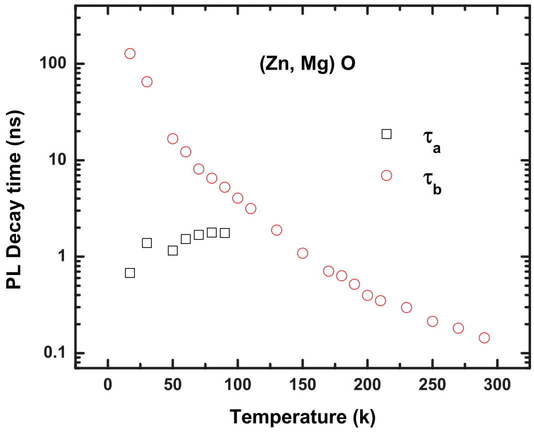

Figure 3.13: PL decay time according to the temperature. For temperature below 90 K, two decay times constant are required to fit the PL decay.

3.3.3.2 Low temperature domain (T<90 K)

The experimental data show that: the recombination processes are radiative, and the energy of the PL peak shift toward higher energy with temperature. The PL decays are biexponential, then we will have to consider the localized state is a system with two levels. The transition energy dependence with temperature indicated that the two levels are separated by 11 meV. The proposed model for the recombination of the localized excitons at low temperature is schematized in figure 3.14.

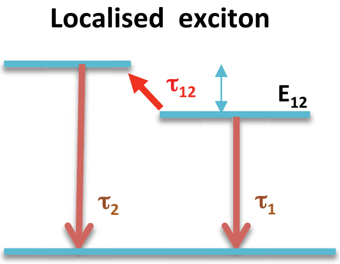

Figure 3.14: Schematic representation of the different recombination phenomena taking into account for localized excitons at low temperature.

The evolution of the population of each level after the excitation pulse are governed by the following system of coupled equations:

$$\begin{cases} \dfrac{dn_1}{dt} = -\dfrac{n_1}{\tau_1} - \dfrac{n_1}{\tau_{12}} \\ \dfrac{dn_2}{dt} = -\dfrac{n_2}{\tau_2} + \dfrac{n_1}{\tau_{12}} \end{cases} \qquad (3.10)$$

where $n_{1,2}$ and $\tau_{1,2}$ are respectively the density and radiative lifetime of exciton on level 1 and 2. τ_{12} is the transfer time between the two levels. The latter parameter is thermally activated and can be written in the following form:

$$\tau_{12} = \tau_{120} \exp\left(\frac{E_{12}}{k_B\ T}\right) \qquad (3.11)$$

τ_{120} is a constant and E_{12} is the energy separation of the two levels. From the equations (3.10) we get temporal evolution of the populations as:

$$\begin{aligned} n_1(t) &= A_1 \exp\left(-t/\tau_{eff}\right) \\ n_2(t) &= A_2 \exp\left(-t/\tau_{eff}\right) + A_3 \exp\left(-t/\tau_2\right) \end{aligned} \qquad (3.12)$$

where τ_{eff} is given by:

$$\frac{1}{\tau_{eff}} = \frac{1}{\tau_1} + \frac{1}{\tau_{12}} \Rightarrow \tau_{eff} = \frac{\tau_1}{1 + \tau_1/\tau_{12}} = \frac{\tau_1}{1 + \frac{\tau_1}{\tau_{120}} \exp\left(\frac{-E_{12}}{k_B\ T}\right)} \qquad (3.13)$$

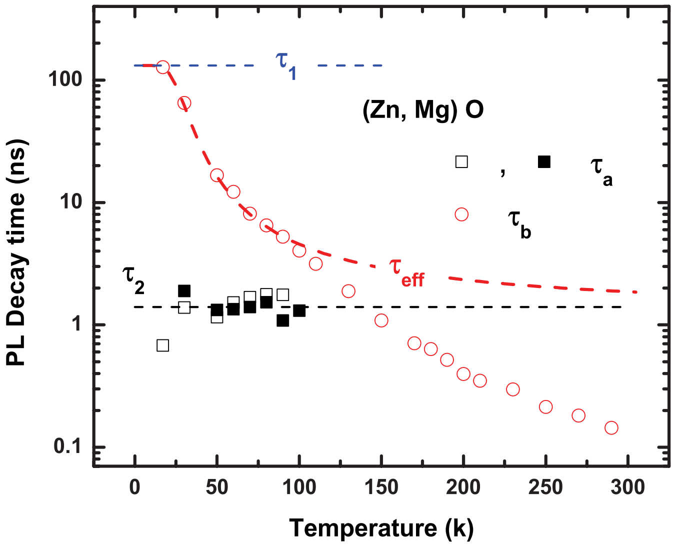

Figure 3.15: Decay times according to the temperature deduced from free fitting (open symbols) and constraint fitting (closed symbols). The red dash line corresponds to the calculated values of τ_{eff} (equation 3.13). The blue and black dash lines indicate the value of respectively τ_1 and τ_2.

These hypothesis allow us to explain the experimental observations: biexponential decays and the long-lifetime (τ_b) dependence with temperature. From the PL decay times measured in the range 17-80 K we deduced the parameters of equation 3.13. Figure 3.15 shows the calculated value of τ_{eff} compared with the measured value. The effective lifetimes are calculated using formula 3.13 with 1.2 ns, 131.5 ns and 11.7 meV for respectively τ_{120}, τ_1 and E_{12}. The value of E_{12} is very close to the one deduced from the temperature dependency of the transition energy. Moreover, we can notice that the formula fit the experimental data until 100 K. However for temperature above 100 K the decay lifetimes still decrease, indicating that other phenomena are involve in the photoluminescence decay.

The open symbols (fig. 3.15) are the τ_a values obtained from free fitting of the PL decays. In order to get more valuable determination of τ_a we have also done fitting with a constraint. Here we use the value of τ_{eff} calculated from equation 3.13 for the one of τ_b. The lifetime is nearly independent of the temperature as expected. We can fixe its value at 1.4 ns.

3.3.3.3 High temperature domain (T>150 K)

In this paragraph we compare the experimental results with the "classical" model of competition of radiative and non-radiative recombination. First we present how one can get the different parameters from the data. As it has been mentioned before, the non-radiative recombination process dominates at elevated temperature. Here we consider the measured lifetimes for temperatures above 150 K.

Determination of the radiative and non-radiative lifetimes. The free exciton emission is expected to have a single decay time determined by interplay of radiative and non-radiative recombination processes as, where Γ_R and Γ_{NR} denote the intrinsic radiative and defect-mediated non-radiative rate of the free exciton, respectively. During the pulse the intensity of photoluminescence can be write in the following form:

$$I = \frac{G\ \Gamma_R}{\Gamma_R + \Gamma_{NR}} = G\ \eta \qquad \textit{(3.14)}$$

where η is the radiative efficiency of the recombination and G is the rate of photo-generation of the carriers. After the pulse (G=0) the population of excitons is governed by:

$$\frac{dn}{dt} = -n\ \left(\Gamma_R + \Gamma_{NR}\right) \Rightarrow n = n_0\ \exp\left(-t\left[\Gamma_R + \Gamma_{NR}\right]\right) \qquad \textit{(3.15)}$$

where n_0 is the initial value of n given by the steady state during the impulsion.

$$n_0 = \frac{G}{\Gamma_R + \Gamma_{NR}} \qquad \textit{(3.16)}$$

The photoluminescence decay is given by:

$$I\left(t\right) = \frac{G\ \Gamma_R}{\Gamma_R + \Gamma_{NR}}\ \exp\left(-t\ \left[\Gamma_R + \Gamma_{NR}\right]\right) = G\ \eta\ \exp\left(-t/\tau_{PL}\right) \qquad \textit{(3.17)}$$

At low-temperature the exciton recombination is dominated by the radiative process. As a consequence we can fix the value of the radiative efficiency to be almost one hundred percent. The integrated time-resolved photoluminescence can be then to write as follow:

$$\frac{I(T)}{I(0)}=\eta(T)=\frac{\Gamma_R(T)}{\Gamma_R(T)+\Gamma_{NR}(T)}=\frac{\Gamma_R(T)}{\Gamma_{PL}(T)} \quad \ldots\ldots (3.18)$$

where $\Gamma_{PL}=1/\tau_{PL}$ is the photoluminescence decay rate. Using this set of equations, from the temperature dependency of the normalized intensity we calculate the radiative lifetime and non-radiative lifetime.

$$\Gamma_R(T)=\frac{1}{\tau_R(T)}=\frac{I(T)}{I(0)}\Gamma_{PL}=\frac{I(T)}{I(0)}\frac{1}{\tau_{PL}}\Rightarrow\tau_R(T)=\tau_{PL}\frac{I(0)}{I(T)} \quad \ldots\ldots (3.19)$$

and

$$\tau_{NR}=\left(1/\tau_{PL}-1/\tau_R\right)^{-1} \quad \ldots\ldots (3.20)$$

Free excitons radiative and non-radiative lifetimes. In this temperature domain we will assume that the photoluminescence signal arise from recombination of free excitons. From the equations (3.19) and (3.20) we calculated the radiative and non-radiative lifetimes (Fig. 3.16) for the temperatures above 150 K. Then these values are compared with the formula (3.3) and (3.6) in order to get the parameters of the dependency with temperature (Table 3.1). Here we set n=3 in the formula (3.6). The activation energy found for non-radiative process is comparable to the one deduced from CW-PL data.

Radiative lifetime	*Non radiative lifetime*
τ_{R0} = 1.8 ps	τ_{NR0} = 5.9 ps E_A = 71 meV

Table 3.1: Temperature-dependency parameters for the radiative and non-radiative lifetimes of the free excitons.

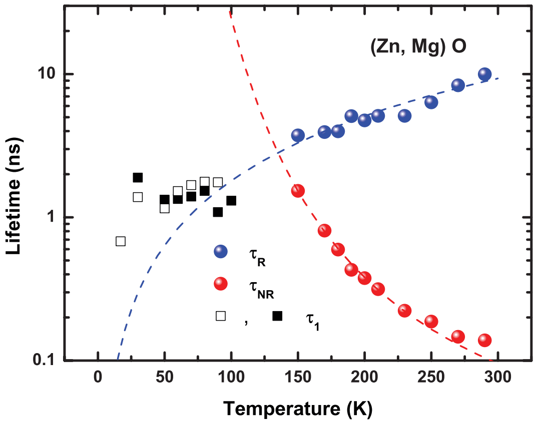

Figure 3.16: Calculated τ_R and τ_{NR} lifetimes with τ_1 measured lifetimes. The dashed lines correspond to the calculated dependence with the temperature of the radiative and non-radiative lifetime.

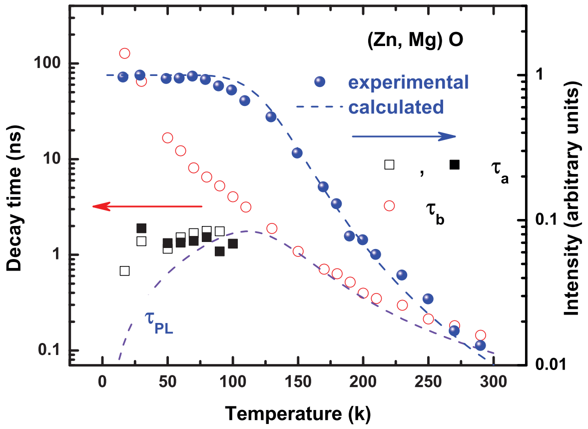

Figure 3.17: Comparison of the experimental data (intensities and lifetimes), with the calculated values (dashed lines).

From formula (3.18) and (3.20), one can calculated the intensity of the photoluminescence as well as the photoluminescence decay time on the whole range of temperature. The experimental results are compared with the experimental values on the figure 3.17. A good agreement is obtained as regards the intensity of photoluminescence. That is not the case for the PL lifetime. However, one can notice here that for temperatures below 125 K the non-radiative process do not have influence on the PL lifetime and intensity.

The discrepancy in PL time decay between the model and the experimental results is not surprising. In the low temperatures domain, the excitons are localized. The model should be completed in order to take into consideration the localization phenomena.

3.3.3.4 PL intensity and lifetime model

For this purpose, we used a model originally proposed in the case of localized excitons in quantum wells potential fluctuations. It has been successfully tested in different systems such as GaN QW.[cor11], [ros14] After presenting the model, we discuss the changes necessity to adapt this one to the case of localization in 3D material. And then we compare the model with the experimental data.

Photoluminescence decay model. The hypotheses of the model are a following one: only the free excitons recombine non-radiatively; the lifetime of localized excitons is independent from the temperature. Fig. 3.18 presents a schematic description of the various phenomena considered.

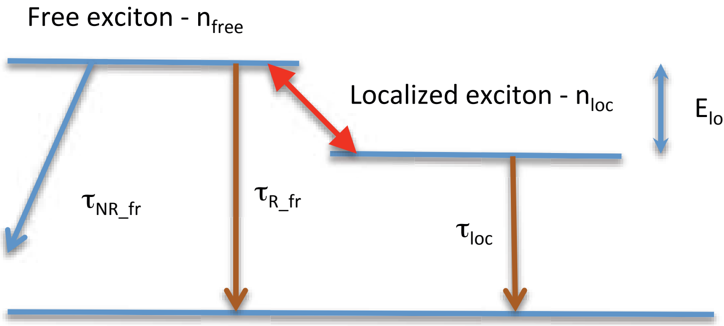

Figure 3.18: Schematic representation of various taken into account recombination phenomenon

The total population of excitons (n_{exc}) is the sum of the density of the free excitons (n_{free}) and of the localized excitons (n_{loc}).

$$n_{exc} = n_{free} + n_{loc} \qquad (3.21)$$

The total recombination rate of the excitons can be written as:

$$\Gamma = \frac{n_{free}}{n_{exc}} \Gamma_{fr} + \frac{n_{loc}}{n_{exc}} \Gamma_{loc} \qquad (3.22)$$

In this equation Γ_{loc} is the radiative recombination rate of localized excitons, which is independent of the temperature. The recombination rate of the free excitons (Γ_{fr}) is given by the sum of radiative (Γ_{R_fr}) and non-radiative (Γ_{NR_fr}) rates. The temperature dependencies of these two rates are deduced from photoluminescence decay time and from the intensity as it as been exposed before. So we get the following expressions for radiative and non-radiative rate of the exciton as function of the densities of localized excitons and free excitons.

$$\Gamma_{rad} = \frac{n_{loc}}{n_{exc}}\,\Gamma_{loc} + \frac{n_{free}}{n_{exc}}\,\Gamma_{R\_fr} = A_{loc}\,\Gamma_{loc} + A_{free}\,\Gamma_{R\_fr} \quad\text{......}(3.23)$$

$$\Gamma_{nrad} = \frac{n_{free}}{n_{exc}}\,\Gamma_{NR\_fr} = A_{free}\,\Gamma_{NR\_fr} \quad\text{......}(3.24)$$

where A_{free} and A_{loc} are the fraction of free and localized excitons. The photoluminescence decay rate is obtained by:

$$\Gamma_{PL} = \left(A_{loc}\,\Gamma_{loc} + A_{free}\,\Gamma_{R\_fr}\right) + A_{free}\,\Gamma_{NR\_fr} = \frac{1}{\tau_{PL}} \quad\text{......}(3.25)$$

Under non-degenerate excitation conditions, the densities of excitons follow Boltzmann distributions:

$$n_{free} \approx \frac{2\,M\,k_B\,T}{\pi\,\hbar^2}\,\exp\left(-\frac{E_{free}(T) - E_F(T)}{k_B\,T}\right) \quad\text{......}(3.26)$$

and

$$n_{loc} \approx N_{loc}\,\exp\left(-\frac{E_{free}(T) - E_{loc} - E_F(T)}{k_B\,T}\right) \quad\text{......}(3.27)$$

where M is the exciton mass ($M = m_e + m_h$), N_{loc} is the areal density of localization centers in the QW, $E_{free}(T)$ is free exciton recombination energy, and E_{loc} is the localization energy determined from energy of the transition temperature dependency. The exciton fractions A_{free} and A_{loc} can thus be expressed as a function of a single unknown parameter N_{loc}.

Development of the model. First, here we deal with a 3D system then the densities of excitons should be adjusted to this situation, i.e. the temperature dependency of the density of state varies with $T^{3/2}$. The localized excitons in the model have a lifetime independent of the temperature. Moreover only one state is considered. Here the localized excitons states have different lifetimes. However, they radiatively recombine in the low temperature domain. At very low temperature, their lifetime is τ_1. When the temperature increases the excitons start to populate the second level and part of them recombine with τ_2 lifetime. As we have demonstrated, the effectif time decay of the photoluminescence varies with temperature. At very low temperature, τ_{eff} is close to

τ_1. When the temperature increases, τ_{eff} decreases and become closer and closer to τ_2. τ_{eff} is then representative of the population repartition of localized excitons on the two levels. In the calculation we used $\tau_{eff}(T)$ as radiative lifetime for the localized excitons. A schematic representation of the model is presented figure 3.19

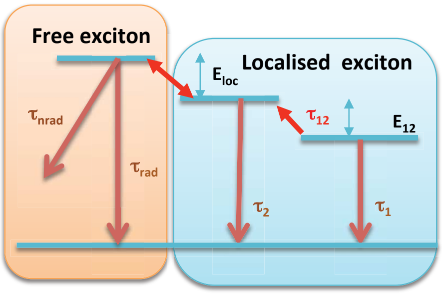

Figure 3.19: Schematic representation of the different recombination phenomena taking into account for the recombination of the excitons in ZnMgO barriers.

The adjustment of the experimental data with the model is presented in Fig. 3.20. The energy of localization is fixed at 60 meV, these value is deduced from the transition energy dependency with temperature. Fig. 3.21 summarizes the temperature dependency of all lifetimes used in the model with the calculated value of the PL lifetime. The best fit is obtained for a value of 5×10^{14} cm^{-3} for the density of localization centers (N_{loc}). A good agreement is obtained for both PL decay time and PL intensity.

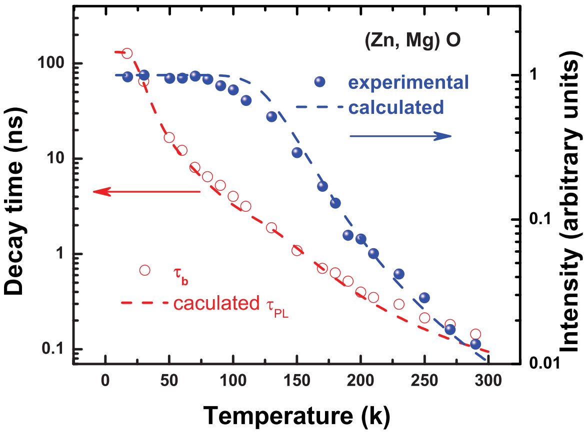

Figure 3.20: Comparison of the calculated PL lifetime and PL intensity with the measures.

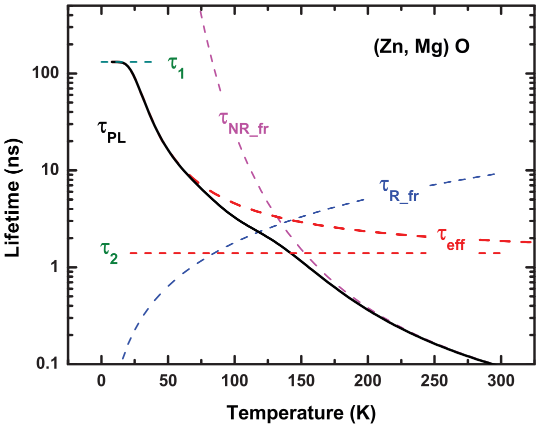

Figure 3.21: Temperature dependency of the different lifetimes considered in the model.

3.4 Conclusion

In this chapter, we resume the results obtained during this study on the ZnO substrate and the (Zn, Mg)O barriers of the quantum well. The PL signal of the substrate is polarized as expected for non-polar A plane. The degree of polarization is 95 % close to the limit of the apparatus. The polarization of the barrier is less around 88 % indicating that the barriers are constrained. At very low temperature, the excitons in the barriers are localized and exhibit a very long lifetime, about 130 ns. The study in temperature of the lifetime showed that the localized exciton can occupied two different states, one with the very long lifetime the other one with a lifetime of 1.4 ns. These two states are in thermal equilibrium. At higher temperature the photoluminescence is dominated by non-radiative recombination of free excitons. Based on the model of localized exciton in quantum wells we proposed a model for the dependency with the temperature at the same time of the intensity and the time of decline of the photoluminescence

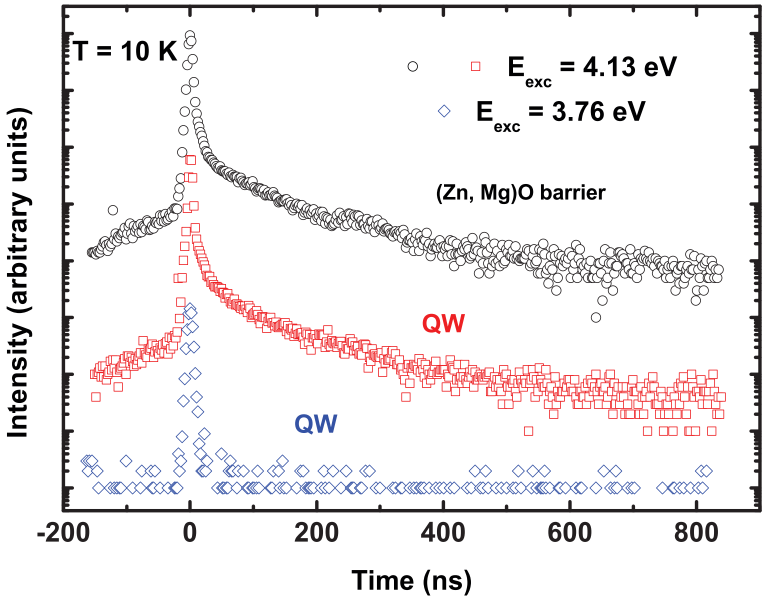

Figure 3.22: Photoluminescence time decays of the barrier (black open circle) and QW (red open square) excited with photon having an energy of4.13 eV and QW (blue open diamond) excited with photon having an energy of 3.76 eV.[bea11b]

To finish this chapter we want to point out the influence of the properties of the barrier on the measures of the decline of photoluminescence of the quantum well. For this purpose we plot different photoluminescence decays with different conditions of excitation in figure 3.22. Two decays are recorded with energy of 4.3 eV for the excitation photon. The first one (black open circle) is the barrier response. The decay shows a non-exponential behavior with a component in time very long. The second one (red open square) recorded at the QW emission energy presents a similar behavior. For PL decay recorded with excitation energy below the bandgap of the barrier (blue open diamond) do not present the long lifetime component. These results are a clear demonstration that the real PL decay of the QW does not have a component with a long lifetime. The apparent component of the decay of the QW at long time could be due to the excitons diffusion from the barrier, or to photons recycling. In the following chapters the experiments of time-resolved photoluminescence of the quantum well are acquired with photons having energy below the barrier bandgap.

Chapter 4

Exciton complexes in ZnO/(Zn, Mg)O quantum well

4.1 Introduction

High quality quantum wells on non-polar surface are grown successfully since a few years by using different technics. What is remarkable in the results published[cha10], [bea11a] on this kind of hétérostructure is that a peak at an energy , which is not the one of the free exciton, dominates the photoluminescence spectra measured at low-temperature. This peak is assigned to the radiative recombination of localized excitons in potential fluctuations.

This chapter is devoted to the results obtained by continuous wave optical spectroscopy, including the effects at the same time of the polarization and the temperature, on a single ZnO/(Zn, Mg)O quantum well growth by MBE on A-oriented ZnO substrate. To understand the observed trends we compare them with models of exciton complexes.

Figure 4.1.a gives a schematic representation of the sample. The width of the quantum well is 3.5 nm and the Mg concentration in the barrier was measured to be ~20%. The figure 4.1.b show a schematic representation of an hexagonal wurtzite structure with the crystallographic axis. The A plane (11-20) is represented in green. In addition, the (x, y, z) coordinate system linked to the plane is indicated. It is important here to notice that the z-axis is parallel to the c-axis [0001] of the crystallographic system.

In a first part, we describe the properties of the main excitonic complexes observed in the quantum wells. The experimental results are the object of two paragraphs. In the first one we included the results obtained in the case of low density of excitation. To understand the observed optical properties we compare them with a model of delocalized and thermalized trions. The other part is dedicated to the results obtained in the case of strong density of excitation. The most important result here is the formation of biexcitons in this quantum well.

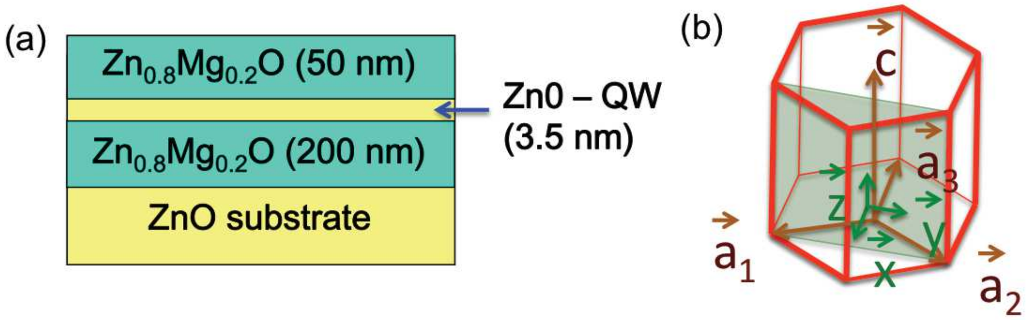

Figure 4.1: (a) Schematic representation of the sample. (b) Orientation of a-plane in hexagonal wurtzite structure, crystallographic axis is indicated. In green, we show the adapted coordinate system linked to a-plane composed by x out-plane axis, and y and z in-planes axis.

4.2 Exciton complexes

4.2.1 Introduction

When the concentration of excitons obtained by optical excitation is sufficiently high or in presence of free carriers (electrons or holes) or foreign atoms in the material exciton complexes can be formed. Here, we consider only two types of excitons complexes. The first one is the biexciton (XX), which consists in two excitons in interaction in a similar way to the H_2 molecule. Biexciton can be observed when the concentration of excitons is high enough. The second one is the trion, in this case it is an exciton in interaction with a free carrier. Consequently two kinds of trions can be formed, negatively charged exciton (X^- exciton in interaction with electron) or positively charged trions (X^+ exciton in interaction with a hole). Moreover, in 2D system like quantum wells the reduction of spatial extension of the wave function leads to an increase the interactions among carriers and to stronger Coulomb-correlation effects.

4.2.2 Biexcitons

Biexcitons has been theoretically predicted in 1958 by Lampert[lam58] and by Moskalenko.[mos58] Evidence for the existence of biexcitons has been found experimentally several years later in CuCl. [mys68] Since this time, biexcitons have been characterized in several bulk materials for example GaAs, [bri73] GaN[kaw96] and ZnO. [ko00], [yam01], [haz03] It has been also experimentally demonstrated that when the excitons are confine in quantum wells the binding energy of the biexciton increases over the bulk value. [cha03], [yam95b]

In photoluminescence experiment the biexciton luminescence arises from the radiative recombination of one of its two electron-hole pairs, leaving behind an exciton. The energy of the emitted photon E_{XX} is given by $E_{XX} = E_X - E_B^{XX}$. Where E_X and E_B^{XX} are respectively the energy of the exciton recombination and the binding energy of the biexciton. From photoluminescence experiments, in bulk ZnO the biexciton binding energy was estimated to be 15-16 meV. [ko00], [yam01], [haz03] In ZnO/(Zn, Mg)O quantum wells, with 26 % Mg contents in the barriers, the biexciton binding energies varied from 19 to 28 meV when the well width goes from 3.7 to 1.75 nm.[sun01], [chi03]

At low temperature, the population evolution of excitons (n_X) and biexcitons (n_{XX}) can be described by a chemical equilibrium model.[gou79], [kim94] This model leads to the pair of coupled differential equations:

$$\begin{aligned} \frac{dn_X}{dt} &= G - \frac{n_X}{\tau_X} + \frac{n_{xx}}{\tau_{XX}} - 2\frac{n_X^2}{n^*}\frac{1}{\tau_C} + \frac{n_{XX}}{\tau_C} \\ \frac{dn_{XX}}{dt} &= -\frac{n_{xx}}{\tau_{XX}} + \frac{n_X^2}{n^*}\frac{1}{\tau_C} - \frac{n_{XX}}{\tau_C} \end{aligned} \qquad \text{.......... (4.1)}$$

where G is the continuous-generation rate (proportional to the density of excitation), τ_X and τ_{XX} are the exciton and biexciton lifetimes. τ_C, is the characteristic interconversion time when $n_X = n_{XX} = n^*$. The two equations take into account the generation of the excitons, the decays of the excitons and biexcitons, and the interconversion between them. The steady-state solutions to this system of equations are:

$$\begin{aligned} n_X &\propto \left[\left(1+\frac{G}{G_0}\right)^{1/2} - 1\right] \\ n_{XX} &\propto \left[\left(1+\frac{G}{G_0}\right)^{1/2} - 1\right]^2 \end{aligned} \qquad \text{.......... (4.2)}$$

where $G_0 = \left(n^*\ \tau_{XX}/4\ \tau_X^2\right)\left(1+\tau_C/\tau_X\right)$ is the characteristic generation rate. These equations indicate that for low generation rates ($G < G_0$) the exciton population grows linearly and the biexciton population grows quadratically. For high generation rates ($G > G_0$), the biexciton population grows linearly and the exciton population grows as the square root of the excitation. In summary, G_0 separates the exciton-dominant from the biexciton-dominant region and the biexciton population is proportional to the square of the exciton population ($n_{XX} \propto n_X^2$).The intensity of the bi-exciton, Ix, thus varies according to that of the exciton, Ix, according to a law of the type: $I_{xx} \propto I_x^{\beta}$ where $\beta = 2$.

The biexciton photoluminescence line exhibits a nearly Lorentzian line shape.[cho73], [kim94] This is because even a biexciton of large wave vector may recombine, the mismatch in wave vector between the biexciton and the photon being given to the remaining exciton.

4.2.3 Trions

The three-particle bound state of an exciton with an additional electron (X^-) or hole (X^+) has been also proposed by Lampert.[lam58] The rather small value of binding energy of third particles makes difficult the observation of such complexes in bulk materials. Two-dimensional confinement is strongly enhanced this energy and subsequently the trions have been observed in quantum well in photoluminescence or absorption spectra.[khe93], [shi95] The effect of the carriers localization on the trion formation in quantum well was previously highlighted.[eyt98] [bri99] Indeed, in real quantum wells, electrons and holes are subject to random potential fluctuations. These can be due to interface roughness, or alloy disorder. It is also due to the presence of remote ionized impurities in the barrier that induces electrostatic potential fluctuations. These can localize the electrons (holes) and the negatively charged trions X^- (positively charged trions X^+), but do not affect much the exciton which are neutral complexes. In such case the trion radiative lifetime is almost independent of the temperature as it was found in single GaAs quantum wells between 2 and 10 K.[fin98]

On the contrary, the concept of delocalized trions is the most appropriate way to describe the broad range of experimental results on trions in quantum wells.[man96], [ess00a], [ess00b], [ciu00] In this model the trions are assumed to be in thermodynamic equilibrium with excitons and free carriers. If we consider the k-vector conservation when a trion X^- radiatively recombines the electron takes away the k-vector of the trion as the photon momentum is small enough to be neglected. Thus X^- with k-vector different from zero can also recombine radiatively. From the point of view of the experimental observations it implies that the peak of photoluminescence is asymmetrical. He has to present a spreading towards low energies corresponding to the recombination of trions with high value of k. Furthermore, this tail is a function of the temperature and has to extend when this one increases.

To understand quantitatively these effects Esser *et al*[ess00a], [ess00b] proposed a model. Here we shall satisfy us with considering only the negative trion because our samples are n-type.[tai11] In this model the X^- thermal distribution is approximate by a Bolzman distribution. The intensity of the photoluminescence is then given, if we neglect the broadening mechanism, by:

$$I_{X^-}(\hbar\omega) \propto \left|M(k)\right|^2 \exp\left(-\frac{\in}{k_B T}\frac{m_e}{M_X}\right)\Theta(\in) \qquad (4.3)$$

where $\in$ is given by $\in = E_{X^-}(k=0) - \hbar\ \omega = \hbar^2k^2M_X/(2m_eM_{X^-})$, $\Theta(\in)$ is the Heaviside step function. $M(k)$ is the optical matrix element, which can be approximated by $\left|M(k)\right|^2 \approx \exp(-\in/\in_1)$. M_X, M_{X^-} and m_e are respectively the exciton, trion and electron masses. The spectral decay constant (E_{Tail}) is deduced from equation (4.3) and is given by:

$$\frac{1}{E_{Tail}} = \frac{1}{k_B T}\frac{m_e}{M_X} + \frac{1}{\in_1} \quad \text{.......} \quad (4.4)$$

To take into account the broadening effect, the trion contribution is obtained from the convolution of the equation 4.3 with the same profile used to fit the exciton line. This procedure is illustrated by the figure 4.2 for two temperatures. It should be noted here that the maximum of the peak does not correspond to the energy of recombination of the trion. The experimental determination of this energy has to be made not on the maximum of the peak but a better choice is the inflexion point on the high-energy part.

A chemical law of action of masses connects the concentration of free electron (n_e) and neutral (n_X) and negatively charged (n_{X^-}) excitons.[siv99]

$$\frac{n_X n_e}{n_{X^-}} = \frac{4\ m_e\ k_B\ T}{\pi\ \hbar^2}\exp\left(-\frac{E_B^{X^-}}{k_B\ T}\right) \quad \text{.......} \quad (4.5)$$

where $E_B^{X^-}$ the trion binding energy.

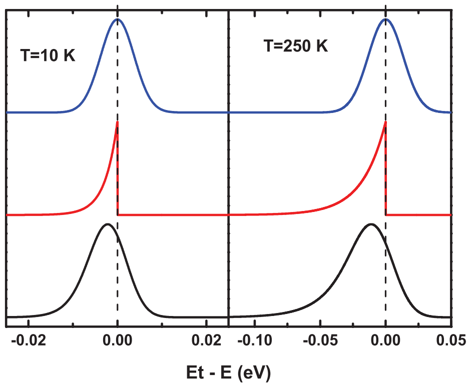

Figure 4.2:.Calculated photoluminescence spectra (black line) in the framework of delocalized trion model at two different temperatures. The spectra are obtained by the convolution of equation 4.3 (red line) by a Gaussian (blue line). The convolution shifts the peak maximum slightly to lower energy.

4.3 Low density of excitation experimental results

4.3.1 Photoluminescence at low temperature

Let us first consider the results obtained in low density of excitation condition. Figure 4.3 present a photoluminescence spectrum of the sample measured at low temperature. The excitation is obtained using a white lamp and the energy (4.3 eV) is selected using a mono-chromator. In such experimental condition the density of excitation is very weak. A peak at 3.399 eV (QW1) dominates the spectrum. At higher energy a second peak at 3.85 eV is related to the recombination of excitons in the (Zn, Mg)O barrier. This value is consistent with a concentration of 20 % of magnesium in the barriers.[yam01] It has been noticed that no line in the spectra can be attributed to recombination of exciton in the ZnO substrate. However, the main line presents a shoulder at high energy, around 3.43 eV (QW2).

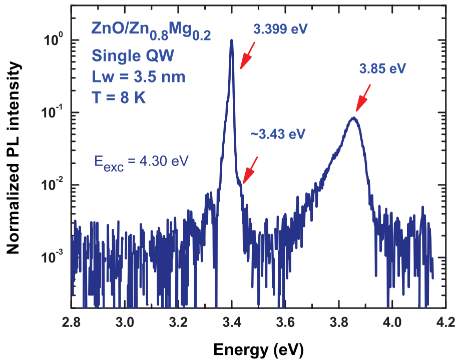

Figure 4.3: Photoluminescence spectra recorded at 8 K. The luminescence was excited at 4.3 eV using a monochromator.

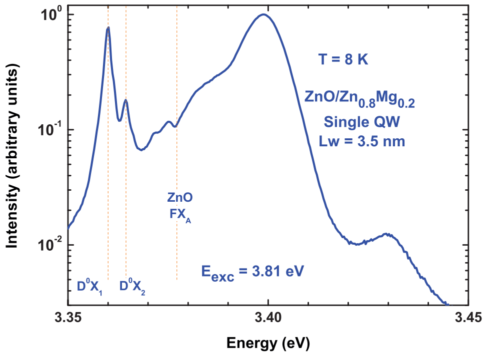

Figure 4.4: PL spectra recorded at 8 K for weak density of excitation and incoming photons energy of 3.81 eV.

In the case of excitation with photons energy below the barrier (Figure 4.4), the PL spectra present two extra lines at 3.360 eV and 3.365 eV. In such condition, both quantum well and ZnO substrate are excited. The two PL lines correspond to the recombination of binding exciton to donors in the ZnO substrate.[mey04] Moreover, a shoulder at low energy complete the main line. It is this shoulder, which becomes the third line when the density of excitement increases as we shall see it later in this chapter.

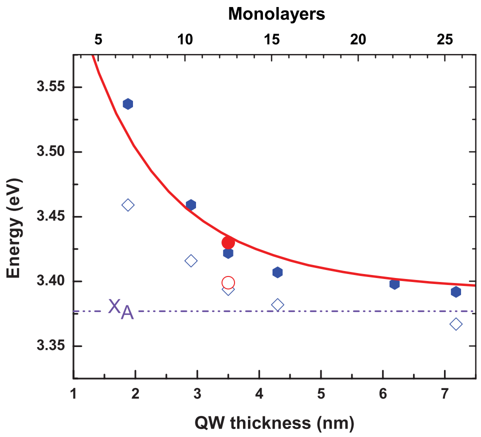

Figure 4.5: Transition energies plotted versus well width for a series of A-plane oriented ZnO/(Zn, Mg)O single quantum wells. The full blue hexagon symbols represent the ground state energies determined by PLE measurements at 2 K.[cha10] The blue open square are the position of the main PL line energies.[cha10] The full and open red circles are the present results. The result of the effective mass envelope function calculation, including hole-electron interactions, is represented by red line.

In figure 4.5, we have reported our results with the ones of J.M. Chauveau[cha10] on the same type of sample. In addition, the figure is completed by the effective mass envelope function calculation, including hole-electron interactions, of transition energy of the exciton in the quantum wells. A good agreement is obtained between the full symbols and the calculated value. The energies are above the energy of the free exciton in ZnO bulk (dashed line dyes purple on the figure). This is a signature of the absence of QCSE in these quantum wells, as expected. Our envelope function calculation shows that the splitting between the two PL lines QW1 and QW2 (~30 meV) is too large to be explained by one or two monolayer QW width fluctuation (~4 meV for 1 ML).

4.3.2 Reflectivity versus photoluminescence

Figure 4.6 presents the reflectivity experiments carried out at low temperature in normal incidence conditions, the light is polarized parallel (blue line) and perpendicular (red line) to the [0001] direction. The positions of the intrinsic excitonics transitions are in agreement with the values[lia68] previously published (indicated by dashes lines). Much more interesting is the presence on these spectra of high-energy feature typical of quantum wells corresponding to the unresolved (A, B) doublet and C confined states.

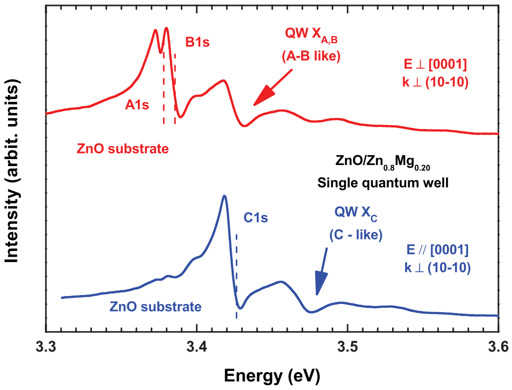

Figure 4.6: Low temperature polarized (red and blue plots) reflectance spectra showing the excitonic selection rules.

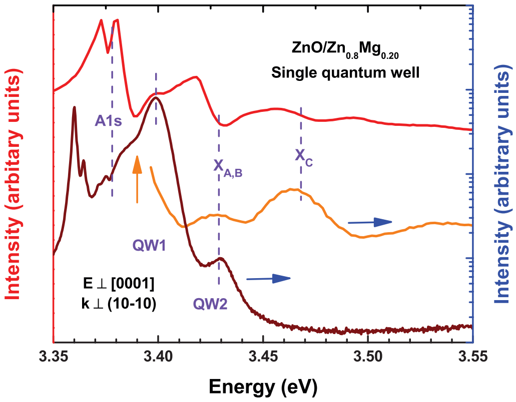

Figure 4.7: Comparison of low temperature polarized reflectance (red line), PL (brown) and PLE (orange) spectra. The PL and PLE spectra are plotted on a semi log scale.

In figure 4.7, we report low-temperature reflectivity spectra (red) associated to photoluminescence (PL - brown) and photoluminescence excitation spectroscopy (PLE – orange) spectrum. The PLE spectrum is taken at energy of 3.39 eV.

On the spectra of PL we do not observe a line associated with the luminescence of C exciton, which according to the experience of reflectivity should be situated towards 3,47 eV. They are at low temperature completely thermalized on the levels A and B as expected. Let us return on the lines of photoluminescence associated to A and B confined exciton in the quantum well. The lines are previously labeled QW1 and QW2. The Stokes-shift between the structure observed in reflectivity, corresponding to the level having the biggest density of state, and the peak of photoluminescence (QW2) is only few meV. This small value of the Stokes-shift indicates reasonable heterointerface smoothness with terraces of the size of the exciton Bohr radius. The line QW2 corresponds well as we had suggested it previously, on the basis of the calculation of the excitonic transitions in these quantum wells, to the recombination of free excitons.

Before going further, I shall want to make some remarks on the dominant peak of PL (QW2). At first, a feature is present on the reflectivity spectra at the same energies. Moreover, the PLE spectrum measured on the low energy side of this peak present two structures corresponding to the energies of the exciton X_{AB} and X_C. What confirms the excitonic nature of the transitions. We have already eliminated the hypothesis of exciton localized on fluctuations in width of well. We have now to envisage the hypothesis of excitonics complexes. The experiments results obtained with high density of excitation described in the paragraph 4.4 show that the line QW1 couldn't be attributed to the recombination of biexcitons. In the following paragraph, we shall analyze the results within the framework of the model of delocalized trions.

4.3.3 Polarization of the photoluminescence spectra

The study of the polarization of the photoluminescence according to the temperature is summarized in the figure 4.8. Each map represents the variation of the PL signal as a function of the angle between the c-axis of the structure, chosen as zero, and the electric field of the outgoing light. The intensity of the PL decreases two orders of magnitude with increasing temperature. The signal related to the barriers disappears for temperatures higher than 150 K. More important, the relative intensity of the lines associated with the quantum well changes when the temperature increases. In the map measured at 150 K, they are clearly resolved and the intensity of the peak $X_{A,B}$ becomes more intense than the peak X^-. Furthermore, from 150 K a signal is clearly present for an angle of zero degrees. The relative intensity of this signal increases with the temperature.

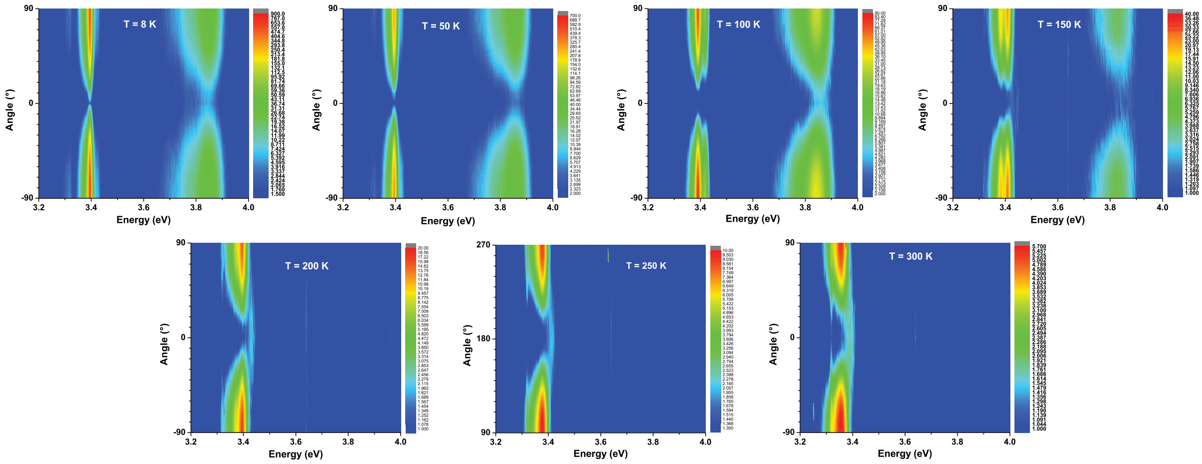

Figure 4.8: Variation of the PL intensity as a function of the angle between the [0001] axis of the structure and the electric field of the outgoing light. The intensity of PL is coded in logarithmic scale.

Before pursuing the analysis of the effect of the temperature, we will first comment on the polarization of the observed signals. In Figures 4.9 and 4.10 we plot the PL spectra measured in two polarizations conditions: electric field of the outgoing light parallel (polarization c) and perpendicular (polarization a,b) to the [0001] axis for two temperature. For both temperatures the signal decreases of about two orders of magnitude when we pass of the polarization a,b in the polarization c. A more interesting feature is the shift towards the high energies of the line associated with the quantum well at 150 K during the change of polarization.

The variation of the intensity of the PL lines as a function of the outgoing light electric field orientation is summarized in figures 4.11 and 4.12. The zero of the polar graph corresponds to light electric field oriented parallel to the [0001] axis. At 8 K (Fig. 4.11), the maximum intensity for all the lines (X_{AB}, X^- and barrier) is obtained when the light electric field is perpendicular to the c-axis. At 150 K (Fig. 4.12), the polar representation shows clearly that the X^- and $X_{A,B}$ lines keep their polarization. It also shows that the polarization of the line QW3 is in quadrature with two others.

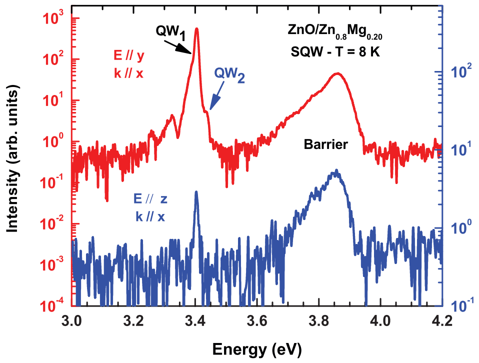

Figure 4.9: Photoluminescence spectra recorded at 8 K in the two polarizations. Note the difference by two orders of magnitude between the two spectra. The luminescence was excited at 4.3 eV using a monochromator.

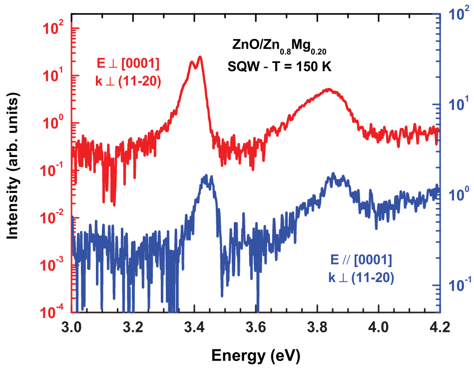

Figure 4.10: Photoluminescence spectra recorded at 150 K in same conditions as in figure 4.11.

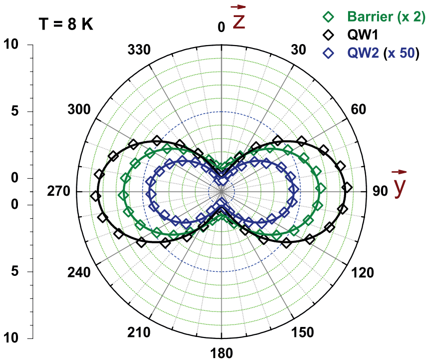

Figure 4.11: Polar representation of photoluminescence intensity measured at 8 K. The Z-axis is parallel to the [0001] axis.

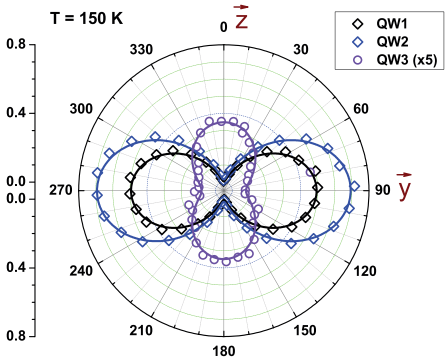

Figure 4.12: Polar representation of photoluminescence intensity measured at 150 K.

The degree of polarization (DOP) of the signal is calculated from the data using the following formula:

$$\mathrm{DOP} = \frac{I_Y - I_Z}{I_Y + I_Z} \qquad (4.6)$$

The values of the DOP for the lines of photoluminescence are collected in the table 4.1.

	X^-	$X_{A,B}$	QW3	Barrier
DOP – 8 K	99 %	99 %	-	88 %
DOP - 150 K	99 %	99 %	-77 %	-

Table 4.1: Degree of polarization of the different CW-PL lines.

The DOP of the X^- and X_{AB} peaks is 99 % whereas it is only 88 % for the line associated to the barrier. The DOP of the line QW3 is about -80 % what corresponds to a polarization of the signal along the axis c. The difference in energy position of the peaks between QW3 and $X_{A,B}$ is of the order of 40 meV what is compatible with the observations made on the reflectivity spectra.

4.3.4 Effect of temperature

To illustrate the effects of the temperature and of the polarization on the photoluminescence spectra we gathered on the figure 4.13 the normalized spectra measured in (a) polarization ab and in (b) polarization c. Figure 4.13 (a) shows the relative change in intensity between the $X_{A,B}$ and X^- lines. When the temperature increases the $X_{A,B}$ line becomes the dominant line. On the low-temperature spectra (Fig. 4.13 (a)), we note the presence of a shoulder on the low energy side of the X^- line that will be in the following attributed to the contribution of the biexcitons. It can be also noticed that the recombination of negative trions shows up as an asymmetric line with a low-energy tail, which broadens with increasing temperature.

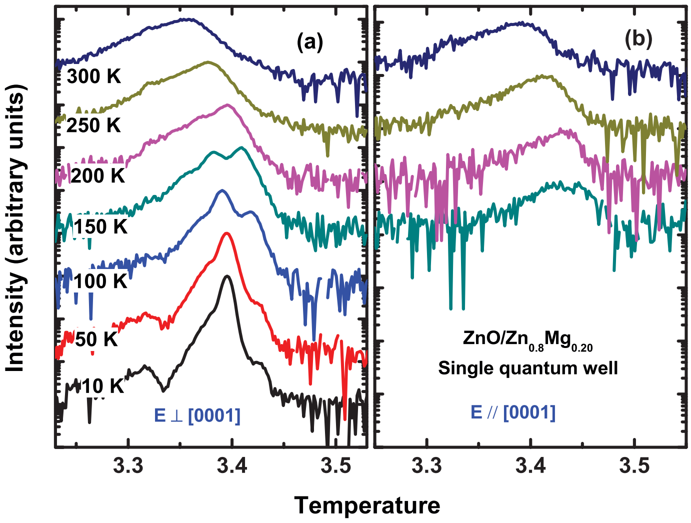

Figure 4.13: Evolution of the normalized photoluminescence spectra according to the temperature. Photoluminescence spectra measured in (a) polarization a,b and (b) polarization c. The luminescence was excited at 4.3 eV using a monochromator.

In order to get quantitative information from the spectra we fit them using the following procedure. The exciton lines are assumed to be Gaussian. To model the asymmetry of the peak of PL associated with the trion we use the convolution product of the equation 4.3 with a Gaussian in order to take into account the broadening effect. The full width at half maximum (FWHM) is chosen equal to the FWHM of the exciton line when these line is clearly defined in the spectra. The E_{tail} parameter of equation 4.3 is adjusted in such a way as that to obtain the best result. At low temperature, a Lorentzian function is used to fit the biexciton contribution. For the spectra recorded in the c polarization only the contributions of the exciton and the trion are considered. The figure 4.16 presents a set of results obtained using this procedure. The figure 4.14 illustrates the procedure to fit the experimental curves. It is remarkable that the dissymmetry of the trion line increases according to temperature.

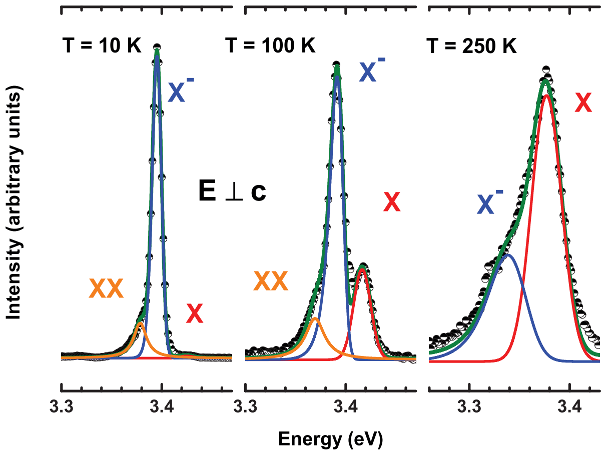

Figure 4.14: Results of fitting procedure utilized to get quantitative information from the experiments. The symbols are the experimental values. The orange, blue, and red curves represent respectively the contribution of the biexciton, the trion and the free exciton. The calculated total photoluminescence curve is green. Note that the maximum of luminescence decreases by a factor of about 60 when the temperature goes from 10 K to 250 K.

The evolution, according to the temperature of the energies of the transitions and the intensity of the associated lines of photoluminescence, is respectively drawn on figures 4.15 and 4.16. We used the model of Varshni[var67] to describe the behavior of the energy of emission of confined excitons in the quantum wells according to the temperature. The expression is the following one:

$$E_g = E_0 - \alpha\, T^2 \big/ \left(T + \beta\right) \tag{4.7}$$

A good agreement with the experimental values is obtained using the parameters $\alpha = 4.7\ 10^{-4}\ (\mathrm{eV/K})$ and $\beta = 900\ (\mathrm{K})$ these values are close to the ones proposed by Meyer *et al.*[mey04] In a general way, we notice a red shift of the energies between 8 and 300 K that corresponds to the decrease of the energy of the forbidden band of ZnO. The gap between the line $X_{A,B}$ and X_C (and X^-_{AB} and X^-_C) is about 38 meV. The one between the line of the exciton is the one of the associated trion is 23 meV. This energy corresponds to the binding energy of the trion. In the case X_{AB}^- a small increase of the energy of photoluminescence occurs for the temperatures lower than 50 K followed at higher temperature by a decrease due to the reduction of the gap of the material. This evolution of the energy of photoluminescence according to the temperature (S shape) is often observed in quantum wells. This behavior correspond to the following physical phenomena:

- At low temperature the excitons (excitons complexes) are localized, the localization energy reduces the transition energy.
- When the temperature increases, the thermal energy allows the delocalization of the exciton (excitons complexes) then the transition energy increases with temperature.
- At high temperature, all the excitons (excitons complexes) are delocalized and the transition energy diminish as the material bandgap with temperature increase.

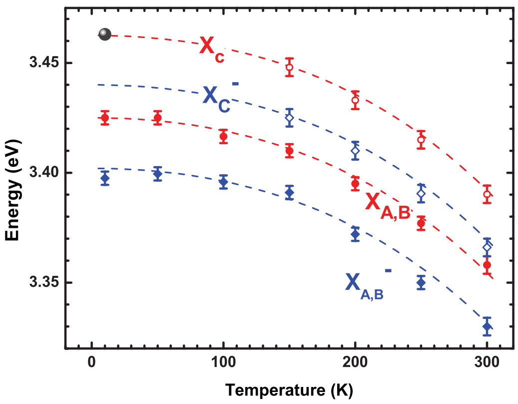

Figure 4.15: Energy of the PL lines as function of temperature. The dashed lines are Varshni function. The full circles correspond to the position in energy of the reflectivity feature on the low temperature spectrum.

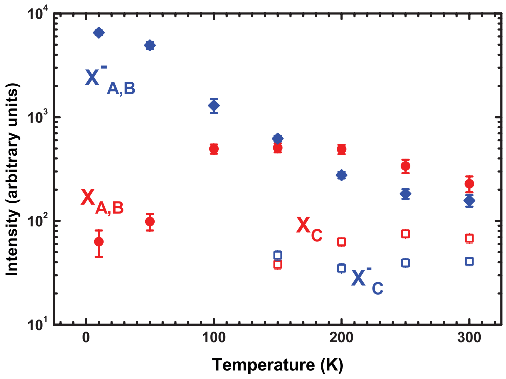

Figure 4.16: Intensity of the PL lines according to temperature.

From the data, we can estimate the localization energy of the negative trions. We found a value of about 5 meV. This value corresponds to a well width fluctuation of one monolayer in the quantum well.

The results show a decrease of the intensity of the X^-_{AB} line (blue full diamond) when the temperature increases, whereas the X_{AB} line (red full circle) has a more complex behavior. At low temperature, the intensity increases with temperature until 100 K. It stays nearly constant till 150 K, next when the temperature increases the intensity decreases. The X_{AB} line becomes dominant in the spectrum from 200 K. The intensities of the lines X_C (red open square) and X_C^- (blue open square) are weak compared to the other ones. The total photoluminescence intensity decreases on one order of magnitude when temperature increases from 10 K to 300 K. This is associated to non-radiative process, which are thermally activated, whether they correspond to level depopulation or to the activation of a non-radiative recombination center.

The photoluminescence intensity of X^-_{AB} line can be fitted (fig. 4.17) with the following expression considering only one non-radiative recombination channel:

$$I\left(T, A, E_1\right) = I_1 \; f\left(T, A, E_1\right) = I_1 \Big/ \left(1 + A \; T \exp\left(-E_1 / k \; T\right)\right) \text{...} \; (4.8)$$

where E_1 is the activation energy of non-radiative process. Its value is 17.1 meV as regards the intensity of the trion, which is very close to trion binding energy. This suggests that the only non-radiative process explaining the disappearance of this line is the trion dissociation in a free exciton and an electron. Assuming that trions are the source for free excitons, the X intensity variation can be approximate by the following expression:

$$I\left(T, B, E_2\right) = \left(I_2\left(1 - f(T, A, E_1)\right) + I_0\right) \Big/ \left(1 + B \; T \exp\left(-E_2 / k \; T\right)\right) \text{..............................} \; (4.9)$$

where I_0 and E_2 correspond respectively to the intensity at low temperature and to the activation energy of non-radiative process. The parameters A and E1 are the ones determined from the X^- line fitting. With a value of E_2=89 meV we obtain a good agreement between the experimental points and this expression.

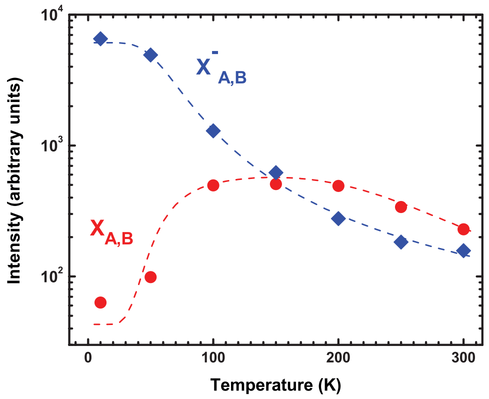

Figure 4.17: Intensity of the PL lines versus temperature. The red and blue dashed lines correspond to the fitting respectively of the intensity of the trions and exciton lines.

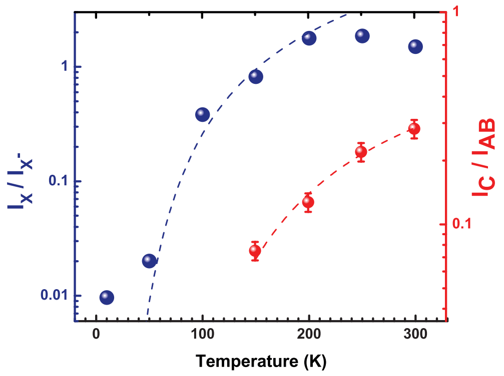

Figure 4.18: The blue and red full circles correspond to the ratio respectively of the intensity of the exciton and trions lines and of the total PL intensity measured in c and ab polarization. The blue and red dashed line correspond to the fitting with respectively the formula 4.5 and a Boltzman distribution.

The ratio between the intensities of the free exciton lines and the trion lines is also presented (blue full circle). The blue dashed line corresponds to the expression 4.5. From this fitting we can estimated the density of electrons in the quantum well. The calculation leads to a value for the electron density of about 10^{12} cm^{-2}. The results showed that the excitons with a c symmetry are populated for temperatures higher than 150 K. The ratio between the intensities of the lines in c polarization and ab polarization is presented in figure 4.18. We assume a thermalized distribution of the excitons and approximate it by a Boltzmann distribution. The fitting of the points gives activation energy of 36.7 meV, which consistent with the separation between the two levels previously determined.

4.4 High density of excitation results

4.4.1 Photoluminescence at low temperature

The figure 4.19 shows the evolution of the photoluminescence spectra according to the incident light intensity of a laser OPO with a repetition rate of 10 Hz. The width of the pulse being 5 ns and the typical lifetime of the excitons being between about ten and some hundreds of picoseconds at low temperature, we can consider the excitation as quasi-continue. The energy of the photons is fixed to 3,75 eV, i.e. below the barrier bandgap, to create excitons directly in the well. The spectra are collected in polarization ab.

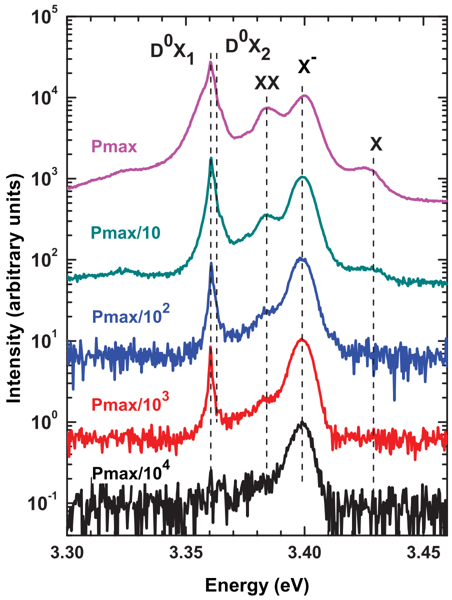

Figure 4.19: Photoluminescence spectra recorded at 10 K. The incident light intensity of a laser is varying on for order of magnitude. (Pmax=8.5 µJ)

In the photoluminescence spectra, an additional line clearly appears at lower energy (3.38 eV) when the excitation power density increases. The intensity of this line increases more quickly with the increase of power which the two other lines (X and X^-). The behavior of this new line is compatible with the biexcitons formation. Quantitative information from the spectra is obtained by using the same fitting procedure used previously. The lines D^0X_1 and D^0X_2 corresponding to the substrate response are assumed to be Gaussian. A Lorentzian function is used to fit the biexciton contribution.

The figure 4.20 presents the evolution of the intensity of the photoluminescence for both excitons localized on neutral donor in the ZnO substrate. The intensity of these lines presents a linear behavior according to the density of the incident light on this graph in logarithmic scale. Therefore the intensity of the PL lines follows a power law ($I \propto \left(P / P\max\right)^{\beta}$). In this case β is equal to 1. The density of the lines is directly proportional to the density of photons absorbed in the substrate as expected.

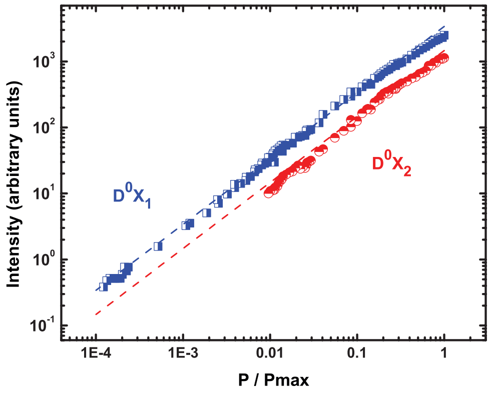

Figure 4.20: Intensity of the PL lines according to the incident light intensity. Noted that scales are logarithmic. (Pmax=8.5 µJ)

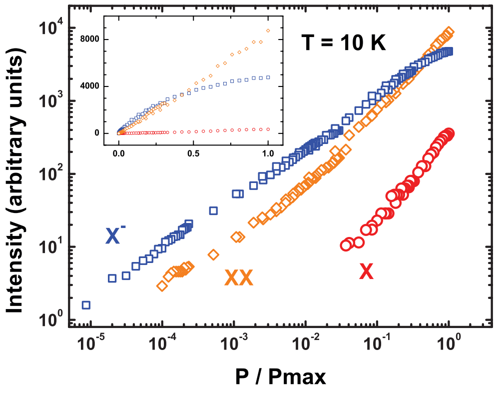

Figure 4.21: Intensity of the X, XX and X^- PL lines according to the incident light intensity in logarithm scale. The same data are plotted in linear scale in the insert. (Pmax=8.5 µJ)

The variations of the intensities of the PL lines associated with the quantum well are more complicated as the figure 4.21 shows it. The insert of the figure 4.21 shows the same data drawn in linear scale. Obviously the intensity of the X^- line has a non-linear behavior. From the classical approximation for long-lived excitons,[kim94] the exciton exhibits a sub linear increase with increasing excitation power density, while the biexciton is close to be linear. From these results we can propose the following scenario. Photons are absorbed in the quantum well and generated excitons. These excitons go either form trions, or biexcitons. At high power densities the excitons that are not involved in a complex give raise to the line associated to the free exciton PL. To go at the end of the model it is necessary to draw the density of biexcitons according to the density of excitons (fig. 4.22).

In our case, the density of excitons will be proportional in the sum of the intensities of the lines X^- and X. The dependence of the biexciton intensity on the exciton intensity for these data gives approximately $I_{biexc} \propto I_{exc}^{1.4}$ which is a reduction in the exponent from the value $\beta = 2$ expected. A factor β lower than 2 has been reported in literature.[phi92], [yam95b] The difference between the theoretical prediction and experimental observation's results maybe from limitations of the model. One postulate of this model is that the interconversion time is much shorter than excitonic lifetime.[gou79], [kim94] This condition can be easy to verify in the case of semiconductors with indirect bandgap, but is far from being verified in the case of semiconductors with direct bandgap such as GaAs[phi92] or ZnSe.[yam95b]

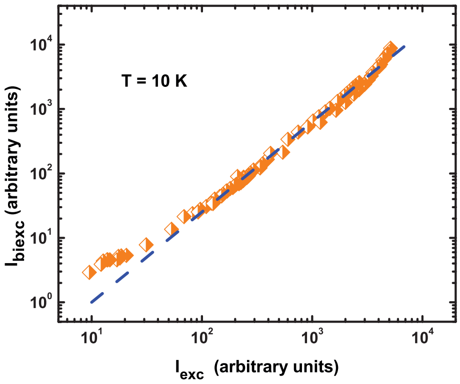

Figure 4.22: Ratio between the intensity of the XX line and the sum of the intensities of X and X^- lines. The slope of the straight line (in blue) is 1.4.

4.4.2 Effect of temperature

The effect of temperature on the photoluminescence spectra was examined. The same conditions of excitation are used and the power density is fixed at 8.5 µJ. The results of this study are summarized on the figure 4.23 on which is traced the energy of photoluminescence according to the temperature, the intensity is coded on a scale of color. The intensity of the D^0X_1 and D^0X_2 decreases quickly with temperature increase. For the response of the quantum well, on the map, we can make the same observations as those that we had made in the study for low density of excitation. At low temperature, the contribution of exciton complexes dominates the spectra. With the temperature increase, the intensity of the free exciton line becomes dominant. This is illustrated on figure 4.24 where some selected spectra are gathered. When temperature increases, due to the thermal broadening, the X^- and XX spectra merge together. Until 250 K, the X contributions remain well separated and then merge with the other contributions at higher temperature. With the help of the results of §4.3.4, the spectra are fitted with the procedure describe before in order to get quantitative information.

The evolutions of the transition energies with temperature are summarized in figure 4.25. The dashed lines correspond to the Varshni function. The full circles correspond to the results measured in the condition of low density of excitation. The energies decrease between 8 and 300 K, which corresponds to the decrease of the energy of the ZnO bandgap. The gap between the line X and X^- is about 19.5 meV. The one between the line of the exciton and the one of the biexciton is 43 meV. As we have noticed before, in the case X^- a small increase (5 meV) of the energy of photoluminescence happens for the temperatures lower than 50 K followed at higher temperature by a decrease (S shape).

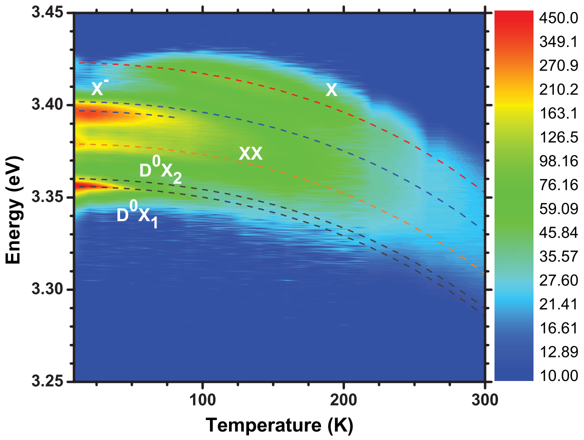

Figure 4.23: Photoluminescence spectra according to the temperature. The intensity is coded in a color logarithmic scale. (P=8.5 μJ)

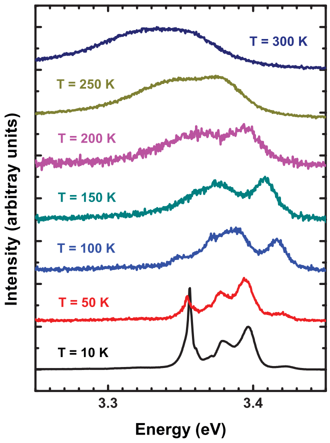

Figure 4.24: Normalized photoluminescence spectra recorded at different temperatures. (P=8.5 μJ)

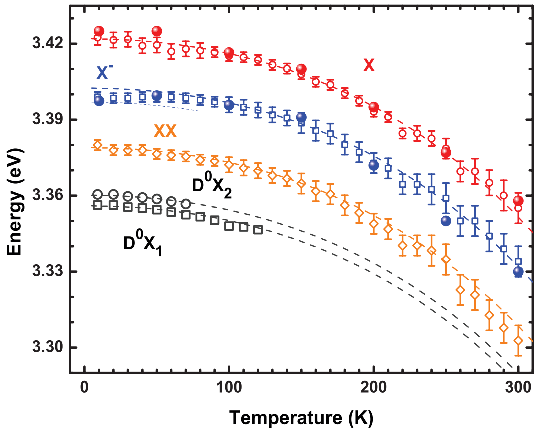

Figure 4.25: Photoluminescence spectra recorded at 10 K. The incident light intensity of a laser is varying on four order of magnitude.

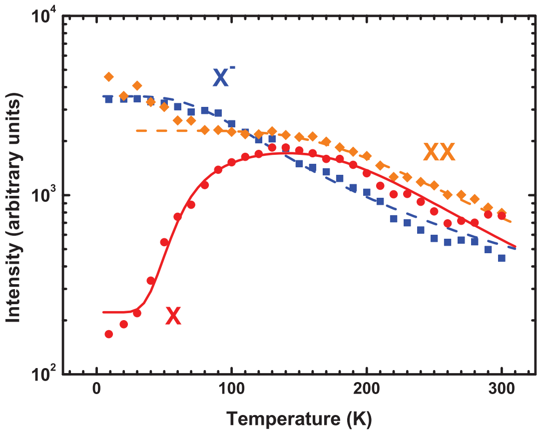

Figure 4.26: Intensity of the PL lines X, X- and XX according temperature.

Figure 4.26 gives the temperature dependence of the X, X^- and XX photoluminescence intensities. The lines intensities of the trion and the biexciton show a decrease on the interval of temperature. The intensity of the trion and the bi-exciton lines are approximate by the formula 4.8. The activation energies are 19.2 meV and 61 meV for respectively the trion and the bi-exciton. These results are in agreement with our previous observations. It confirms the hypotheses that the non-radiative channel associated with the quenching of these lines are the thermal dissociation of the exciton complexes. At lower temperature, the phenomena involved in the biexciton line quenching appears to be more complex. The biexciton population is dependent on the dissociation of the biexciton but also possibly of the formation of biexciton, consequence of the increase of the exciton density due to dissociation of the trions. The X line shows first an increase till 100 K followed by a decrease. The increase is a consequence of the exciton complexes dissociation. For temperature higher than 100 K the non-radiative process govern the exciton density. The intensity is approximate by the formula 4.10. The activation energy of the non-radiative process is 73 meV.

$$I(T,B,E_2) = \left(I_2\left(1-f(T,A,E_1)\right) + I_3\left(1-f(T,C,E_3)\right) + I_0\right) \Big/ \left(1 + B\ T\ \exp\left(-E_2/k\ T\right)\right) \quad (4.10)$$

To compare the results obtained in the two conditions of excitation the radiative efficiency (η) of the quantum well can be estimated. This value is defined as the ratio between the number of radiative recombination and the total number of recombination (radiative and non radiative). From the measures of photoluminescence intensity it is possible to estimate this value by making the hypothesis that at the lowest temperature all the recombination are radiative. In this case, the variation of η is given by the variation of the intensity of PL normalized in its low-temperature value. This hypothesis is valid all the more as the intensity of photoluminescence remains constant on a large range of temperature. In any cases, it gives information about the variation of η according to the temperature. Here η is calculated using the sum of the intensities of the different lines attributed to the quantum well in the photoluminescence spectra.

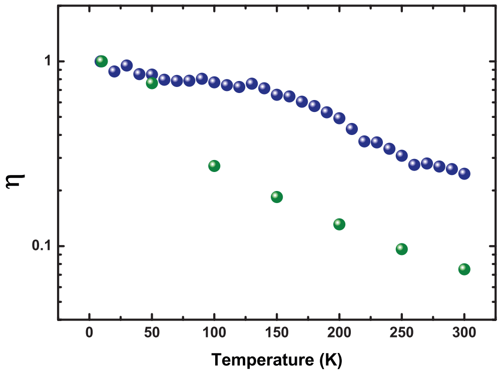

Figure 4.27: Radiative efficiency of the quantum well estimated from the total PL intensity. The full circles blue and green correspond respectively to high density and low density of excitation.

To report these experimental results we propose the following simple model. At low temperature exciton are optically generated and then form complexes. As the temperature increases the complexes are dissociated according to their binding energy. The density of exciton then increases. The excitons can then move towards non-radiative recombination center or can dissociate themselves. At low excitation density, only the trions are created in high concentration so the PL efficiency is mainly governed by the trions dissociation with activation energy of about 20 meV. Whereas at high excitation density, both the trion and biexciton are created, the PL efficiency now depends on dissociation of the trion and of the biexciton. The binding energy of the biexciton is about twice the one of the trion. As a result the radiative efficiency is improved. This is illustrated by the figure 4.27 where we can see that the radiative efficiency is 0.08 at 300 K in the case of low density of excitation while it is 0.25 for the results obtained in the condition of high density of excitation.

4.5 Discussion

In this chapter, the results obtained in continuous optical spectroscopy were analyzed by considering both free excitons and exciton complexes. In particular, one of the lines observed is attributed to the recombination of the negatively charged trion. In order to get this exciton complex, electrons should exist in the quantum well. In spite of the absence of information about the electric properties of our sample, we can estimate simply the density of electrons in the quantum well from what is known on these materials. It is well known that ZnO non intentionally doped (nid) has residual doping n-type.[tai11] The undoped ZnMgO layer is also n-type[tam08] with a doping level in the order of 1x10^{17} cm^{-3}. A value of 0.8 eV for the barrier height at the surface of (Zn, Mg)O has been measured by Kelvin probe force microscopy.[tam09] The total width of (Zn, Mg)O is 250 nm in the sample. Using textbook equations, one can calculate the width of space charged region. A value of 75 nm is found. The quantum well is located in it. It is possible then to calculate the distance in between the Fermi level and the fundamental state of electron in quantum well. The electron density is obtained considering that the electronic levels below the Fermi level are filled by electrons. A value of about 3x10^{11} cm^{-2} is obtained close to the one previously determinate.

4.6 Conclusion

The binding energy of the trion deduced from the measurement is 19.5±2 meV. The largest value reported, in materials other than Zn0, so far is 9 meV in ZnSe QW[fu88] to our best knowledge. From photoluminescence experiments, in bulk ZnO the biexciton binding energy was estimated to be 15-16 meV.[ko00], [yam01], [haz03] Consequently, a further increase of trion binding energy can be expected for ZnO-related QWs. In ZnO a value of 5 meV was reported by Makino *et al*[mak09] for SQW with a width of 5nm and 12 % magnesium contents in the barrier. More recently a value of 13 meV has been reported in ZnO/Zn$_{0.9}$Mg$_{0.1}$O MQW.[pul12]

In ZnO/(Zn, Mg)O quantum wells, with 26 % Mg contents in the barriers, the biexciton binding energies varied from 19 to 28 meV when the well width goes from 3.7 to 1.75 nm.[sun01], [chi03] In this study, for a well of 3.5 nm of thickness we find an binding energy of 45±5 meV. This energy is much bigger than those previously reported in the literature. However, it is necessary to note that in this study samples are grown according to the c-axis. In this case, the internal electric field is responsible for the reduction of the binding energy of the exciton but also for bi-exciton

In the next chapter, we are going to examine the dynamics of recombination of the excitons and the trion in this quantum well.

Chapter 5

Time resolved study of a ZnO/(Zn, Mg)O quantum well

5.1 Introduction

In this last chapter, we present the results of time-resolved investigation of the non-polar quantum well. This technic allows us to characterize the dynamic of the recombination of the exciton complexes. The analysis leads to the determination of the behavior of the optical properties according to the temperature among which the evolutions of the radiative and non-radiative contributions in the photoluminescence. We can also get information about the localization of the excitonic complexes.

As we have already indicated it in a previous chapter the lifetime of exciton is a function of the degree of freedom of the considered system. Here, we shall limit ourselves to the two-dimensional systems. The theoretical study of the dynamics of the exciton in the quantum wells gave rise to numerous publications.[fel87], [han88], [and91], [cit92b] The exciton radiative lifetime can be written as follow: [bea11a]

$$\tau(T) = \frac{k_B}{\hbar^2} \frac{\overline{M_X}}{\omega_{LT}\ a_B^3} \frac{\lambda^2}{n\ k_0^3\ I_{eh}^2} T \quad (5.1)$$

where n is the background refractive index, a_B the Bohr radius in the bulk and ω_{LT} the excitonic longitudinal transverse splitting pulsation. λ is a variational parameter corresponding to the two-dimensional confined Bohr radius, and I_{eh} the electron-hole envelope function integral. The calculated values by Béaur[bea11b] for the three excitons are summarized in table 5.1.

	$d\tau_A/dT$	$d\tau_B/dT$	$d\tau_C/dT$
QW – 1.7 nm (ps/K)	27	1.9	1.7
QW – 3.6 nm (ps/K)	36	2.5	2.3

Table 5.1: Calculated increase of the radiative lifetime according to temperature calculated for A, B and C exciton in quantum wells with width of 1.7 and 3.6 nm.[bea11b]

The increase of the radiative lifetime with the temperature is in order of picosecond by kelvin in non-polar (Zn, Mg)O/ZnO quantum wells. These values are lower than the values reported for others semiconductors. They vary between some tens (GaN/(Ga, Al)N quantum wells)[lef98] up to some hundreds (GaAs/(Ga, Al)As quantum wells)[fel87] of picosecond by kelvin. The reduction is directly related to the increase of the oscillator strength, represented by ω_{LT}. Indeed, the excitonic longitudinal transverse splitting is approximately ten times as big in the ZnO as in the GaN,[hof97] this last value is more important than the value of GaAs[Ada85] by a half of order of magnitude.

If the behavior with the temperature of the lifetime of the exciton is well documented, it is not the case of the lifetime of the trion. The electrostatic potential fluctuations localize the negatively charged trions X^- (positively charged trions X^+). In this case, the radiative lifetime is almost independent of the temperature as it has been observed in single GaAs quantum wells between 2 and 10 K.[fin98] In the model of delocalized trions[man96], [ess00a], [ess00b], [ciu00], the trions are in thermodynamic equilibrium with excitons and free carriers. It has been reported as a linear increase of the trion lifetime in CdTe related quantum well (fig. 5.1) with a slope of about 5 ps/K. [ciu00] A theoretical model was also proposed to support these results.[ciu00], [ess00b] The figure 5.2 illustrates the results of these calculations in the case of quantum well GaAs.[ess00b]

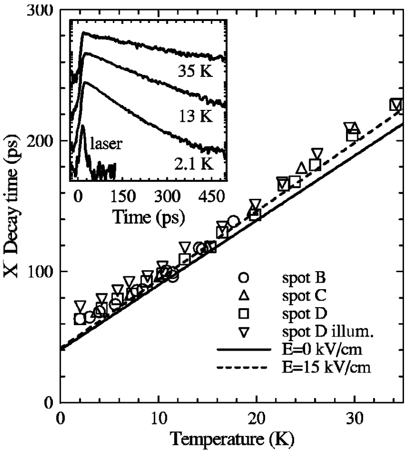

Figure 5.1: Inset: Time-resolved spectra for different temperatures. Main panel: Decay time of the X- PL when exciting resonantly on X- as a function of temperature.[ciu00]

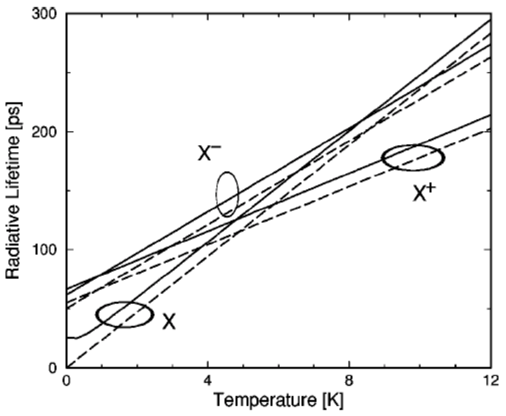

Figure 5.2: Calculated radiative lifetime of excitons (X), electron trions (X-), and hole trions (X+) for GaAs related quantum wells.[ess00b]

In this work, the lifetime of the exciton and the trion are both considered. The radiative lifetime of excitons is found to change linearly with temperature according to:

$$\tau_X = \frac{3}{2}\frac{\tau_{0,X}}{E_0}\left(k_B T + \frac{3}{5}E_0\right) \quad (5.2)$$

Here, E_0 is the exciton kinetic energy on the light cone. The temperature-independent pre-factor $\tau_{0,X}$ is the lifetime of an excitonic bright state at Q=0. The radiative recombination of the exciton is restricted to the light cone. In contrast, trions with arbitrary Q>0 can radiatively recombine. This fact introduces an additional offset at zero temperature. The temperature dependence of the radiative lifetime of the trion is given by:

$$\tau_T = \frac{3}{4}\frac{M_X}{M_T}\frac{\tau_{0,T}}{E_0}\left(k_B T + \in_1 \frac{m_e}{M_X} + \frac{3}{5}\frac{M_T}{M_X}E_0\right) \quad (5.3)$$

M_X, M_T and m_e are respectively the masses of the exciton, trion and free electron. Figure 5.2 presents the numerical evaluation of these expressions. Two important remarks must be underlined here. The first one concerns the lifetime to T=0K who is almost zero for the exciton, while its value is not insignificant for the trion. The second, the increase with the temperature of the lifetime of the exciton and the trion are different. In this article, for GaAs quantum wells, the report between the temperature slopes of the lifetime of the negatively charged trion and the exciton has a value of 0.75.

In a simple approach to the problem of the dynamics of recombination of the excitons, there is competition between the radiative and non-radiative phenomena. The radiative lifetime increases linearly, with the temperature while the not radiative lifetime decreases exponentially with the temperature. Experimentally, it is expected, at first, that the constant of a decline of the intensity of photoluminescence increases with temperature. After which, the competition between the radiative time and the non-radiative time leads to a decrease of the intensity and decay time of photoluminescence with the temperature. Such variations of the lifetime of the PL were observed by various teams in quantum wells of GaAs / (Ga, Al)As,[fel87], [gur91] (In, Ga)N / GaN[lan10] or GaN / (Ga, Al)N.[ros14]

These theoretical conclusions are confronted with the experimental results during the next part.

5.2 Experimental results

In order to prevent the exciton diffusion from the barrier, or photon recycling, the energy of the incoming photons is fixed at 3.48 eV. This energy is widely below the bangap of the barrier to be confident that the excitons are created only in the quantum well. Consequently, we are assured that the dynamic of the PL measured are related to the exciton complexes in the quantum well.

5.2.1 Time integrated

The normalized time-integrated spectra for different temperatures are presented in fig. 5.3. The evolution of the spectra according to the temperature is comparable to the one observed in CW-PL investigation. At low temperature, the line associated to the trions recombination dominates the spectrum. The ratio between the intensities of the exciton line and trion line increases with the temperature increasing. At high temperature, the exciton line dominates the spectrum.

The spectra are analyzed with the procedure presented in §4.3.4. The temperature dependencies of the intensities of the trion and exciton lines are presented in figure 5.4. The intensity of the X- line is nearly constant until 40 K. Then it decreases regularly with the increase of temperature. The behavior of the intensity of the X line is more complex. At first, it is constant and then, it increases until 100 K. And finally, it decreases regularly at high temperature. The dashed lines correspond to the expression (4.8) and (4.9) of the previous chapter. We get a good agreement between the experimental data and the calculated intensities with 19.2 meV and 67 meV for respectively E_1 and E_2. These two values are close to the ones determined from dependency with temperature of the CW-PL intensities.

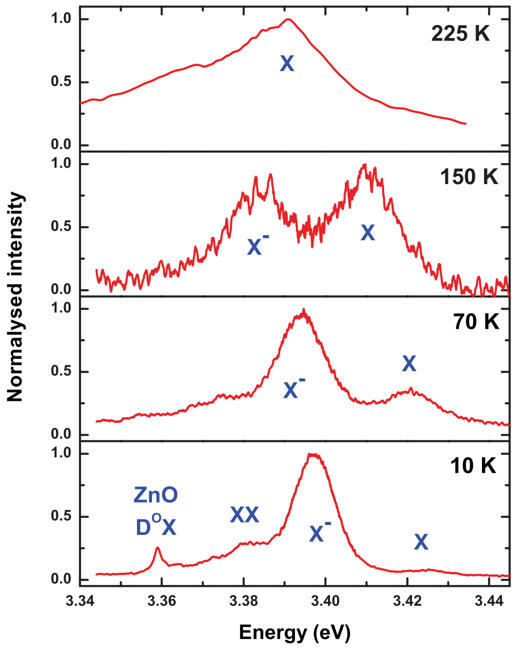

Figure 5.3: Time integrated spectra recorded at different temperatures ranged from 10 K to 225 K.

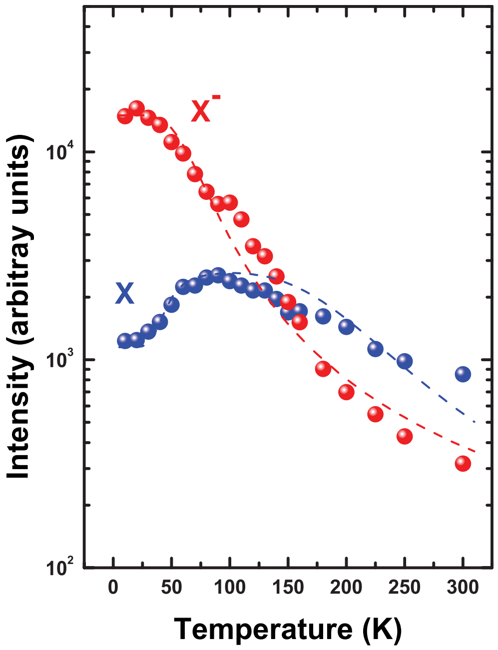

Figure 5.4: Intensity of the X- and X lines according to the temperature.

During this chapter, to interpret the photoluminescence decays, we shall consider the following scenario. At low temperature, the trions dominate the spectrum. With the temperature increase, the trions is dissociated in free excitons and free electrons. The non-radiative recombination process of the exciton is thermally activated with activation energy E_2.

5.2.2 Parameters involved in the PL time decays

From this study and from the temperature dependency of the CW-PL and the ITRPL, we can propose the following scheme (fig. 5.5) for the PL decay. The hypotheses are the following:

- the dissociation of the trion in a free exciton and electron is thermally activated;
- the non-radiative process concerns only the free excitons.

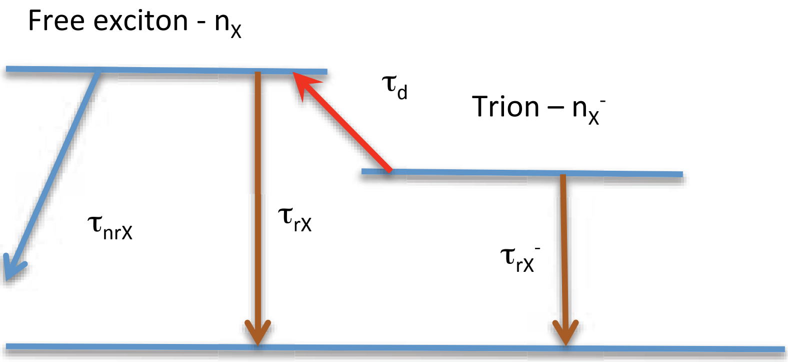

Figure 5.5: Schematic representation of the different recombination phenomena taking into account.

Where $n_{X^-, X}$ and τ_{rX^-}, τ_{rX} are respectively the density and radiative lifetime of the trion and the free exciton. τ_d is a lifetime associated to the dissociation of the trion. $\tau_{rX,}$ is the lifetime associated to non-radiative process. The two latter parameters are thermally activated. The evolution of the population of each level after the excitation pulse are governed by the following system of coupled equations:

$$\begin{cases} \dfrac{dn_{X^-}}{dt} = -\dfrac{n_{X^-}}{\tau_{rX^-}} - \dfrac{n_{X^-}}{\tau_d} \\ \dfrac{dn_X}{dt} = -\dfrac{n_X}{\tau_{rX}} - \dfrac{n_X}{\tau_{nrX}} + \dfrac{n_{X^-}}{\tau_d} \end{cases} \qquad (5.4)$$

From the equations (5.4) we get temporal evolution of the populations as:

$$\begin{aligned} n_{X^-}(t) &= A_1 \exp(-t/\tau_1) \\ n_X(t) &= A_2 \exp(-t/\tau_2) + A_3 \exp(-t/\tau_1) \end{aligned} \qquad (5.5)$$

where τ_1 and τ_2 are given by:

$$\begin{aligned} \frac{1}{\tau_1} &= \frac{1}{\tau_{rX^-}} + \frac{1}{\tau_d} \\ \frac{1}{\tau_2} &= \frac{1}{\tau_{rX}} + \frac{1}{\tau_{nrX}} \end{aligned} \qquad (5.6)$$

The temporal evolution of the trion population is a simple exponential decay with a temperature dependent decay time. Due to the coupling of the two equations, the temporal evolution of the exciton population is more complex and involves two decays times that are both temperature dependent.

5.2.3 Detailed study of PL decays

In this paragraph, we present a detailed study of PL decay time on the whole range of energies of the PL spectra for different temperatures. For this purpose we have carefully analyzed the PL line across the spectral window. In order to measure the PL decay lifetime we used a spectral window of 1 nm width, that correspond to an energy window with a width of about 9.4 meV. The signal to noise ratio is high enough to get valuable information. Moreover, more one order of magnitude change in the intensity is observed for all the spectra.

Low temperature. The PL spectrum recorded at 10 K is presented in fig. 5.6. In addition, the contributions to the spectrum of the different recombination process considered are also plotted. The PL decay times are obtained considering a mono-exponential decay. The procedure is illustrated in figure 5.7. At low energies, the PL decay is clearly mono-exponential, what is not the case at high PL energy. At 3.42 eV, the decay shows a fast component at short time following by a slower component. Unfortunately, it is not possible to resolve accurately the two lifetimes in this spectrum. However, it is not possible to determine accurately two lifetimes from the data. The combination of the two components results in a decrease of the PL decay time for high energies PL (see fig 5.6).

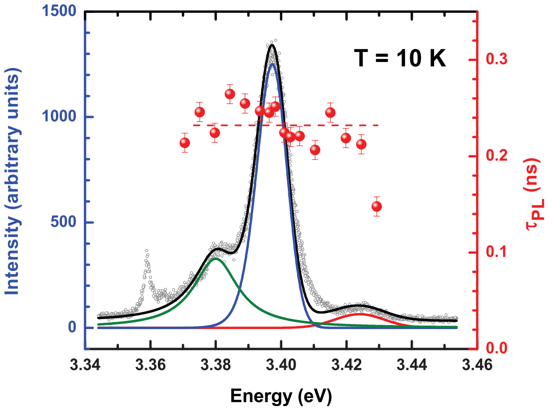

Figure 5.6: Photoluminescence spectra recorded at 10K. The solid lines correspond to contribution of the exciton (red), trion (blue) and biexciton (green) recombination to the PL spectrum. PL decay times according to the energy.

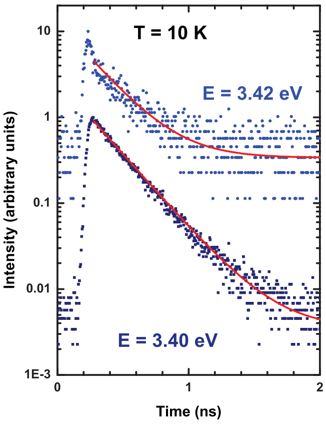

Figure 5.7: PL decay recorded at 10 K for two different PL energies. The solid lines correspond to the mono-exponential decay model.

These observations are consistent with the model. The intensity decay of photoluminescence associated to the trion is mono-exponential as expected, whereas the recombination of the exciton shows two regimes. The rapid one corresponds to the radiative recombination of free exciton whereas the slow one is due to the production of free exciton by trion dissociation.

Intermediate temperatures. We chose to present the results at two intermediate temperatures. At 70 K (fig. 5.8) the spectrum is still dominated by the trion contribution but the exciton contribution cannot be neglected. At 200 K (fig. 5.10), the spectrum shows the reverse situation, the exciton contribution dominates the spectrum and the trion contribution cannot be neglected. Between this two temperatures, the ratio between the intensities of the exciton line and the trion line increases. Despite this the PL decay time show a similar behavior according to the emission energy.

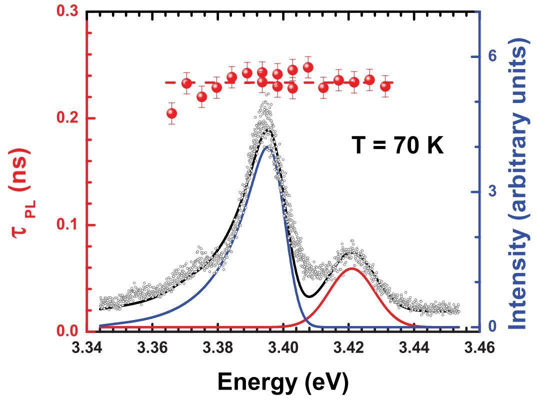

Figure 5.8: Photoluminescence spectra recorded at 70K. The solid lines correspond to contribution of the exciton (red) and trion (blue) recombination to the PL spectrum. PL decay times according to the energy.

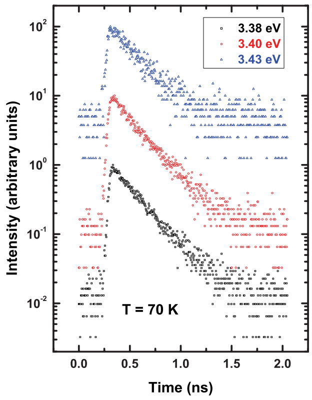

Figure 5.9: PL decay recorded at 70 K for three different PL energies.

At the two temperatures, the PL decays show a mono-exponential behavior (fig 5.9 and 5.11). Moreover, the PL decay times are nearly constant over the PL spectra. In a wide range of temperature the photoluminescence, associated to trion and free exciton, exhibits a similar temporal evolution.

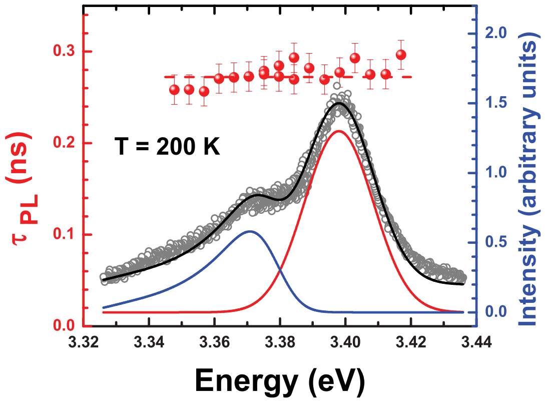

Figure 5.10: Photoluminescence spectra recorded at 200K. The solid lines correspond to contribution of the exciton (red) and trion (blue) recombination to the PL spectrum. PL decay times according to the energy.

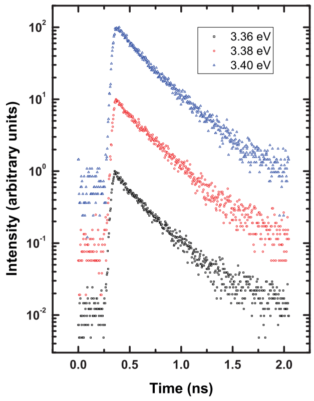

Figure 5.11: PL decay recorded at 200 K for three different PL energies.

High temperature. In this domain of temperature, the free exciton contribution dominates the PL spectrum as illustrated in fig. 5.12. At 300 K, the shape of the PL decays varies significantly with the energy. Fig. 5.13 presents two examples taken at two energies. At 3.37 eV, the PL decay is mono-exponential whereas it is bi-exponential for energy of 3.28eV. The results of the analysis of the PL decay are presented in fig. 5.12. For energies below 3.35 eV bi-exponential can be used to fit the PL decays. The PL decay times are presented for the short component (blue dots) and for the long component (black dots). The short component stays nearly constant until 3.31 eV whereas the long component increases. In this range of energy the PL spectrum is dominated by the trion contribution. Consequently, we conclude that the short lifetime is related to the trion.

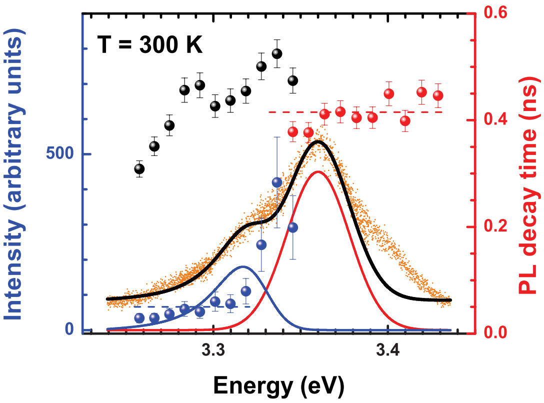

Figure 5.12: Photoluminescence spectra recorded at 300K. The solid lines correspond to contribution of the exciton (red) and trion (blue) recombination to the PL spectrum. PL decay times according to the energy. The bleu and black dots correspond to bi-exponential decays, the red one to mono-exponential decays.

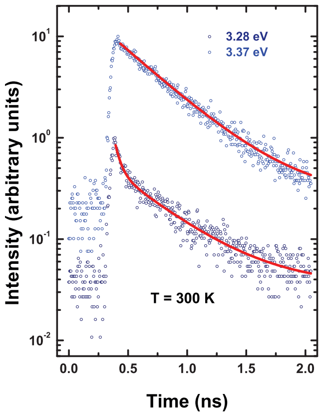

Figure 5.13: PL decay recorded at 300 K for two different PL energies.

For energies above 3.35 eV, the PL decay can be approximated with a mono-exponential. The decay lifetime stays nearly constant in this energy domain. Between 3.31 and 3.35 eV the short lifetime is increasing, the long lifetime has a value close to the one found for energies above 3.35 eV. For these energies both exciton and trion contribute to the photoluminescence intensity. Then is difficult to separate each contribution in the PL decay.

In conclusion, due to the overlap of the two PL lines, which increases with temperature, it is difficult to separate clearly the two contributions in the PL decays. In the intermediate temperature domain, the observed lifetime is a contribution of two mixed decays. Later in this chapter, the PL decay lifetime is determined using a 2 nm spectral window centered on the maximum of the PL peaks.

5.2.4 PL lifetime - temperature dependency

The photoluminescence decay with time recorded for a series of temperatures, going of 10K to 250K, are collected in fig. 5.14 and fig 5.15 for respectively the trion line and the exciton line. The decays are mono-exponential in the case of X^- line until 200 K. It becomes bi-exponential at

250 K. From 250 K to 50 K the decay of the X line shows a mono-exponential behavior whereas at 10 K it is not the case. For all the PL decays, the slope of the long component increases with temperature.

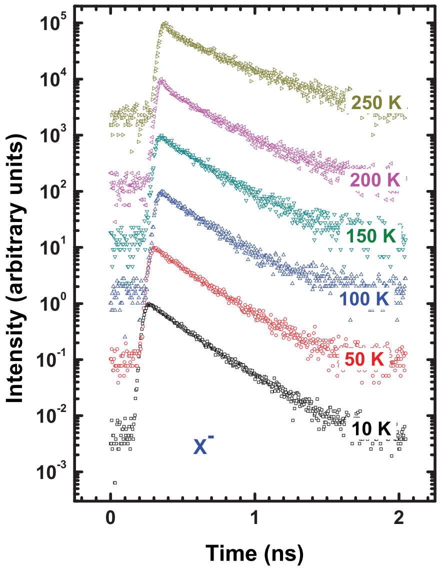

Figure 5.14: Normalized X- PL decay recorded at different temperatures.

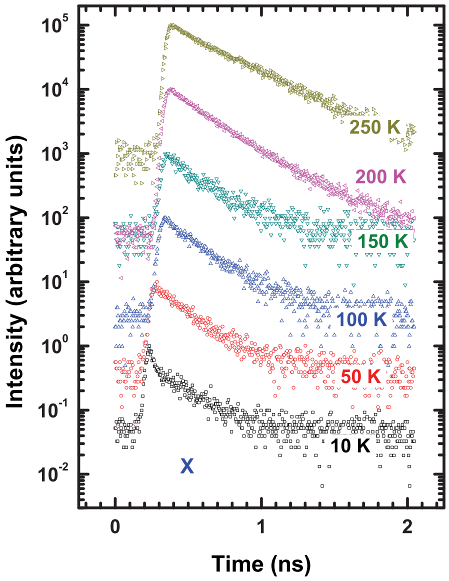

Figure 5.15: Normalized X PL decay recorded at different temperatures.

The PL decay lifetimes are gathered on fig. 5.16. Here, we report only the value of the long lifetimes. They are close to being constant for temperatures below 100 K. It is an indication that we have dealing, in this temperature range, with localized excitons complexes. The lifetimes start to increase linearly with temperature after 200 K with a slope of 1.1 ps/K.

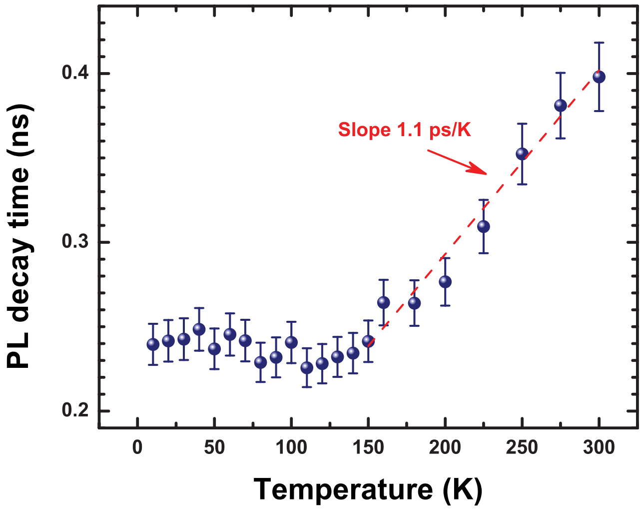

Figure 5.16: PL decay lifetimes according to the temperature.

This result is closed to the ones obtained in the case of non-polar quantum wells grown on M plane.[bea11b] The value of the slope of the linearly increase of the lifetime is smaller than the one reported for 1.7 nm width which is 7 ps/K. [bea11a] However, it can be noticed that in this last case the total intensity is constant with the temperature and consequently that non-radiative process are not involved in the PL decays. Here, the increase of the decay time of the photoluminescence comes along with a decrease of the intensity with the temperature. It is characteristic that non-radiative recombination become dominant in the disappearance of the signal of photoluminescence.

5.2.5 Discussion

In this part we are going to try to extract information on dependence in temperature of the lifetime. Here we deal with two populations in thermal equilibrium. For it we are separately going to consider the dynamics of recombination of the trion and the exciton.

Trion. The equation of evolution of the population of trion (5.1) is comparable to that of the evolution of a population of exciton that can recombine radiatively or non-radiatively. The thermal dissociation of the trion plays here the role of non-radiative channel. Thus, it is possible to obtain information directly from experimental data from the following equations:

$$\tau_{rX^-}(T) = \tau_{PL}\frac{I(0)}{I(T)} \quad (5.7)$$

$$\tau_d = \left(1/\tau_{PL} - 1/\tau_{rX^-}\right)^{-1} \quad (5.8)$$

However, it is necessary to be careful for the choice of the interval of temperature on which these equations can be used. We indicate earlier that from a certain temperature the decay time of the photoluminescence results from multiple phenomena. We shall restrict the domain of temperature in temperature lower than 80 K, at this temperature the exciton contributes for less of 30 % to the total signal of photoluminescence. In addition, we used also the short lifetime extracted from the PL decays of the trion measured at 300 K. The radiative lifetime, τ_{rX^-}, and the non-radiative rate, $\Gamma_{nrT} = 1/\tau_d$ are presented in figure 5.17. The blue dashed line corresponds to a linear increase of radiative lifetime with a slope of 7.1 ps/K for temperature above 50 K. This value is much higher than the apparent increase in lifetime and comparable to previously value reported for the exciton in non-polar quantum wells.[bea11a], [bea11b] The non-radiative recombination rate has an exponential behavior as expected. The activation energy is 17.8 meV. Such value is close to the trion binding energy and confirms our hypothesis that the diminution of the intensity of the trion line is mainly related to its thermal dissociation.

For temperature below 50 K, the radiative lifetime stay constant. In this case, we have to deal with localized trions. The energy of localization is set at 5 meV according to the CW-PL and ITRPL investigations. By using the same model as in the chapter three, we fit the experimental results. Both the PL decay time and the intensity of the trion signal are fitted using a value of

$N_D = 6x10^{12}\ cm^{-2}$. A reasonable agreement is observed between the calculations and the experimental values as shown in figure 5.18.

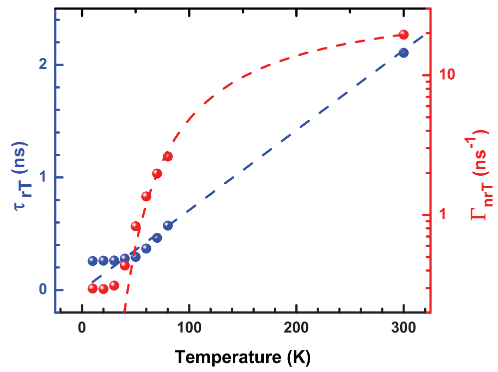

Figure 5.17: Radiative lifetime and non-radiative rate deduced from the experimental data.

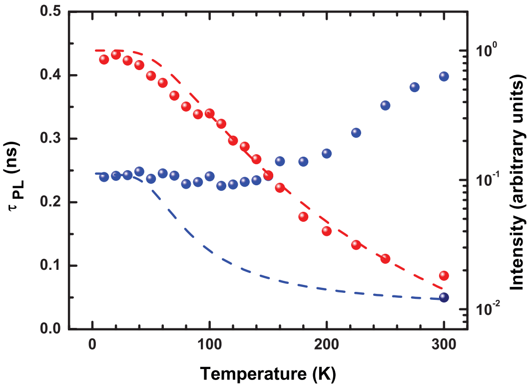

Figure 5.18: Comparison between the calculated value of intensity and PL decay time with experimental data.

Exciton. In this case, the situation is more complex. The model previously used cannot be used to describe the PL decays of the exciton. In fact, here we deal with competition between the exciton disappearances due to both radiative and non-radiative recombination and the creation of exciton by thermal dissociation of the trions.

At low temperature, the recombination of the trion dominates the radiative processes. The exciton lifetime is very short. However, during the duration of the decline of the PL related to trions some of them are dissociated and excitons are created. These excitons recombine radiatively quickly and the PL decay of the exciton line shows the same PL decay time as the trion line. At these temperatures, the decays of exciton photoluminescence are non exponential.

On the other side of the domain of temperature, the situation is inverted. The effective lifetime of the trion is dominated by the dissociation time and it is very short. Due to this short time the trions can be formed during the decline. The decay of PL of the trion is not mono-exponential and follows at long time the one of the exciton. As we have done in the case of the trion, we can define a restricted domain of temperature in order to obtain value on radiative and non-radiative processes of the exciton. At temperature above 200 K, the trions recombination participate for less of 30 % to the total signal. By using an unrefined approximation from the equations (5.6) and (5.7) we found a value of about 10 ps/K for the increase of the radiative lifetime and around 20 meV for the energy of activation of the non-radiative processes. The increase in temperature for the exciton is higher than the value of the trion. The activation energy value of the non-radiative processes is smaller than the value deduced from CW-PL. However, it is necessary to be careful with these values because their determinations are based on very strong approximations.

At intermediate temperatures, the competition between the different phenomena involve results in a photoluminescence decays of trion and exciton very close. In this temperature range, the effective lifetime of the trion decreases with the temperature in the same time the exciton radiative lifetime shows an increasing. The two lifetimes become commensurable and then cannot be separated in the fitting process of the photoluminescence declines.

5.3 Conclusion

The recombination dynamic of the trions and the excitons show a complex behavior as function temperature. The detailed analyze through the PL line presents different configuration for the time decays. At low temperature, the intensity of the decline is non exponential for the exciton and mono-exponential for the trion. At intermediates temperatures, both decline are mono-exponential. And finally at high temperature, the decline of the exciton is mono-exponential whereas the one of the trion is bi-exponential. The main PL lifetime is constant at low temperature signature of particles localization. At temperature higher than 100 K it increases linearly with the temperature.

The radiative lifetime of both the trion and the exciton are found increasing linearly with temperature. It can be noticed here that the apparent increase of the PL decay time does not correspond to the increase of the lifetimes.

Conclusion

When heterostructure wurtzite was grown according to the axis c present an important internal electric field. This one has a disastrous effect on the optical properties of the quantum wells; in particular the radiative efficiency is dramatically strongly impacted. In order to avoid the effects of the internal electric field in heterostructure it is possible to grow them along the non-polar directions, i.e., with the polar c-direction lying in the growth plane. ZnO/(Zn, Mg)O QWs without internal electric field have been successfully grown on the A-plane $(11\bar{2}0)$ or the M-plane $(1\bar{1}00)$.

In this manuscript, we present a detailed study of the optical properties of non-polar quantum well of ZnO/(Zn, Mg)O grown along the A axis on a ZnO substrate. For this purpose, different technique of optical spectroscopy are implemented (reflectivity, continuous photoluminescence (CW-PL), photoluminescence resolved in time (TRPL)).

The first results concern the barrier of (Zn, Mg)O. The signal of photoluminescence of the barrier is less polarized than that of the substrate, the polarization of which is superior to 95 % as expected in the case of a non-polar sample. We confirm the important role played by the effects of localization of exciton in this type of ternary alloy. From the results of the of time-resolved photoluminescence measures, we propose a model for the behavior of the exciton in this material. At low temperature, excitons are localized in potential fluctuations. Two excitonic states with lifetime very different are involved. With the increase of temperature the distribution of the populations of both states changes and is translated by an evolution of the PL decay times with the temperature. The evolutions in temperature of the intensity and the decay time of PL are modeled. In the model are included the effects of localization of the exciton, their distribution between both localized states, the dependence in temperature of the lifetime of the free exciton as well as the temperature dependency of non-radiative process. This study highlights the importance of the energy of the photons used for the optical excitation. In particular, in the case of the TRPL measurements, it is important for characterizing strictly the quantum well to use photons of lower energy the band gap of the barriers.

The PL signal of the quantum well presents three contributions. To identify the nature of the transitions involved in each of them, different measurements were realized. In a first step, the results obtained in continuous optical spectroscopy are analyzed according to the polarization of the out coming signal and to the density of excitation. The entire PL signal arising from the quantum well is polarized at close to 100 %. The temperature dependence investigation of CW-PL shows that for temperature higher than 150 K a new exciton state is populated. This new line has a polarization in quadrature with the main lines. It is attributed to the recombination of the C exciton.

The consideration of the results of reflectivity and the calculation by the variational method of the energy of the fundamental transition allows identifying the signal with higher energy as resulting from the recombination of the free exciton in the well. On the basis of the results of CW-PL according to the density of excitation the contribution low energy is clearly due to the recombination of the biexciton (two exciton in interaction). As regards the main peak situated in an intermediate energy the identification is more delicate. It cannot be attributed to the recombination of localized exciton in a fluctuation in width of well (1-2 ML) because the difference in energy with the emission attributed to the free exciton is too important if it is compared with the calculation. When the temperature increases, the decrease of the intensity of PL of this line is accompanied with an increase of the intensity of the line attributed to the free exciton. This indicates clearly the excitonic nature of the recombination partner in this line. Moreover, the line shape of the PL line is dissymmetric with a tail at low energy, which varies with temperature. It is characteristic of the line of PL attributed to the recombination of trion (complex form by an exciton in interaction with a free carrier). As our samples are n-type we identify this line to the recombination of negatively charged trion. To finish we studied dynamics of recombination of the trions and excitons. The lifetime increases linearly with temperature for both the exciton and the trion.

In conclusion, we have demonstrated that the PL signal of a non-polar quantum well arise from the recombination of exciton and exciton complexes such as negatively charged trion and biexciton. In order to characterize the PL dynamic in these quantum wells a particular attention should be devoted to the energy of the excitation photons, it will be at energy below the barriers band gap. In regard to these conclusions the interpretation of results on non-polar quantum well should be revisited.

References

[Ada85] S Adachi. *GaAs, AlAs, and Al(x)Ga(1-x)As material parameters for use in research and device applications*. J. Appl. Phys. **58**, 1–29 (1985).

[and91] L.C. Andreani, F. Tassone, and F. Bassani. *Radiative lifetime of free excitons in quantum wells.* Solid State Commun. **77**, 641 (1991).

[bea11a] L. Beaur, T. Bretagnon, B. Gil, A. Kavokin, T. Guillet, C. Brimont, D. Tainoff, M. Teisseire, J.M. Chauveau. *Exciton radiative properties in nonpolar homoepitaxial ZnO/(Zn,Mg)O quantum wells.* Phys. Rev. B **84**, 165312 (2011). DOI : 10.1103/PhysRevB.84.165312

[bea11b] L. Beaur. *Propriétés excitoniques de puits quantiques ZnO/(Zn,Mg)O*. PhD thesis - Université de Montpellier 2 (2011).

[bea13] L. Beaur, T. Bretagnon, T. Guillet, C. Brimont, M. Gallart, B. Gil, P. Gilliot, C. Morhain. *Phonon-assisted exciton formation in ZnO/(Zn, Mg)O single quantum wells grown on C-plane oriented substrates*. Journal of Luminescence **136**, 355 (2013). DOI: 10.1016/j.jlumin.2012.11.010

[bra20] WL Bragg. *The crystalline structure of zinc oxide*. Philos. Mag. 647 (1920).

[bre06a] T. Bretagnon, P. Lefebvre, P. Valvin, B. Gil, C. Morhain, X.D. Tang. *Time resolved photoluminescence study of ZnO/(Zn,Mg)O quantum wells.* J. Cryst. Growth **287**, 12 (2006). DOI: 10.1016/j.jcrysgro.2005.10.034

[bre06b] T. Bretagnon, P. Lefebvre, P. Valvin, R. Bardoux, T. Guillet, T. Taliercio, B. Gil, N. Grandjean, F. Semond, B. Damilano, A. Dussaigne, and J. Massies. *Radiative lifetime of a single electron-hole pair in GaN/AlN quantum dots*. Phys. Rev. B **73**, 113304 (2006). DOI: 10.1103/PhysRevB.73.113304

[bre07] T. Bretagnon, P. Lefebvre, T. Guillet, T. Taliercio, B. Gil and C. Morhain. *Barrier composition dependence of the internal electric field in ZnO/*$Zn_{1-x}Mg_xO$ *quantum wells*. Appl. Phys. Lett. **90**, 201912 (2007). DOI: 10.1063/1.2740576

[bre14] T. Bretagnon. *Optical properties of ZnO/(Zn, Mg)O quantum wells.* Turk. J. Phys. **38**, 420 (2014). doi:10.3906/z-1407-17

[bri73] W. F. Brinkman, T. M. Rice, and B. Bell, Phys. Rev. B **8**, 1570 (1973).

[bri99] D. Brinkmann J. Kudrna, P. Gilliot, B. Hönerlage, A. Arnoult, J. Cibert, and S. Tatarenko. *Trion and exciton dephasing measurements in modulation-doped quantum wells: A probe for trion and carrier localization.* Phys. Rev. B **60**, 4474 (1999).

[cha03] S. Charbonneau, T. Steiner, M. L. W. Thewalt, Emil S. Koteles, J. Y. Chi, and B. Elman. *Optical investigation of biexcitons and bound excitons in Gaks quantum wells.* Phys. Rev. B **38**, 3583 (1988)

[cha07] J.M. Chauveau, D.A. Buell, M. Laugt, P. Vennegues, M. Teisseire-Doninelli, S. Berard-Bergery, C. Deparis, B. Lo, B. Vinter, C. Morhain. *Growth of non-polar ZnO/(Zn,Mg)O quantum well structures on R-sapphire by plasma-assisted molecular beam epitaxy*. J. Cryst. Growth **301–302**, 366 (2007). DOI: 10.1016/j.jcrysgro.2006.11.320

[cha08] J.-M. Chauveau, P. Vennéguès, M. Laügt, C. Deparis, J. Zuniga-Perez, and C. Morhain. *Interface structure and anisotropic strain relaxation of nonpolar wurtzite (112¯0) and (101¯0) orientations: ZnO epilayers grown on sapphire.* J. Appl. Phys. **104**, 073535 (2008). DOI: 10.1063/1.2996248

[cha10] J.M. Chauveau, M. Teisseire, H. Kim-Chauveau, C. Deparis, C. Morhain, B. Vinter. *Benefits of homoepitaxy on the properties of nonpolar (Zn,Mg)O/ZnO quantum wells on a-plane ZnO substrates*. Appl. Phys. Lett. **97**, 081903 (2010). DOI: 10.1063/1.3481078

[cha13] J.M. Chauveau, Y. Xia, I. Ben Taazaet-Belgacem, M. Teisseire, B. Roland, M. Nemoz, J. Brault, B. Damilano, M. Leroux, B. Vinter. *Built-in electric field in ZnO based semipolar quantum wells grown on (101-2) ZnO substrates.* Appl. Phys. Lett. **103**, 262104 (2013). DOI: 10.1063/1.4851116

[che10] A. Chernikov, S.Horst, M.Koch, K.Volz, S.Chatterjee, S.W.Koch, T.A.Wassner, B. Laumer, M.Eickhoff. *Investigation of carrier dynamics in* $Zn_{1-x}Mg_xO$ *by time-resolved photoluminescence*. Journal of Luminescence **130** 2256 (2010).

[che16] H.R. Chen, C.Y. Tsai, Y.C. Huang, C.C. Kuo, H.C. Hsu and W.F. Hsieh. *Optical properties of one- and two-dimensional excitons in m-plane ZnO/MgZnO multiple quantum wells*. J. Phys. D: Appl. Phys. **49**, 095105 (2016). DOI:10.1088/0022-3727/49/9/095105

[cho73] Kikuo Cho. *Emission line shapes of exciton molecules in direct and indirect gap materials*. Opt. Commun. **8**, 412 (1973).

[chi03] C. H. Chia, T. Makino, K. Tamura, Y. Segawa, M. Kawasaki, A. Ohtomo, and H. Koinuma. *Confinement-enhanced biexciton binding energy in ZnO/ZnMgO multiple quantum wells*. Appl. Phys. Lett. **82**, 1848 (2003). DOI: 10.1063/1.1561158

[chi11] S.F. Chichibu, K. Hazu, Y. Kagamitani, T. Onuma, D. Ehrentraut, T. Fukuda, T. Ishiguro. *Time-Resolved Photoluminescence of a Two-Dimensional Electron Gas in an Al 0.2 Ga 0.8 N/GaN Heterostructure Fabricated on Ammonothermal GaN Substrates*. Appl. Phys. Express. **4** (2011) 45501. DOI:10.1143/APEX.4.045501.

[chu95] T.L. Chu, S.S. Chu, *Thin film II-VI photovoltaïcs*. Solid State Electronics, **38**, 3, 533 (1995).

[cit92a] D.S. Citrin. *Long intrinsic radiative lifetimes of excitons in quantum wires*. Phys. Rev. Lett. **69**, 3393 (1992).

[cit92b] D.S. Citrin. *Homogeneous-linewidth effects on radiative lifetimes of excitons in quantum wells.* Solid State Commun. **84**, 281 (1992).

[ciu00] V. Ciulin, P. Kossacki, S. Haacke, J.-D. Ganière, B. Deveaud, A. Esser, M. Kutrowski and T. Wojtowicz. *Radiative behavior of negatively charged excitons in CdTe-based quantum wells: A spectral and temporal analysis.* Phys. Rev. B **60**, R16 310 (2000).

[col01] Giuliano Coli and K. K. Bajaj. *Excitonic transitions in ZnO/MgZnO quantum well heterostructures.* Appl. Phys. Lett. **78** (19), 2861 (2001). DOI: 10.1063/1.1370116

[col06] V.A. Coleman, C. Jagadish, *Basic Properties and Applications of ZnO, Zinc Oxide Bulk*, Thin Film. Nanostructures. (2006) 1–20. DOI:10.1016/B978-008044722-3/50001-4.

[cor11] P. Corfdir, J. Levrat, A. Dussaigne, P. Lefebvre, H. Teisseyre, I. Grzegory, T. Suski, J.-D. Ganière, N. Grandjean, and B. Deveaud-Plédran. *Intrinsic dynamics of weakly and strongly confined excitons in nonpolar nitride-based heterostructures*. Phys. Rev B **83**, 245326 (2011). DOI: 10.1103/PhysRevB.83.245326

[dav06] Jeffrey A. Davis, Lap Van Dao, Xiaoming Wen, Peter Hannaford, V. A. Coleman, H. H. Tan, C. Jagadish, K. Koike, S. Sasa, M. Inoue, and M. Yano. *Observation of coherent biexcitons in ZnO/ZnMgO multiple quantum wells at room temperature*. Appl. Phys. Lett. **89**, 182109 (2006). DOI: 10.1063/1.2372747

[des98] S. Desgreniers. *High-density phases of ZnO: Structural and compressive parameters.* Phys. Rev. B, **58**, 21, 14102 (1998).

[din74] R Dingle, W Wiegmann, and CH Henry. *Quantum States of Confined Carriers in Very Thin Al(x)Ga(1-x)As - GaAs – Al(x)Ga(1-x)As Heterostructures.* Phys. Rev. Lett **33**, 827–830 (1974).

[ess00a] A. Esser, E. Runge, R. Zimmermann, and W. Langbein. *Trions in GaAs Quantum Wells: Photoluminescence Lineshape Analysis.* Phys. Status Solidi A **178**, 489 (2000).

[ess00b] A. Esser, E. Runge, R. Zimmermann, and W. Langbein. *Photoluminescence and radiative lifetime of trions in GaAs quantum wells*. Phys. Rev. B **62**, 8232 (2000).

[eyt98] G. Eytan, Y. Yayon, M. Rappaport, H. Shtrikman, and I. Bar-Joseph. *Near-Field Spectroscopy of a Gated Electron Gas: A Direct Evidence for Electron Localization*. Phys. Rev. Lett. **81**, 1666 (1998).

[fel87] J. Feldmann, G. Peter, E.O. Göbel, P. Dawson, K. Moore, C. Foxon, and R.J. Elliott. *Linewidth dependence of radiative exciton lifetimes In quantum wells.* Phys. Rev. Lett. **59**, 2337 (1987).

[fin95] G. Finkelstein, H. Shtrikman, I. Bar-Joseph, *Optical spectroscopy of a two-dimensional electron gas near the metal-insulator transition*, Phys. Rev. Lett. **74** (1995) 976–979. DOI:10.1103/PhysRevLett.74.976.

[fin98] G. Finkelstein, V. Umansky, I. Bar-Joseph, V. Ciulin, S. Haacke, J.-D. Ganière, and B. Deveaud. *Charged exciton dynamics in GaAs quantum wells*. Phys. Rev. B 58, 12657 (1998).

[fox14] M. Fox, *Optical Properties of Solids*. Am. J. Phys. **70** (2014) 1–415. DOI:10.1119/1.1691372.

[fu88] Q Fu, D Lee, A Mysyrowicz, AV Nurmikko, RL Gunshor, and LA Kolodziejski. *Excitonic molecules in ZnSe quantum wells*. Phys. Rev. B **37**, 8791–8794 (1988).

[gil00] B. Gil, P. Lefebvre, H. Morkoç. *Strain effects in GaN epilayers*. C. R. Acad. Sci. Paris, t. 1, Série IV, 51 (2000).

[gou79] P. L. Gourley and J. P. Wolfe. *Thermodynamics of excitonic molecules in silicon*. Phys. Rev. B 20, 3319 (1979)

[gop06] P. Gopal, N.A. Spaldin. *Polarization, Piezoelectric Constants, and Elastic Constants of ZnO, MgO, and CdO*. J. Electron. Mater. **35** (4), 538 (2006).

[gru03] T. Gruber, C. Kirchner, R. Kling, F. Reuss, A. Waag, F. Bertram, D. Forster, J. Christen, M. Schreck, *Optical and structural analysis of ZnCdO layers grown by metalorganic vapor-phase epitaxy*, Appl. Phys. Lett. **83** (2003) 3290–3292. DOI:10.1063/1.1620674.

[gru04] Th. Gruber, C. Kirchner, R. Kling, F. Reuss, A. Waag. *ZnMgO epilayers and ZnO-ZnMgO quantum wells for optoelectronic applications in the blue and UV spectral region.* Appl. Phys. Lett. **84** (26) 5359 (2004). DOI: 10.1063/1.1767273

[gru06] M. Grundmann, The physics of semiconductors: An introduction including devices and nanophysics, (2006). DOI:10.1007/3-540-34661-9.

[gru09] Marius Grundmann and Christof P. Dietrich. *Lineshape theory of photoluminescence from semiconductor alloys*. J. Appl.Phys. **123**, 521 (2009). https://doi.org/10.1063/1.3267875

[gru16] M. Grundmann, and J. Zuniga-Perez. *Pseudomorphic ZnO-based heterostructures: From polar through all semipolar to nonpolar orientations*. Phys. Status Solidi B **253** (2), 351 (2016). DOI: 10.1002/pssb.201552535

[gru06] M. Grundmann, The physics of semiconductors: An introduction including devices and nanophysics, (2006). DOI:10.1007/3-540-34661-9.

[gu07] X. Q. Gu, L. P. Zhu, Z. Z. Ye, H. P. He, Y. Z. Zhang, F. Huang, M. X. Qiu, and Y. J. Zeng, F. Liu, W. Jaeger. *Room-temperature pho-toluminescence from ZnO/ZnMgO multiple quantum wells grown on Si(111) substrates*. Appl. Phys. Lett. **91**, 022103 (2007). DOI: 10.1063/1.2755922

[gur91] M Gurioli, A Vinattieri,M Colocci, C Deparis, J Massies, G Neu, A Bosacchi, and S Franchi. *Temperature dependence of the radiative and nonradiative recombination time in GaAs/Al(x) Ga(1-x) As quantum-well structures.* Phys. Rev. B **44**, 3115 (1991).

[han88] E Hanamura. *Rapid radiative decay and enhanced optical nonlinearity of excitons in a quantum well*. Phys. Rev. B **38**, 1228 (1988).

[haz03] K. Hazu, T. Sota, K. Suzuki, S. Adachi, SF. Chichibu, G. Cantwell, D. B. Eason, D. C. Reynolds and C. W. Litton. *Strong biexcitonic effects and exciton-exciton correlations in ZnO*. Phys. Rev. B **68**, 033205 (2003)

[hei07] S. Heitsch, G. Zimmermann, D. Fritsch, C. Sturm, R. Schmidt-Grund, G. Schulz, H. Hochmuth, D. Spermann, G. Benndorf, B. Rheinländer, Th Nobis, M. Lorenz, M. Grundmann. *Luminescence and surface properties of thin films grown by pulsed laser deposition*. J. Appl. Phys. **101**, 083521 (2007). doi: 10.1063/1.2719010.

[hel93] R. Hellmann, M. Koch, J. Feldmann, S. T. Lundiff, E. O. Gobel, D. R. Yakovler, A. Waag, and G. Landwehr. *Homogeneous linewidth of excitons in semimagnetic CdTe/*$Cd_{1-x}Mn_xTe$ *multiple quantum wells*. Phys. Rev. B **48**, 2847 (1993).

[hof97] A Hoffmann. *Dynamics of excited states in GaN*. Mat. Sci. Eng. B **43**, 185–191 (1997).

[hu15] Y. Hu, B. Cai, Z. Hu, Y. Liu, S. Zhang, H. Zeng, *The impact of Mg content on the structural, electrical and optical properties of MgZnO alloys: A first principles study*. Curr. Appl. Phys. **15,** 423 (2015). DOI:10.1016/j.cap.2015.01.015.

[jaf93] J.E. Jaffe, A.C. Hess. *Hartree-Fock study of phase changes in ZnO at high pressure.* Phys. Rev. B, **48**, 7903, (1993).

[joh96] M.A.L. Johnson, Shizuo Fujita, W.H. Rowland JR., W.C. HUGHES, J.W. COOK JR., and J.F. Schetzina. *MBE Growth and Properties of ZnO on Sapphire and SiC Substrates*. Journal of Electronic Materials **25** (5), 855 (1996).

[kam16] A. Kaminska, A. Duzynska, M. Nowakowska, A. Suchocki, T.A. Wassner, B. Laumer, M. Eickhoff. *Luminescent properties of ZnO and ZnMgO epitaxial layers under high hydrostatic pressure*. Journal of Alloys and Compounds **672**, 125 (2016). DOI 10.1016/j.jallcom.2016.02.128

[kaw96] Yoichi Kawakami, Zhi Gang Peng, Yukio Narukawa, Shizuo Fujita, Shigeo Fujita, and Shuji Nakamura. *Recombination dynamics of excitons and biexcitons in a hexagonal GaN epitaxial layer*. Appl. Phys. Lett. **69** (10), 1414 (1996).

[khe93] K. Kheng, R.T. Cox, Y. Merle d'Aubigne, Franck Bassani, K. Saminadayar, and S. Tatarenko. *Observation of Negatively Charged Excitons* X^- *in Semiconductor Quantum Wells.* Phys. Rev. Lett. **71**, 1752 (1993).

[ko00] H. J. Ko, Y. F. Chen, T. Yao, K. Miyajima, A. Yamamoto, and T. Goto. *Biexciton emission from high-quality ZnO films grown on epitaxial GaN by plasma-assisted molecular-beam epitaxy.* Appl. Phys. Lett. **77**, 4, 537 (2000).

[ko10] T.S. Ko, T.C. Lu, L.F. Zhuo, W.L. Wang, M.H. Liang, H.C. Kuo, S.C. Wang, L. Chang, D.Y. Lin. *Optical characteristics of a-plane ZnO/Zn0.8Mg0.2O multiple quantum wells grown by pulsed laser deposition*. J. Appl. Phys. **108**, 073504 (2010). DOI: 10.1063/1.3488898

[koi05] K Koike, K Hama, I Nakashima, G Takada, K Ogata, S Sasa, M Inoue, and M Yano. *Molecular beam epitaxial growth of wide bandgap ZnMgO alloy films on (1 1 1)-oriented Si substrate toward UV-detector applications*. J. Cryst. Growth **278**, 288–292 (2005).

[koi06] K. Koike, G.-Y. Takada, K. Fujimoto, S. Sasa, M. Inoue and M. Yano. *Characterization of* $[ZnO]_m[ZnMgO]_n$ *multiple quantum wells grown by molecular beam epitaxy*. Physica E **32**, 191 (2006).

[kon08] J. F. Kong, W. Z. Shen, Y. W. Zhang, C. Yang, and X. M. Li. *Resonant Raman scattering probe of alloying effect in ZnMgO thin films*. Appl. Phys. Lett. **92**, 191910 (2008). DOI 10.1063/1.2930676

[kim94] JC Kim, DR Wake, and JP Wolfe. *Thermodynamics of biexcitons in a GaAs quantum well*. Phys. Rev. B **50**, 15099 (1994).

[kim00] H. S. Kim, R. A. Mair, J. Li, J. Y. Lin, and H. X. Jiang. *Time-resolved photoluminescence studies of* $Al_xGa_{1-x}N$ *alloys*. Appl. Phys. Lett. **76** (10), 1252 (2000). doi: 10.1063/1.126000

[kim09] J. H. Kim, S. K. Han, S. I. Hong, S. K. Hong, J. W. Lee, J. Y. Lee, J. H. Song, J. S. Park, and T. Yao, J. Vac. Sci. Technol. B **27**, 1625 (2009).

[lam58] M.A. Lampert. *Mobile and immobile effective mass-particle complexes in nonmetallic solid.* Phys. Rev. Letters **1**, 450 (1958).

[lan10] T Langer, H Jönen, D Fuhrmann, U Rossow, and A Hangleiter. *Recombination of free excitons in polar and non-polar nitride quantum wells.* JPCS **210**, 012056 (2010).

[lan12] M. Lange, J. Kupper, C. P. Dietrich, M. Brandt, M. Stölzel, G. Benndorf, M. Lorenz, and M. Grundmann. *Exciton localization and phonon sidebands in polar ZnO/MgZnO quantum wells*. Phys. Rev. B **86**, 045318 (2012). DOI: 10.1103/PhysRevB.86.045318

[lau10] S. Lautenschlaeger, S. Eisermann, M.N. Hofmann, U. Roemer, M. Pinnisch, A. Lau-fer, B.K. Meyer, H. von Wenckstern, A. Lajn, F. Schmidt, M. Grundmann, J. Blaesing, A. Krost. *Morphological, structural and electrical investigations on non-polar a-plane ZnO epilayers*. J. Cryst. Growth **312**, 2078 (2010). DOI: 10.1016/j.jcrysgro.2010.04.029

[lau11] B. Laumer, T. A. Wassner, F. Schuster, M. Stutzmann, J. Schörmann, M. Rohnke, A. Chernikov, V. Bornwasser, M. Koch, S. Chatterjee, and M. Eickhoff. *Exciton confinement in homo- and heteroepitaxial ZnO/*$Zn_{1-x}Mg_xO$ *quantum wells with* $x<0.1$. J. Appl. Phys. **110**, 093513 (2011). doi:10.1063/1.3658020

[lau13] B. Laumer, F. Schuster, M. Stutzmann, A. Bergmaier, G. Dollinger, M. Eickhoff. *Accurate determination of optical bandgap and lattice parameters of* $Zn_{1-x}Mg_xO$ *epitaxial films* ($0\leq x\leq 0.3$) *grown by plasma-assisted molecular beam epitaxy on a-plane sapphire.* Journal of Applied Physics **113**, 233512 (2013). DOI 10.1063/1.4811693

[lef98] P Lefebvre, J Allegre, B Gil, A Kavokine, H Mathieu, W Kim, A Salvador, A Botchkarev, and H Morkoç. *Recombination dynamics of free and localized excitons in GaN/Ga(0.93) Al(0.07) N quantum wells*. Phys. Rev. B **57**, 9447–9450 (1998).

[lef01] P. Lefebvre, A. Morel, M. Gallart, T. Taliercio, J. Allègre, B. Gil, H. Mathieu, B. Damilano, N. Grandjean, J. Massies. Appl. Phys. Lett. **78** (2001) 1252, and references cited therein.

[ler99a] M. Leroux, N. Grandjean, J. Massies, B. Gil, P. Lefebvre, P. Bigenwald. *Barrier-width dependence of group-III nitrides quantum-well transition energies.* Phys. Rev. B, **60**, 1496 (1999).

[ler99b] M. Leroux, N. Grandjean, B. Beaumont, G. Nataf, F. Semond, J. Massies, P. Gibart. *Temperature quenching of photoluminescence intensities in undoped and doped GaN*. J. Appl.Phys. **86**, 3721 (1999).

[li2003] J. Li, K.B. Nam, M.L. Nakarmi, J.Y. Lin, H.X. Jiang, P. Carrier, S.H. Wei, *Band structure and fundamental optical transitions in wurtzite AlN*, Appl. Phys. Lett. **83** (2003) 5163–5165. DOI:10.1063/1.1633965.

[li10] S.M. Li, B.J. Kwon, H.S. Kwack, L.H. Jin, Y.H. Cho, Y.S. Park, M.S. Han, Y.S. Park. *Optical transition dynamics in ZnO/ZnMgO multiple quantum well structures with different well widths grown on ZnO substrates.* J. Appl. Phys **107**, 033513 (2010) DOI: 10.1063/1.3284959

[lia67] W. Y. Liang. *Transmission spectra of ZnO single Crystal.* Phys. Rev. Lett. **20,** 59–61(1967).

[lia68] W. Y. Liang and A. D. Yoffe. *Transmission spectra of ZnO single crystals*. Phys. Rev. Lett. 20, 59 (1968).

[liu09] Z.L. Liu, Z.X. Mei, T.C. Zhang, Y.P. Liu, Y. Guo, X.L. Du, A. Hallen, J.J. Zhu, A.Y. Kuznetsov, *Solar-blind 4.55 eV band gap* $Mg_{0.55}Zn_{0.45}O$ *components fabricated using quasi-homo buffers*. J. Cryst. Growth. **311,** 4356–4359 (2009). DOI:10.1016/j.jcrysgro.2009.07.030.

[lu05] Y.M. Lu, C.X. Wu, Z.P. Wei, Z.Z. Zhang, D.X. Zhao, J.Y. Zhang, Y.C. Liu, D.Z. Shen, X.W. Fan. *Characterization of ZnO/*$Mg_{0.12}Zn_{0.88}O$ *heterostructure grown by plasma-assisted molecular beam epitaxy.* Journal of Crystal Growth **278**, 299 (2005). doi:10.1016/j.jcrysgro.2005.01.023

[mal07] A. Malashevich, D. Vanderbilt. *First-principles study of polarization in* $Zn_{1-x}Mg_xO$. Phys. Rev. B **75**, 045106 (2007). DOI: 10.1103/PhysRevB.75.045106

[mak00] T. Makino, C.H. Chia, N.T. Tuan, H.D. Sun, Y. Segawa, M. Kawasaki, A. Ohtomo, K. Tamura, H. Koinuma. *Room-temperature luminescence of excitons in ZnO/(Mg, Zn)O multiple quantum wells on lattice-matched substrates.* Appl. Phys. Lett. **77** (7), 975 (2000). DOI: 10.1063/1.1289066

[mak01] T. Makino and Y. Segawa, M. Kawasaki, A. Ohtomo, R. Shiroki, and K. Tamura, T. Yasuda and H. Koinuma. *Band gap engineering based on* $Mg_xZn_{1-x}O$ *and* $Cd_yZn_{1-y}O$ *ternary alloy film.* Appl. Phys. Lett. **78** (9), 1237 (2001).

[mak02] T. Makino, K. Tamura, C. H. Chia, Y. Segawa, M. Kawasaki, A. Ohtomo, and H. Koinuma. *Size dependence of exciton-longitudinal-optical-phonon coupling in ZnO/$Mg_{0.27}Zn_{0.73}O$ quantum wells*. Phys. Rev B **66** (23), 233305 (2002). DOI: 10.1103/PhysRevB.66.233305

[mak02b] T. Makino, K. Tamura, C. H. Chia, Y. Segawa, M. Kawasaki, A. Ohtomo, and H. Koinuma. *Radiative recombination of electron-hole pairs spatially separated due to quantum-confined Stark and Franz-Keldish effects in ZnO/Mg0.27Zn0.73O quantum wells*. Appl. Phys. Lett. **81** (13), 2355 (2002). DOI: 10.1063/1.1507606.

[mak04] T. Makino, A. Ohtomo, C. H. Chia, Y. Segawa, H. Koinuma and M. Kawasaki. *Internal electric field effect on luminescence properties of ZnO/(Mg,Zn)O quantum wells*. Physica E **21**, 671 (2004).

[mak04a] T. Makino, Y. Segawa, M. Kawasaki, H. Koinuma, *Optical Properties of Excitons in ZnO-based Quantum Well Heterostructures*, Semicond. Sci. Technol. **78** (2004) 20. DOI:10.1088/0268-1242/20/4/010.

[mak05] T. Makino, Y. Segawa and M. Kawasaki. Analytical study on exciton-longitudinal-optical-phonon coupling and comparison with experiment for ZnO quantum wells. J. Appl. Phys. **97**, 106111 (2005). DOI: 10.1063/1.1900294

[mak08] T. Makino, Y. Segawa, A. Tsukazaki, A. Ohtomo, M. Kawasaki. *Photoexcitation screening of the built-in electric field in ZnO single quantum wells*. Appl. Phys. Lett. **93**, 121907 (2008). DOI: 10.1063/1.2981523

[mak09] T. Makino, Y. Furuta, Y. Segawa, A. Tsukazaki, A. Ohtomo, Y. Hirayama, R. Shen, S. Takeyama, Y. Takagi, M. Kawasaki. *Magneto-optical study of n-type modulation-doped ZnO/$Mg_xZn_{(1-x)}O$ single quantum well structures*. Phys. Rev B **80**, 155333 (2009). DOI: 10.1103/PhysRevB.80.155333

[man96] A. Manassen, E. Cohen, Arza Ron, E. Linder, and L. N. Pfeiffer. *Exciton and trion spectral line shape in the presence of an electron gas in GaAs/AlAs quantum wells*. Phys. Rev. B **54**, 10609 (1996).

[mey04] B. K. Meyer, H. Alves, D. M. Hofmann, W. Kriegseis, D. Forster, F. Bertram, J. Christen, A. Hoffmann, M. Straßburg, M. Dworzak, U. Haboeck, and A. V. Rodina. *Bound exciton and donor–acceptor pair recombinations in ZnO*. Phys. stat. sol. (b) **241**, No. 2, 231– 260 (2004) / DOI 10.1002/pssb.200301962

[mor09] H. Morkoç, Ü. Özgür, *Zinc Oxide: Fundamentals, Materials and Device Technology*, (2009). DOI:10.1002/9783527623945.

[mor05a] C. Morhain, X. Tang, M. Teisseire-Doninelli, B. Lo, M. Laügt, J.-M. Chauveau, B. Vinter, O. Tottereau, P. Vennégués, C. Deparis, G. Neu. *Structural and electronic properties of ZnMgO/ZnO quantum wells.* Superlattices and Microstructures **38**, 455 (2005). DOI:10.1016/j.spmi.2005.08.055

[mor05b] C. Morhain, T. Bretagnon, P. Lefebvre, X. Tang, P. Valvin, T. Guillet, B. Gil, T. Taliercio, M. Teisseire-Doninelli, B. Vinter, and C. Deparis. *Internal electric field in wurtzite ZnO/$Zn_{0.78}Mg_{0.22}O$ quantum wells*. Phys Rev B 72 (24), 241305(R) (2005). DOI: 10.1103/PhysRevB.72.241305

[mos58] S.A Moskalenko. J. Opt. Spectroscop. 5, 147 (1958).

[mys68] A. Mysyrowicz, J.B. Grun, R. Levy, A. Bivas, S. Nikitine. *Excitonic molecule in CuCl*. Phys. Letters **26** A, 615 (1968).

[neu11] M.D. Neumann, C. Cobet, N. Esser, B. Laumer, T.A. Wassner, M. Eickhoff, M. Feneberg, R. Goldhahn. *Optical properties of MgZnO alloys: Excitons and exciton-phonon complexes*. J. Appl. Phys. **110**, 013520 (2011). DOI 10.1063/1.3606414

[oga03] K. Ogata, K. Koike, T. Tanite, T. Komuro, F. Yan, S. Sasa, M. Inoue, M. Yano. *ZnO and ZnMgO growth on a-plane sapphire by molecular beam epitaxy*. J. Cryst.Growth **251**, 623 (2003).

[ozg05] Ü. Özgür, Y.I. Alivov, C. Liu, A. Teke, M.A. Reshchikov, S. Doğan, V. Avrutin, S.J. Cho, H. Morkọ, *A comprehensive review of ZnO materials and devices*. J. Appl. Phys. **98** (2005) 1–103. DOI:10.1063/1.1992666.

[oht98a] A. Ohtomo, M. Kawasaki, Y. Sakurai, I. Ohkubo, R. Shirold, Y. Yoshida, T. Yasuda, Y. Segawa, H. Koinuma. *Fabrication of alloys and superlattices based on ZnO towards ultraviolet laser*. Materials Science and Engineering B **56**, 263 (1998). DOl: 10.1016/S0921-5107(98)00218-9

[oht98b] A. Ohtomo, M. Kawasaki, T. Koida, K. Masubuchi, H. Koinumab, Y. Sakurai, Y. Yoshida, T. Yasuda and Y. Segawa. *$Mg_xZn_{1-x}O$ as a II–VI widegap semiconductor alloy*. Appl. Phys. Lett. **72** (19), 2466 (1998).

[oht99a] A. Ohtomo, M. Kawasaki, I. Ohkubo, H. Koinuma, T. Yasuda, Y. Segawa. *Structure and optical properties of ZnO/$Mg_{0.2}Zn_{0.8}O$ superlattices*. Appl. Phys. Lett. **75** (7), 980 (1999). DOI 10.1063/1.124573

[oht99b] A Ohtomo, R Shiroki, I Ohkubo, H Koinuma, and M Kawasaki. *Thermal stability of supersaturated MgZnO alloy films and MgZnO/ZnO heterointerfaces*. Appl. Phys. Lett. **75**, 4088 (1999).

[oht00] A. Ohtomo, K. Tamura, M. Kawasaki, T. Makino, Y. Segawa, Z.K. Tang, G.K.L. Wong, Y. Matsumoto, H. Koinuma, *Room-temperature stimulated emission of excitons in ZnO/(Mg, Zn)O superlattices*, Appl. Phys. Lett. **77** (2000) 2204. DOI:10.1063/1.1315340.

[one93] M. O'Neill, M. Oestriech, W. W. Ruhle, and D. E. Ashenford. *Exciton radiative decay and homogeneous broadening in CdTe/$Cd_{0.85}Mn_{0.15}$Te multiple quantum wells*. Phys. Rev. B **48**, 8980 (1993).

[onu04] T. Onuma, S. F. Chichibu, A. Uedono, T. Sota, P. Cantu, T. M. Katona, J. F. Keading, S. Keller, U. K. Mishra, S. Nakamura, and S P. DenBaars. *Radiative and nonradiative processes in strain-free $Al_xGa_{1-x}N$ films studied by time-resolved photoluminescence and positron annihilation techniques.* J. Appl. Phys., **95** (5), 2495 (2004).

[pal44] C. Palache, H. Berman, C. Frondel. "*The system of mineralogy*", *7th. revised edition John Wiley & Sons*, NewYork, 1, 504 (1944).

[pag98] N. Paganotto, J. Siviniant, D. Coquillat, D. Scalbert, J.-P. Lascaray, A. V Kavokin, *Donor bound or negatively charged excitons in thin CdTe/Cd1-xMnx Te quantum wells*, Phys. Rev. B. **58** (1998) 4082–4088. DOI:10.1103/PhysRevB.58.4082.

[par66] Y.S. Park, C.W. Litton, T.C. Collins, D.C. Reynolds, *Exciton spectrum of ZnO*, Phys. Rev. **143** (1966) 512–519. DOI:10.1103/PhysRev.143.512.

[par05] S.-H. Park, D. Ahn. *Spontaneous and piezoelectric polarization effects in wurtzite ZnO/MgZnO quantum well lasers*. Appl. Phys. Lett. **87**, 253509 (2005). DOI: 10.1063/1.2149294

[pea05] S.J. Pearton, D.P. Norton, K. Ip, Y.W. Heo, T. Steiner, *Recent progress in processing and properties of ZnO*, Prog. Mater. Sci. **50** (2005) 293–340. DOI:10.1016/j.pmatsci.2004.04.001.

[pea12] S. Pearton, Jeffrey Davis and Chennupati Jagadish, *GaN and ZnO-based Materials and Devices*, Springer Berlin Heidelberg, Berlin, Heidelberg, 2012. DOI:10.1007/978-3-642-23521-4.

[pee02] F.M. Peeters, C. Riva, K. Varga, *Trions in Quantum Wells*, Few-Body Syst. **31** (2002) 97–100. DOI:10.1007/s006010200005.

[phi92] RT Phillips, DJ Lovering, GJ Denton, and GW Smith. *Biexciton creation and recombination in a GaAs quantum well*. Phys. Rev. B **45**, 4308 (1992).

[pul12] J. Puls, S. Sadofev, F. Henneberger. *Trions in ZnO quantum wells and verification of the valence band ordering.* Phys. Rev. B **85**, 041307(R) (2012). DOI: 10.1103/PhysRevB.85.041307

[ree70] R.R. Reeber. Lattice parameters of ZnO from 4.2 to 296K. J. Appl. Phys., 41, 13, 5063 (1970).

[rey99] D.C. Reynolds, D.C. Look, B. Jogai, C. Litton, G. Cantwell, W. Harsch, *Valence-band ordering in ZnO*, Phys. Rev. B. **60** (1999) 2340–2344. DOI:10.1103/PhysRevB.60.2340.

[ros14] D. Rosales, B. Gil, T. Bretagnon, B. Guizal, F. Zhang, S. Okur, M. Monavarian, N. Izyumskaya, V. Avrutin, Ü. Özgür, H. Morkoç, and J. H. Leach. *Excitonic recombination dynamics in non-polar GaN/AlGaN quantum wells.* J. Appl. Phys. **115**, 073510 (2014. DOI: 10.1063/1.4865959

[sad05] S. Sadofev, S. Blumstengel, J. Cui, J. Puls, S. Rogaschewski, P. Schafer, Y.G. Sadofyev, F. Henneberger. Growth of high-quality ZnMgO epilayers and ZnO/ZnMgO quantum well structures by radical-source molecular-beam epitaxy on sapphire. Appl. Phys. Lett. **87**, 091903 (2005). DOI: 10.1063/1.2034113

[sch03] R. Schmidt, B. Rheinländer, M. Schubert, D. Spemann, T. Butz, J. Lenzner, E. M. Kaidashev, M. Lorenz, A. Rahm, H. C. Semmelhack, and M. Grundmann. *Dielectric functions (1 to 5 eV) of wurtzite $Mg_xZn_{1-x}O$ ($x \leq 0.29$) thin films.* Appl. Phys. Letters **82** (147), 2260 (2003). DOI: 10.1063/1.1565185

[sen03] R.T. Senger, K.K. Bajaj. *Binding energies of excitons in polar quantum well heterostructures*. Phys. Rev. B **68**, 205314 (2003). DOI: 10.1103/PhysRevB.68.205314

[ser05] R.A. Sergeev, R.A. Suris, G. V. Astakhov, W. Ossau, D.R. Yakovlev, *Universal estimation of X- trion binding energy in semiconductor quantum wells*, Eur. Phys. J. B. **47** (2005) 541–547. DOI:10.1140/epjb/e2005-00362-5.

[shi95] A.J. Shields, J.L. Osborne, M.Y. Simmons, M. Pepper, and D.A. Ritchie. *Magneto-optical spectroscopy of positively charged excitons in GaAs quantum well.* Phys. Rev. B **52**, R5523 (1995).

[siv99] J. Siviniant, D. Scalbert, A. V. Kavokin, D. Coquillat, and J-P. Lascaray. *Chemical equilibrium between excitons, electrons, and negatively charged excitons in semiconductor quantum wells*. Phys. Rev. B **59**, R1602 (1999)

[sha99] A.K. Sharma, J. Narayan, J.F. Muth, C.W. Teng, C. Jin, A. Kvit, R.M. Kolbas, O.W. Holland, *Optical and structural properties of epitaxial $Mg_xZn_{1-x}O$ alloys*. Appl. Phys. Lett. **75** (1999) 3327–3329. DOI:10.1063/1.125340.

[ski92] A.J. Skinner, J.P. Lafemina. *Surface atomic and electronic structure of ZnO polymorphs*. Phys. Rev. B, **45**, 7, 3557 (1992).

[smo15] T. Smolenski, T. Kazimierczuk, M. Goryca, P. Wojnar, and P. Kossacki. *Mechanism and dynamics of biexciton formation from a long-lived dark exciton in a CdTe quantum dot.* Phys. Rev. B **91**, 155430 (2015). DOI: 10.1103/PhysRevB.91.155430

[sun2000] H.D. Sun, T. Makino, N.T. Tuan, Y. Segawa, Z.K. Tang, G.K.L. Wong, M. Kawasaki, A. Ohtomo, K. Tamura, H. Koinuma. *Stimulated emission induced by exciton-exciton scattering in ZnO/ZnMgO multiquantum wells up to room temperature*. Appl. Phys. Lett. **77** (26), 4251 (2000). DOI: 10.1063/1.1333687.

[sun01] H.D. Sun, T. Makino, Y. Segawa, M. Kawasaki, A. Ohtomo, K. Tamura, H. Koinuma. *Biexciton emission from ZnO/Zn0.74Mg0.26O multiquantum wells*. Appl. Phys. Lett. **78** (22), 3385 (2001). DOI: 10.1063/1.1375830

[sun02] H.D. Sun, Y. Segawa, M. Kawasaki, A. Ohtomo, K. Tamura, H. Koinuma. *Phonon replicas in ZnO/ZnMgO multiquantum wells*. J. Appl. Phys. **91** (10), 6457 (2002). DOI: 10.1063/1.1467627

[tai11] D. Taïnoff, M. Al-Khalfioui, C. Deparis, B. Vinter, M. Teisseire, C. Morhain, and J.-M. Chauveau. *Residual and nitrogen doping of homoepitaxial nonpolar m-plane ZnO films grown by molecular beam epitaxy*. Appl. Phys. Lett. **98**, 131915 (2011).

[tam08] H. Tampo, H. Shibata, K. Maejima, A. Yamada, K. Matsubara, P. Fons, S. Kashiwaya, S. Niki, Y. Chiba, T. Wakamatsu, and H. Kanie. *Polarization-induced two-dimensional electron gases in ZnMgO/ZnO heterostructures*. Appl. Phys. Lett. **93**, 202104 (2008)

[tam09] H. Tampo, H. Shibata, K. Maejima, T.-W. Chiu, H. Itoh, A. Yamada, K. Matsubara, P. Fons, Y. Chiba, T. Wakamatsu, Y. Takeshita, H. Kanie, and S. Niki. *Band profiles of ZnMgO/ZnO heterostructures confirmed by Kelvin probe force microscopy*. Appl. Phys. Lett. **94**, 242107 (2009).

[tek04] A. Teke, Ü. Özgür, S. Doğan, X. Gu, H. Morkoç, B. Nemeth, J. Nause, H.O. Everitt. *Excitonic fine structure and recombination dynamics in single-crystalline ZnO*. Phys. Rev. B. **70** (2004) 1–10. DOI:10.1103/PhysRevB.70.195207.

[tri14] R. Triboulet. *Growth of ZnO bulk crystals: A review*. Progress in Crystal Growth and Characterization of Materials **60**, 1 (2014). DOI : 10.1016/j.pcrysgrow.2013.12.001 and references cited therein.

[thi10] C. Thiandoume, A. Lusson, P. Galtier, V. Sallet. *Temperature dependence of $Zn_{1-x}Mg_xO$ films grown on c-plane sapphire by metal organic vapor phase epitaxy.* J. Cryst. Growth **312**, 1529 (2010). DOI: 10.1016/j.jcrysgro.2010.01.018

[tho60] D.G. Thomas, *The exciton spectrum of zinc oxide*, J. Phys. Chem. Solids. **15** (1960) 86–96. DOI:10.1016/0022-3697(60)90104-9.

[var67] Y. P. Varshni. *Temperature dependence of the energy gap in semiconductors*. Physica **34**, 149 (1967).

[ven08] P. Vennéguès, J. M. Chauveau, M. Korytov, C. Deparis, J. Zuniga-Perez, and C. Morhain. *Interfacial structure and defect analysis of nonpolar ZnO films grown on R-plane sapphire by molecular beam epitaxy*. J. Appl. Phys. **103**, 083525 (2008). DOI: 10.1063/1.2905220

[vis99] R. D. Vispute, S. Choopun, R. Enck, A. Patel, V. Talyansky, R. P. Sharma, T. Venkatesan, W. L. Sarney, L. Salamancariba, S. N. Andronescu, A. A. Iliadis, and K. A. Jones. *Pulsed Laser Deposition and Processing of Wide Band Gap Semiconductors and Related Materials*. Journal of Elec Materi **28** (3), 275 (1999).

[yam95] Yoichi Yamada, Tomobumi Mishina, Yasuaki Masumoto, Yoichi Kawakami, Shigeo Yamaguchi, Kunio Ichino, Shizuo Fujita, and Shigeo Fujita. *Time-resolved spectroscopy of biexciton luminescence in $Zn_xCd_{1-x}Se$-ZnS_ySe_{1-y} multiple quantum wells*. Phys. Rev B **51**, 2596 (1995).

[yam95b] Y Yamada, T Mishina, Y Masumoto, Y Kawakami, J Suda, S Fujita, and S Fujita. *Time-resolved nonlinear luminescence of biexcitons in ZnSe-Zn(x) Mg(1-x) S(y) Se(1-y) single quantum wells*. Phys. Rev. B **52**, 2289 (1995).

[yam01] A. Yamamoto, K. Miyajima, T. Goto, H. K. Ko, and T. Yao. *Biexciton luminescence in high-quality ZnO epitaxial thin films*. J. Appl. Phys. **90**, 4973 (2001).

[zha05] B. P. Zhang, N. T. Binh, K. Wakatsuki, C. Y. Liu, and Y. Segawa, N. Usami. *Growth of ZnO/MgZnO quantum wells on sapphire substrates and observation of the two-dimensional confinement effect*. Appl. Phys. Lett. **86**, 032105 (2005). DOI: 10.1063/1.1850594

[zip10] J. Zippel, S. Heitsch, M. Stolzel, A. Muller, H. von Wenckstern, G. Benndorf, M. Lorenz, H. Hochmuth, M. Grundmann. *Optical properties of homo- and heteroepitaxial ZnO/$Mg_xZn_{1-x}O$ single quan-tum wells grown by pulsed-laser deposition*. Journal of Luminescence **130**, 520 (2010). DOI: 10.1016/j.jlumin.2009.10.025

[zhu17] L. Zhu, Laurent L C Lem, T.-P. Nguyen, K. Fair, S. Ali, M. J Ford, M. R Phillips and C. Ton-That. *Indirect excitons in hydrogen-doped ZnO*. J. Phys. D: Appl. Phys. **50**, 115104 (2017). doi:10.1088/1361-6463/aa5c23

[was09] Thomas A. Wassner, Bernhard Laumer, Stefan Maier, Andreas Laufer, Bruno K. Meyer, Martin Stutzmann, and Martin Eickhoff. *Optical properties and structural characteristics of ZnMgO grown by plasma assisted molecular beam epitaxy*. J. Appl.Phys.**105**, 023505 (2009). DOI 10.1063/1.3065535.

Résumé en français

L'oxyde de zinc est un matériau qui fait l'objet d'étude depuis de nombreuses années. Son usage est multiple puisqu'il est utilisé dans des domaines très variés allant de la cosmétique à la réalisation de détecteur UV en passant par la réalisation de revêtements pour les métaux. Son intérêt en tant que matériaux semiconducteurs a été ravivé ces vingt dernières années suite à la réalisation d'hétéro-structures quantiques à base de ZnO et de ses alliages (Zn, Mg)O et (Zn, Cd)O. Plusieurs de ses propriétés en font un candidat intéressant pour la réalisation de composants optoélectroniques émetteurs (DEL, DL) ou détecteur de lumière. C'est un matériau qui lorsqu'il cristallise dans la structure wurtzite a un gap direct dont la valeur à température ambiante (3.37 eV) en fait un matériau comparable au GaN qui est le matériau emblématique de la famille des nitrure d'élément III. Ces matériaux sont actuellement utilisés par l'industrie pour la réalisation d'émetteurs et de détecteurs dans le domaine du bleu et du proche UV. De plus l'énergie de liaison de son exciton (60 meV) est le double de celle de GaN (25.4 meV) et surtout deux fois l'énergie thermique à température ambiante. Cette propriété remarquable ouvre un champ d'investigation important pour l'exploitation des effets excitoniques à température ambiante.

Dans ce travail nous avons étudié les propriétés optique de puits quantiques ZnO/(Zn, Mg)O crus sur la face non polaire d'un substrat de ZnO massif. Les faces non polaires, A ou M, sont utilisées, malgré les difficultés liées à la croissance de ces matériaux dans cette configuration, afin d'éviter les effets désastreux de l'effet Stark quantique confiné (ESQC). En effet, dans le cas de puits quantiques crus selon l'axe c (axe facile de croissance) du ZnO, un champ électrique interne résultant à la fois des propriétés piézoélectrique et de polarisation spontanée du matériau apparaît dans les structures. Ce champ, en séparant les paires électron-trou photo-crées réduit la force d'oscillateur des transitions radiatives et l'énergie de liaison de l'exciton. Ces deux effets combinés réduisent considérablement le rendement radiatif des puits quantiques.

Les échantillons étudiés sont des puits quantique unique crus par MBE au CHREA sur la face A de substrats de ZnO massif. La largeur du puits est de 3.5 nm. Dans un premier temps une couche de 200 nm de (Zn, Mg)O est crue, suivit de 3.5 nm de ZnO. L'hétéro-structure est complété par une couche de 50nm de (Zn, Mg)O. La concentration de magnésium dans les barrières est de 20 %.

La présentation des résultats est organisée en trois parties. D'abord une étude détaillée de la recombinaison des excitons dans le substrat et la barrière. Ensuite, les résultats obtenus en excitation continue du puits quantique. Pour finir, avec l'étude de la dynamique temporelle de la recombinaison des excitons dans le puits.

Propriétés optiques du substrat de ZnO et des barrières de (Zn, Mg)O

Si les propriétés optiques du ZnO massif sont bien documentées, il n'en est pas de même de celle du (Zn, Mg)O. En particulier, il y a que très peu de résultat dans la littérature sur ce dernier matériau en terme de dynamique de recombinaison des excitons.

Les mesures de photoluminescence en excitation continue (CW - PL) avec des photons d'énergie inférieure au gap du matériau barrière permettent d'obtenir des informations sur le substrat utilisé. Le spectre de PL présente trois pics avec des énergies qui correspondent à la recombinaison d'excitons liés à des donneurs neutres. Le signal émis présente un taux de polarisation d'environ 95 %. Cette valeur confirme la bonne qualité du matériau massif. L'intensité de photoluminescence décroit d'un ordre de grandeur entre 10 et 50 K. Cette variation est modélisée en considérant un mécanisme de libération des excitons sous l'effet de l'énergie thermique qui ensuite se recombine non-radiativement dans le matériau.

Le comportement des excitons dans la barrière de (Zn, Mg)O est bien différent. Dans ce cas, les spectres de PL sont obtenus avec une énergie des photons du faisceau incident supérieure à l'énergie du gap du matériau barrière. Le taux de polarisation du signal émis n'est que de 88 %. Ce fait peu s'expliquer en prenant en compte les effets de contrainte, résultant de la différence des paramètres de maille entre le ZnO et le (Zn, Mg)O. Les spectres de photoluminescence en excitation continue, mesurés entre 10 K et 200 K, sont analysés en utilisant des fonctions gaussiennes pour ajuster les spectres. Ceux ci se composent de plusieurs raies, celle à plus haute énergie correspond à la transition fondamentale. Elle est accompagné de répliques phonons à plus base énergie avec une différence en énergie entre les différentes raie de 71 meV. Le comportement en température de l'intensité, de la largeur à mi-hauteur et de l'énergie est modélisé (fig. R.1). La variation de l'énergie d'émission dans la gamme 10-100 K montre un S-shape caractéristique soit d'un effet de délocalisation, soit d'un changement d'état des excitons. L'intensité reste quasi constante sur cette gamme de température, avant de décroitre d'environ deux ordres de grandeur entre 100 K et 200 K.

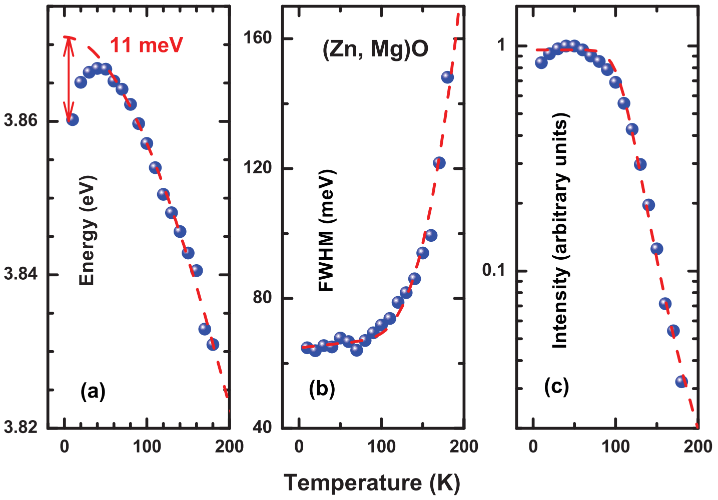

Figure R.1 : Energie de la transition, largeur à mi-hauteur et intensité de la luminescence en fonction de la température.

Pour compléter, nous avons réalisé une étude de la photoluminescence résolue en temps en fonction de la température entre 10 K et 300 K. L'analyse des spectres intégrés en temps nous a permis de compléter les résultats de CW-PL. Le résultat le plus intéressant est la mise en évidence d'un second S-shape sur l'énergie d'émission entre 150 K et 250 K (fig. R.2-c).

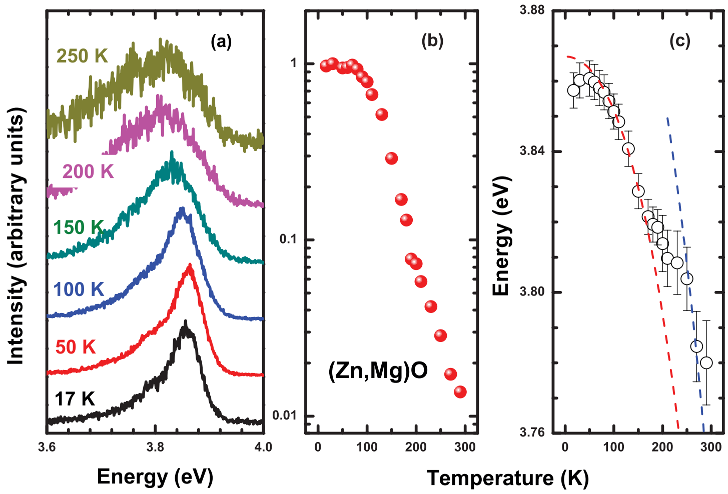

Figure R.2 : Energie de la transition, largeur à mi-hauteur et intensité de la luminescence en fonction de la température obtenue par ITRPL.

Les déclins de l'intensité de PL sont à base température sont non exponentiel. Ils deviennent mono-exponentiels pour les températures au-delà de 100 K. Les déclins mesurés à base température sont ajustés en utilisant une fonction bi-exponentielle. La constante de temps rapide, τ_a, est invariante avec la température. Par contre, la constante de temps lente, τ_b, elle décroit rapidement avec la température. Au delà de 100 K, une seule constante de temps est nécessaire pour reproduire le comportement temporel de l'intensité. Celle-ci décroit de manière monotone avec la température jusqu'à 300 K.

Pour comprendre et modéliser le comportement en température du temps de déclin et de l'intensité de PL nous avons considéré deux domaines de température. D'abord considérons les résultats obtenus à des températures inférieures à 90 K. L'intensité de PL est quasi constante, l'énergie de la transition présente un S-shape correspondant à une variation de 11 meV de l'énergie de transition. La durée de vie longue varie rapidement avec la température alors que la plus rapide est constante. Ces différents éléments nous conduisent à proposer le scénario suivant.

A très base température les excitons sont piégés sur des fluctuations de potentiel. Cette situation est souvent rencontrée pour des composés ternaires dans lesquels la répartition aléatoire des éléments entraine des fluctuations de potentiel importantes. Ces fluctuations ont des extensions spatiale réduites, les excitons sont localisés dans un espace 0 D. Dans ce cas la durée de vie est indépendante de la température.

Le système d'excitons localisés comporte deux états distincts. Sous l'effet de la température, les excitons passe de l'état de plus basse énergie, qui à la durée de vie la plus longue, vers l'état de plus haute énergie séparé du précédent de 11 meV. Par conséquent les évolutions de la population des deux niveaux peuvent être décrite par les équations suivantes :

$$\begin{aligned} n_1(t) &= A_1 \exp\left(-t/\tau_{eff}\right) \\ n_2(t) &= A_2 \exp\left(-t/\tau_{eff}\right) + A_3 \exp\left(-t/\tau_2\right) \end{aligned} \quad \text{...} \ (\text{R.01})$$

avec :

$$\frac{1}{\tau_{eff}} = \frac{1}{\tau_1} + \frac{1}{\tau_{12}} \Rightarrow \tau_{eff} = \frac{\tau_1}{1+\tau_1/\tau_{12}} = \frac{\tau_1}{1+\dfrac{\tau_1}{\tau_{120}} \exp\left(\dfrac{-E_{12}}{k_B\ T}\right)} \quad \text{................................} \ (\text{R.02})$$

L'ajustement de τ_b avec l'expression (R.02) permet de terminer les valeurs de τ_1, τ_{12} et E_{12}. Le meilleur ajustement est obtenue pour 131.5 ns, 1.2 ns et 11.7 meV pour respectivement τ_1, τ_{12} et E_{12}. La valeur de τ_{120} est proche de celle de τ_a et l'énergie d'activation correspond à l'énergie déterminée à partir de l'évolution de l'énergie de transition.

Dans le domaine haute température (T>200 K), nous avons affaire à des excitons libres. L'intensité et le temps de déclin de la photoluminescence décroient de manière monotone avec la température. Ce comportement est observé lorsque les phénomènes de recombinaison non-radiatifs prennent le pas sur les recombinaisons radiatives. Dans ce cas il est facile de démontrer que les durées de vie radiative (τ_R) et non radiative (τ_{NR}) sont données par les expressions suivantes :

$$\tau_R(T) = \tau_{PL} \frac{I(0)}{I(T)} \quad \text{et} \quad \tau_{NR} = \left(1/\tau_{PL} - 1/\tau_R\right)^{-1} \quad \text{..} \ (\text{R.03})$$

Ou I(T) est l'intensité de la photoluminescence, τ_{PL} le temps de déclin de la photoluminescence. A partir des données expérimentales la dépendance en température de ces deux durées de vie peut être déterminée. Elles sont données par les expressions suivantes :

$$\tau_R = 1.8(\mathrm{ps/K})\ T^{3/2} \text{ et } \tau_{NR}(T) = 5.9(\mathrm{ps})\ \exp\left(71(\mathrm{meV})/kT\right)$$

La durée de vie radiative varie en $T^{3/2}$ comme attendue et l'énergie d'activation des phénomènes non-radiatifs est de 71 meV.

Pour finir le modèle il faut connecter les deux domaines de température. Pour cela nous nous appuyons sur le modèle couramment utilisé pour rendre compte des phénomènes de localisation dans les puits quantiques. Dans ce modèle le τ_{PL} et l'intensité de PL sont obtenus à partir des expressions suivantes :

$$\Gamma_{PL}(T) = \Gamma_R(T) + \Gamma_{NR}(T) = \frac{1}{\tau_{PL}(T)} \quad \text{(R.04)}$$

$$\frac{I(T)}{I(0)} = \frac{\Gamma_R(T)}{\Gamma_R(T) + \Gamma_{NR}(T)} = \Gamma_R(T)\ \tau_{PL}(T) \quad \text{(R.05)}$$

Dans ces expressions Γ_R et Γ_{NR} sont les taux de recombinaisons radiatif et non radiatif. Ils sont calculé en prenant comme hypothèse que seul les excitons libres peuvent se recombiner non radiativement. Dans ce cadre ils peuvent être calculés à partir des expressions suivantes :

$$\Gamma_R = A_{loc}\ \Gamma_{loc} + A_{free}\ \Gamma_{R\_fr} \text{ et } \Gamma_{NR} = A_{free}\ \Gamma_{NR\_fr} \quad \text{(R.06)}$$

Ici Γ_{loc}, Γ_{R_fr} et Γ_{NR_fr} sont respectivement les taux de recombinaison radiatif des excitons localisés et les taux de recombinaisons non radiatif et non-radiatif des excitons libres. Les coefficients A_{loc} et A_{free} sont les ratios de respectivement la population d'excitons localisés (n_{loc}) et d'excitons libres (n_{free}) et de la population totale d'excitons ($n_{exc}=n_{loc}+n_{free}$). Dans des conditions de faible excitation, cas non-dégénérée, les densités d'excitons suivent les distributions Boltzmann :

$$n_{free} \approx \frac{2\ M\ k_B\ T}{\pi\ \hbar^2} \exp\left(-\frac{E_{free}(T) - E_F(T)}{k_B\ T}\right) \quad \text{(R.07)}$$

et

$$n_{loc} \approx N_{loc}\ \exp\left(-\frac{E_{free}(T) - E_{loc} - E_F(T)}{k_B\ T}\right) \quad \text{(R.08)}$$

Le seul paramètre permettant d'ajuster les deux courbes aux mesures est N_{loc} est la densité de centres de localisation. Une valeur de $5\mathrm{x}10^{14}$ cm^{-3} pour N_{loc} permet d'avoir un très bon accord entre le modèle et l'expérience (fig. R.3).

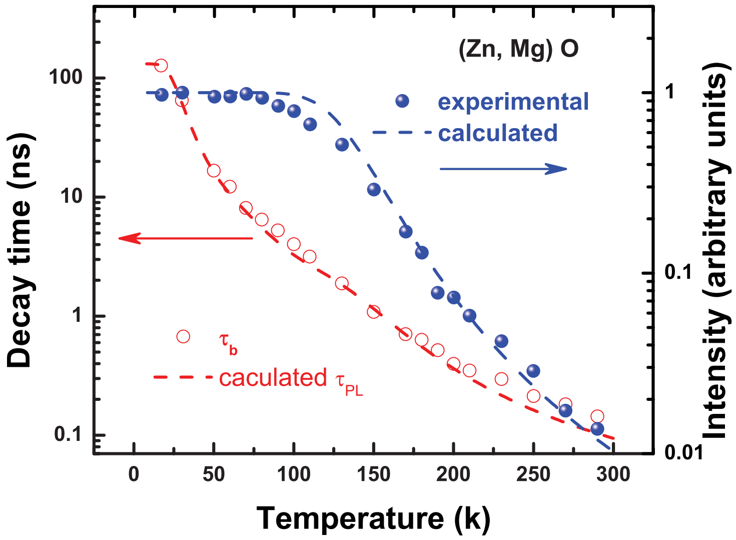

Figure R.3 : Comparaison des valeurs expérimentales de l'intensité et du temps de déclin de la photoluminescence en fonction de la température avec le modèle.

Complexes excitoniques dans les puits quantique

L'existence de complexes excitoniques, à savoir d'un exciton en interaction soit avec un porteur de charge soit avec un autre exciton a été proposé théoriquement en 1958. La mise en évidence expérimentale a suivit quelques années plus tard dans les matériaux semiconducteurs. Nous envisagerons dans ce travail, le ZnO étant de type n, que la formations de deux type de complexes, les biexcitons (deux excitons en interaction) et les trions chargés négativement (un excitons en interaction avec un électron libre).

Les spectres de photoluminescence mesurés à basse température publiés dans la littérature de puits quantique crus sur les surfaces non polaires de ZnO sont tous dominés par un pic dont l'énergie ne correspond pas à celle de la transition fondamentale dans le puits. Cet effet est généralement attribué à des effets de localisations sur des défauts du matériau. Dans cette étude nous nous sommes appliqué à reconsidérer cette interprétation. Pour cela nous avons fait des mesures de photoluminescence avec des conditions d'excitations différentes, et analysé le comportement en température et en polarisation.

Nous avons dans un premier temps regardé la polarisation de la photoluminescence du puits. Le degrés de polarisation du signal est de 99 % ce qui est attendu pour une structure crue sur une surface non-polaire contenant l'axe c.

Sur la fig. R.4 nous avons reporté deux spectres, mesurés à base température avec des densités d'excitation différentes, normalisés sur le maximum d'intensité de la réponse du puits quantique. Pour la densité la plus faible la réponse du puits quantique se résume à un seul pic avec un maximum à 3.4 eV. Par contre à forte excitation trois pics sont résolus, un à plus haute énergie un autre à plus basse énergie. En comparant ce spectre avec le spectre de réflectivité de l'échantillon le pic à 3.43 eV est attribué à la recombinaison des exciton libres. Cette identification est renforcée par le calcul de l'énergie de la transition dans le formalisme des fonctions enveloppes. L'intensité du pic à 3.38 eV a, comme nous le verrons plus loin, un comportement en fonction de la densité d'excitation qui permet de l'attribuer à la recombinaison du biexciton.

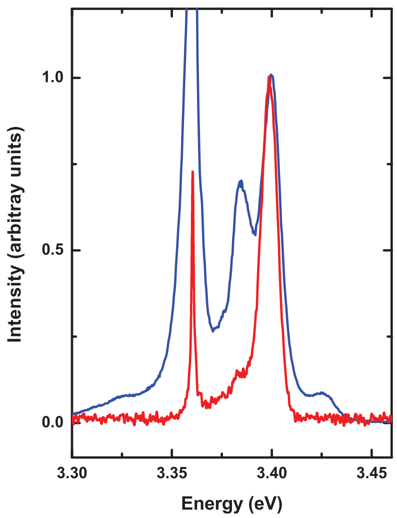

Figure R.4 : Spectres de PL mesurés à 10 K pour deux densités d'excitation.

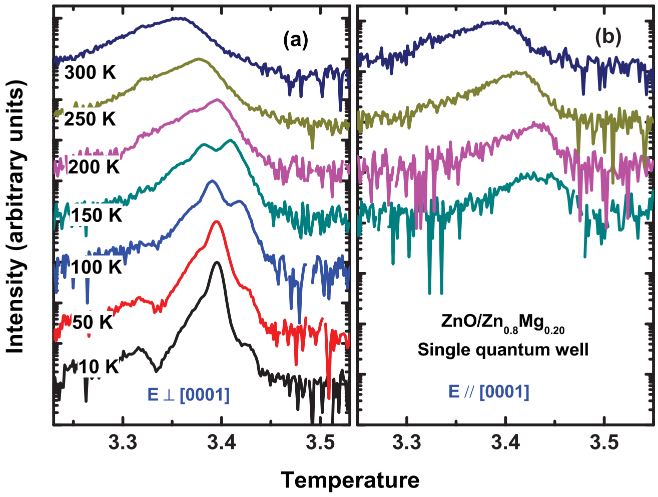

Figure R.5 : Spectres de photoluminescence mesurés à différente température dans les polarisations (ab) et (c).

Afin d'identifier la nature de la transition responsable de ce pic de luminescence nous avons fait une étude en température. La figure R.5 résume cette étude pour les deux polarisations étudiées. Le panel a (polarisation ab) démontre que lorsque la température augmente le ratio entre le pic attribué à l'exciton libre (X) est le pic dominant augmente avec la température. La raie dominante est donc liée à la recombinaison d'un complexe excitonique. Quand la température augmente il se dissocie et la densité d'excitons libres augmente dans le puits quantique et conséquemment l'intensité de la raie X. D'autre part, la raie de luminescence est dissymétrique, elle présente une extension vers les bases énergie. Cette dissymétrie augmente avec la température. Ce comportement est caractéristique de la luminescence du trion. En effet dans ce complexe formé de trois particules la règle de conservation de la quantité de mouvement est assurée par la troisième particule. A partir de 150 K dans la polarisation c une raie à plus haute énergie apparaît sur les spectres séparés d'environ 40 meV de la raie principale. Cette énergie est compatible avec la différence en énergie entre les exciton A, B et C dans ZnO. En conclusion le spectre de PL à base température est dominé par la raie du trion chargé négativement.

Les pics de luminescence ont été approximé en prenant : un fonction gaussienne pour la contribution de l'exciton, une fonction lorentzienne pour celle du bi-exciton et de la convolution d'une fonction gaussienne avec une distribution de Boltzmann pour le trion. Dans le cas d'une faible densité d'excitation, ou les contributions du trion et de l'exciton sont à considérer, les résultats sont présentés fig. R.6. L'intensité du trion décroit de manière monotone avec la température alors que l'intensité de l'exciton croit jusqu'à 100 K pour ensuite décroitre avec l'augmentation de la température. Ce comportement peut être modélisé par les équations R.09 pour le trion et R.10 pour l'exciton. Ici nous considérons que sous l'effet de la température la dissociation du trion est responsable de la diminution de l'intensité de photoluminescence. L'augmentation de l'intensité de l'exciton est du à ce phénomène. A plus hautes températures les recombinaisons sur des centres non-radiatifs expliquent la diminution de l'intensité de l'exciton. Un bon accord est obtenu avec les points expérimentaux pour E_1=17.1 meV valeur proche de la différence entre les énergies des deux transitions. La recombinaison non radiative a une énergie d'activation E_2=89 meV.

$$I\left(T,A,E_1\right)=I_1\ f\left(T,A,E_1\right)=I_1\Big/\left(1+\ A\ T\ \exp\left(-E_1/k\ T\right)\right)\ \ldots\ldots\ldots\ldots\ldots\ldots\ldots\ldots\ (R.09)$$

$$I\left(T,B,E_2\right)=\left(I_2\left(1-f(T,A,E_1)\right)+I_0\right)\Big/\left(1+\ B\ T\ \exp\left(-E_2/k\ T\right)\right)\ \ldots\ldots\ldots\ldots\ldots\ (R.10)$$

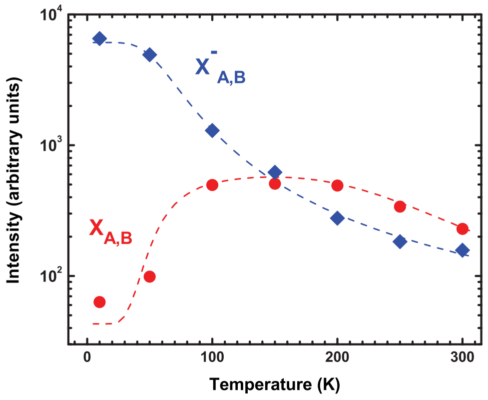

Figure R.6 : Intensité de photoluminescence mesurée à différente température.

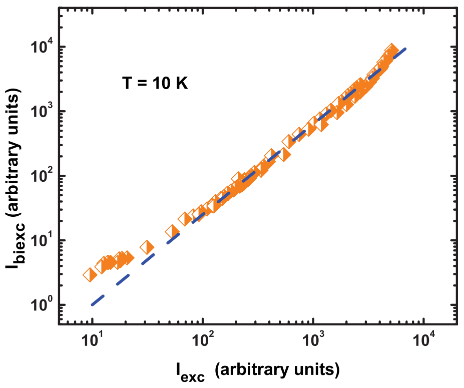

Figure R.7 : Intensité du biexciton en fonction de celle de l'exciton.

Pour caractériser le bi-exciton nous avons procédé à une étude à base température de la photoluminescence en fonction de la densité d'excitation. L'évolution des densités des excitons et des bi-excitons peut être décrite dans le cadre d'un modèle d'équilibre chimique, dans lequel les bi-excitons sont créés par interaction entre excitons. Dans le cadre de ce modèle l'intensité du bi-exciton I_{xx} varie en fonction de celle de l'exciton I_x selon une loi du type $I_{xx} \propto I_x^{\beta}$ avec $\beta = 2$. Le résultat présenté fig. R.7 montre une dépendance linéaire de la forme $I_{biexc} \propto I_{exc}^{1.4}$. Cette différence entre la prévision théorique et l'expérience provient de limitations du modèle. Un des postulats du modèle est notamment que le temps caractéristique d'inter-conversion est beaucoup plus court que les durées de vies excitoniques. Cette condition, qui n'était pas contraignante pour les matériaux à gap indirect comme le silicium, n'est peut-être pas remplie dans le cas de nos échantillons.

Etude résolue en temps de la réponse du puits quantique

Dans cette dernière partie nous nous sommes intéressé aux dynamiques temporelles de recombinaison des excitons et des trions en fonction de la température. Les spectres intégrés en temps de photoluminescence résolue en temps (ITRPL) présentent le même comportement en température que les spectres de CW-PL. Les intensités des raies liées au trion et à l'exciton montrent des comportements comparables à ceux illustrés figure R.6. Nous avons analysé en détail les déclins de photoluminescences à différente température. A très base température le déclin de PL du trions est mono-exponentielle alors que celui de l'exciton montre deux régimes. Dans une gamme de température intermédiaire les deux déclins montrent un comportement mono-exponentiel avec des constantes de temps comparable. A haute température, le déclin de l'exciton reste mono-exponentiel et celui du trion devient bi-exponentiel. La figure R.8 résume cette étude du temps de déclin en fonction de la température.

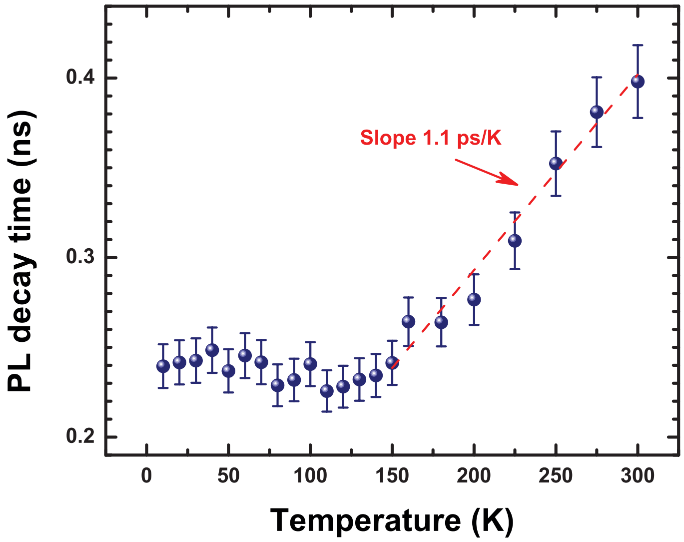

Figure R.8 : Temps de déclin de la photoluminescence en fonction de la température.

Le temps de déclin reste quasi constant pour les températures inférieures à 100 K. Il augmente linéairement avec la température jusqu'à 300 K. La valeur de la pente est de 1.1 ps/K qui est inférieure aux valeurs précédemment publié pour des puits non-polaire ZnO/(Zn, Mg)O.

Pour analyser les résultats nous supposons : les trions peuvent soit se recombiner radiativement soit se dissocier thermiquement pour donner des excitons libres ; les excitons libres peuvent eux soit se recombiner radiativement soit disparaître lors de processus non-radiatifs. A partir de ce modèle il est possible en étant prudent sur les domaines de température considérés d'évaluer la pente de l'accroissement linéaire des durée de vie radiative des excitons et des trions. Pour cela nous avons d'abord considérer les déclins mesurés à basse température (T<80 K). Dans ce domaine de température les recombinaisons radiatives des trions domine le signal de photoluminescence. Il donc possible de le traiter en terme de compétition radiatif versus non radiatif. Dans ce cas c'est la dissociation thermique des trions qui joue le rôle du canal non-radiatif. A haute température (T>200 K) c'est la situation inverse. Et dans une approche grossière, car ne tenant pas compte de l'alimentation de la population d'exciton par dissociation du trion on peut effectuer le même traitement des résultats.

Conclusion

Nous présentons une études détaillées du comportement des excitons dans un puits quantique non-polaire cru sur la face A d'un substrat de ZnO massif. Dans une première partie le comportement des excitons dans la barrière à fait apparaître un comportement non-usuel de l'exciton localisé dans les fluctuation de potentiel. Les observations ont été modélisées à partir d'un modèle à deux niveaux excitoniques et par une prise en compte des effets de localisation. L'importance des complexes excitoniques dans le puits quantique est mise en évidence dans les seconde et troisième parties à partir de mesures de différentes spectroscopies optiques résolues en polarisation, en température et en temps. La dissociation des trions négativement chargés sous l'effet de l'énergie thermique est clairement mise en évidence. De même le peuplement d'un état de symétrie c. Les études en fonction de la densité d'excitation ont permis de mettre en évidence la formation de bi-excitons et d'étudier leur comportement en fonction de la température. La dynamique des déclins de photoluminescence est étudiée dans le détail.

Au vue de ces résultats il nécessaire de revisiter les interprétations des résultats de photoluminescence publiés sur les puits quantiques Zn0/(Zn, Mg)O. En effet, il est couramment admis que le pic dominant de photoluminescence doit être attribué à la recombinaison des excitons localisés soit sur des fluctuations de potentiel soit sur des défauts intrinsèques.

L’oxyde de zinc est un matériau prometteur pour la réalisation de composants optoélectroniques dans la gamme des émetteurs UV. Pour cela, il faut développer des hétéro-structures tel que des puits quantiques ZnO/(Zn, Mg)O afin de mieux contrôler les propriétés d’émissions. Ce travail porte sur la caractérisation de telles structures crûes sur le plan A, surface non polaire, de ZnO massif. A partir de mesures de spectroscopie optiques (réflectivité, photoluminescence en excitation continue et photoluminescence résolue en temps) nous avons déterminé les différents phénomènes physiques mis en jeux lors de la recombinaison radiative des porteurs dans ces puits quantiques. Dans un premier temps, nous avons étudié en détail l’émission des photons par les barrières de (Zn, Mg)O. Grace à l’étude en température nous avons montré que l’émission optique de la barrière correspond à la recombinaison de paires électron trou en interactions (excitons) qui sont à basses températures localisées dans des fluctuations de potentiel. Sous l’effet de la température ils se délocalisent et se recombinent comme des exciton libres. L’étude détaillée des déclins temporels de photoluminescence nous à permis de démontrer que nous avions affaire à deux états excitoniques différents qui présentent des dynamiques de recombinaisons différentes. Un modèle est proposé pour rendre compte des différentes observations. La partie principale de ce travail porte sur le comportement des excitons dans le puits quantique. Le résultat majeur de cette étude est la démonstration expérimentale que dans ce cas des complexes excitoniques, ici des trions chargé négativement (exciton en interaction avec un électron libre), se forment à basse température et sont responsable de la luminescence observée. De plus, en variant la densité d’excitation nous avons montré que se former également des bi-excitons (pseudo particule formée de deux exciton en interactions). Le comportement en température de la photoluminescence obtenue dans différente conditions d’excitation à permis de démontrer que sous l’effet de l’énergie thermique les complexes excitoniques se dissociés pour créer des excitons libres. Des mesures en fonction de la polarisation de la lumière émise et de la température ont permis également d’étudier l’état C de l’exciton dans le puits. Les dynamiques de recombinaison des différents complexes excitoniques sont examinées en fonction de la température.

The zinc oxide is a promising material for the realization of optoelectronic devices in the blue-UV range. For this, it is necessary to develop hetero-structures such as ZnO/(Zn, Mg)O quantum wells in order to have better control of the properties of emissions. This work concerns the characterization of such structures grown on the A-plane (non-polar surface) of bulk ZnO. From optical spectroscopies measurements (reflectivity, continuous wave and time-resolved photoluminescence) we determined the various physical phenomena involve during the radiative recombination of the carriers in these quantum wells. At first, we studied in detail the emission of photons by the barriers of (Zn, Mg)O. Thanks to the study in temperature we showed that the optical emission of the barrier corresponds to the recombination of electron hole pairs in interactions (excitons), which are at low temperatures localized in the fluctuations of the potential. Under the influence of the temperature they delocalize and recombine as free exciton. From the detailed study of the temporal decays of photoluminescence we can demonstrate that we deal with two different excitonic states, which present different dynamics of recombination. A model is proposed that explain the various observations. The main part of this work concerns the behavior of the excitons in the quantum well. The major result is the experimental demonstration that excitonics complexes are formed at low temperature, negatively charged trion (exciton in interaction with a free electron), in this system and they are responsible for the observed luminescence. Furthermore, by varying the density of excitation we showed that biexcitons are also form (pseudo-particles formed by two excitons in interactions). The behavior in temperature of the photoluminescence obtained in different conditions of excitation demonstrates that under the influence of the thermal energy the exitonic complexes are broken to create free excitons. Measures according to the polarization of the emitted light and the temperature also allowed studying the C state of the exciton in the quantum well. The dynamics of recombination of the various excitonics complexes are examined according to the temperature.